



Measurement of differential cross sections of isolated-photon plus heavy-flavour jet production in pp collisions at $\sqrt{s}=8$ TeV using the ATLAS detector

Aaboud, M.; Aad, G.; Abbott, B.; Abdinov, O.; Abeloos, B.; Abidi, S.H.; Abouzeid, Ossama Sherif Alexander; Abraham, NL; Abramowicz, H.; Abreu, H.; Abreu, R.; Abulaiti, Y.; Acharya, B.S.; Adachi, Shin-ichi; Adamczyk, L.; Adelman, J.; Adersberger, M.; Adye, T.; Affolder, A. A.; Dam, Mogens; Besjes, Geert-Jan; Alonso Diaz, Alejandro; Hansen, Peter Henrik; Hansen, Jørgen Beck; Hansen, Jørn Dines; Wiglesworth, Graig; Galster, Gorm Aske Gram Krohn; de Almeida Dias, Flavia; Thiele, Fabian Alexander Jürgen; Monk, James William; Bajic, Milena; Petersen, Troels Christian; Stark, Simon Holm; Xella, Stefania

Published in:
Physics Letters B

DOI:
[10.1016/j.physletb.2017.11.054](https://doi.org/10.1016/j.physletb.2017.11.054)

Publication date:
2018

Document version
Publisher's PDF, also known as Version of record

Document license:
[CC BY](#)

Citation for published version (APA):
Aaboud, M., Aad, G., Abbott, B., Abdinov, O., Abeloos, B., Abidi, S. H., Abouzeid, O. S. A., Abraham, NL., Abramowicz, H., Abreu, H., Abreu, R., Abulaiti, Y., Acharya, B. S., Adachi, S., Adamczyk, L., Adelman, J., Adersberger, M., Adye, T., Affolder, A. A., ... Xella, S. (2018). Measurement of differential cross sections of isolated-photon plus heavy-flavour jet production in pp collisions at $\sqrt{s}=8$ TeV using the ATLAS detector. *Physics Letters B*, 776, 295-337. <https://doi.org/10.1016/j.physletb.2017.11.054>



Measurement of differential cross sections of isolated-photon plus heavy-flavour jet production in pp collisions at $\sqrt{s} = 8$ TeV using the ATLAS detector

The ATLAS Collaboration^{*}

ARTICLE INFO

Article history:

Received 26 October 2017

Received in revised form 21 November 2017

Accepted 22 November 2017

Available online 5 December 2017

Editor: W.-D. Schlatter

ABSTRACT

This Letter presents the measurement of differential cross sections of isolated prompt photons produced in association with a b -jet or a c -jet. These final states provide sensitivity to the heavy-flavour content of the proton and aspects related to the modelling of heavy-flavour quarks in perturbative QCD. The measurement uses proton–proton collision data at a centre-of-mass energy of 8 TeV recorded by the ATLAS detector at the LHC in 2012 corresponding to an integrated luminosity of up to 20.2 fb^{-1} . The differential cross sections are measured for each jet flavour with respect to the transverse energy of the leading photon in two photon pseudorapidity regions: $|\eta^\gamma| < 1.37$ and $1.56 < |\eta^\gamma| < 2.37$. The measurement covers photon transverse energies $25 < E_T^\gamma < 400 \text{ GeV}$ and $25 < E_T^\gamma < 350 \text{ GeV}$ respectively for the two $|\eta^\gamma|$ regions. For each jet flavour, the ratio of the cross sections in the two $|\eta^\gamma|$ regions is also measured. The measurement is corrected for detector effects and compared to leading-order and next-to-leading-order perturbative QCD calculations, based on various treatments and assumptions about the heavy-flavour content of the proton. Overall, the predictions agree well with the measurement, but some deviations are observed at high photon transverse energies. The total uncertainty in the measurement ranges between 13% and 66%, while the central $\gamma + b$ measurement exhibits the smallest uncertainty, ranging from 13% to 27%, which is comparable to the precision of the theoretical predictions.

© 2017 The Author. Published by Elsevier B.V. This is an open access article under the CC BY license (<http://creativecommons.org/licenses/by/4.0/>). Funded by SCOAP³.

1. Introduction

The production of isolated prompt photons in association with a jet containing a b - or c -hadron provides a testing ground for perturbative quantum chromodynamics (pQCD), the content of the proton and the treatment of heavy quarks in matrix element (ME) and parton shower (PS) computations. Prompt photons, which refer to those not arising from hadron decays, are targeted by requiring that their signals are isolated, i.e. well separated from other energetic signals. The most recent measurements of these final states were performed at the Tevatron proton–antiproton collider by the D0 [1,2] and CDF [3] collaborations. The Large Hadron Collider (LHC) produces proton–proton (pp) collisions at much higher centre-of-mass energies. Compared to the proton–antiproton collisions of the Tevatron, these collisions exhibit smaller contributions from t -channel quark–antiquark processes, allowing other processes sensitive to the heavy-quark content of the proton to play a more significant role.¹

Prompt photons (γ) can be used as a colourless non-hadronizing probe of parton dynamics that yields a clean experimental signature [4–16]. Processes containing final state b - or c -quarks play an important role in many LHC physics analyses and therefore the accuracy of the description of this heavy-flavour (HF) content of the proton must be investigated [17–21]. HF jets are defined as jets which contain either a b - or c -hadron.

At the LHC, prompt photons arise mainly through the Compton process, initiated by a quark (q) and a gluon (g), $qg \rightarrow q\gamma$. HF quarks arise in the proton through either extrinsic or intrinsic mechanisms. Extrinsic refers to HF quarks arising through perturbative mechanisms in the proton, while intrinsic refers to non-perturbative mechanisms. Presently, global parton distribution function (PDF) fits show that HF quarks in the proton are almost entirely extrinsic, however non-zero values of the intrinsic contribution have not been ruled out [22]. The photon transverse energy observable provides sensitivity to these effects, by taking advantage of its precise calibration while integrating over the less precise jet kinematic observables. The effect of intrinsic HF quarks in the PDF would be manifest at large Bjorken- x , which in the context of this measurement would give rise to larger cross-section values at large absolute photon pseudorapidities, $|\eta^\gamma|$, with high photon

^{*} E-mail address: atlas.publications@cern.ch.

¹ In the context of a photon + jet final state, s -channel quark–antiquark processes are suppressed due to the isolation requirement imposed on the photon.

transverse energy, E_T^γ .² Due to their smaller mass, c -quarks are more sensitive to these effects than b -quarks.

As the value of the mass of the b -quark, m_b , is much greater than the non-perturbative scale of QCD, it can be included explicitly in pQCD calculations. The calculations of the $\gamma + b$ cross sections can thus be done in two different schemes: the four-flavour scheme (4F) and the five-flavour scheme (5F) [23]. In the 4F scheme, the u -, d -, s - and c -quarks are treated as massless in the ME, while the b -quark is treated as massive. PDFs describing the proton with only the lightest four quarks are used in the calculations. Most of the b -quarks are dynamically generated in the matrix element through the splitting of a gluon. In the 5F scheme, the b -quark is also treated as massless and PDFs describing the proton with these five quarks are used in the calculations. The b -quark can thus be an initial-state quark in the matrix element. As such, the diagrams considered at a particular order in pQCD differ between the 4F and 5F schemes. In the 4F scheme, the mass of the b -quark gives rise to terms proportional to $\log(Q^2/m_b^2)$. At energies far above m_b , these logarithmic terms are large and spoil the convergence of the perturbative series. The 5F scheme avoids this issue since these logarithmic terms are resummed into the b -quark PDF. As such the 5F scheme is expected to give a better description of processes at energies far above m_b . In a calculation to all orders in pQCD, however, both schemes should yield the same result.

Theoretical predictions using leading-order (LO) and next-to-leading-order (NLO) pQCD matrix element calculations, interfaced to a PS, are computed using different PDF sets and compared to the measurement. In addition to the nominal sets with no intrinsic charm component in the 5F scheme, predictions are made using sets in the 4F scheme for $\gamma + b$ and sets that incorporate various degrees of intrinsic charm contribution for $\gamma + c$.

This Letter presents a fiducial differential measurement of the production cross section of a prompt isolated photon in association with a b -jet or a c -jet in pp collisions using the ATLAS detector. The transverse photon energy, E_T^γ , is required to satisfy $E_T^\gamma > 25$ GeV, the jet transverse momentum, p_T^{jet} , is required to satisfy $p_T^{\text{jet}} > 20$ GeV and the absolute pseudorapidity of the jet, $|\eta^{\text{jet}}|$, is required to satisfy $|\eta^{\text{jet}}| < 2.5$. In each bin of the measurement a background-enriched sideband technique is used to extract the prompt photon signal, while a template fit of a neural-network jet flavour-tagging discriminant is used to extract the HF signal. The measured signal is then corrected for detector effects, mapping it from the detector level to the particle level. The measurement is performed in bins of E_T^γ for two regions of $|\eta^\gamma|$: the central region with $|\eta^\gamma| < 1.37$ reaching up to 400 GeV in E_T^γ and the forward region with $1.56 < |\eta^\gamma| < 2.37$ reaching up to 350 GeV in E_T^γ . The ratios of the cross sections in the central to the forward regions are also presented for each flavour, as systematic and theoretical uncertainties that are correlated between the two regions then cancel out.

2. ATLAS detector

The ATLAS detector [24] is designed to measure the particles produced by the collisions provided by the LHC with almost complete solid angle coverage of the collision point. The inner de-

tector (ID), immersed in a 2 T axial magnetic field provided by an encompassing thin superconducting solenoid, is located nearest to the beam pipe and comprises a high-granularity pixel detector, a silicon microstrip tracker and a straw-tube transition radiation tracker. The ID provides tracking and vertexing information, which plays a crucial role in this measurement identifying photons and HF decay vertices associated with jets. Its acceptance, up to $|\eta| = 2.5$, imposes the upper bound on the $|\eta|$ acceptance of the analysis. The electromagnetic calorimeter (ECAL) surrounds the ID and is used to measure electromagnetic showers. Within the $|\eta|$ acceptance of this analysis, the ECAL is a high-granularity lead/liquid-argon sampling calorimeter using an accordion geometry that provides complete azimuthal coverage and comprises three radial layers augmented by a thin presampler. The presampler, which covers $|\eta| < 1.8$ and is located in front of the ECAL strips, is used to measure early electromagnetic showers. The innermost ECAL layer is the thinnest and uses highly segmented strips in η , which help to characterize shower shapes. The second layer is the thickest with a coarser granularity and collects most of the photon energy. The third layer is the least granular and is used to correct high-energy signals for leakage. Between the ECAL barrel and endcap detectors there is a transition region, located at $1.37 < |\eta| < 1.56$, where the photon reconstruction and identification are poorer. The hadronic calorimeter (HCAL) encloses the ECAL and is used to measure hadronic showers. The HCAL consists of a steel/plastic-scintillator sampling calorimeter for $|\eta| < 1.7$ and a copper/liquid-argon sampling calorimeter for $1.5 < |\eta| < 3.2$. Surrounding the HCAL is the muon spectrometer, equipped with large superconducting air-core toroidal magnets and comprising separate sets of detectors for triggering and for precision muon track reconstruction. A three-level trigger system is used to select photon signals. The first-level trigger is a coarse-granularity hardware-based trigger that limits the event rate to 75 kHz. The second- and third-level triggers are software-based and make use of the full detector granularity, reducing the event rate to about 400 Hz.

3. Monte Carlo simulations and theoretical predictions

The SHERPA 1.4.5 [25] and PYTHIA 8.160 [26] Monte Carlo (MC) event generators are used to simulate signal events of prompt photons accompanied by jets at LO in pQCD. The cross sections predicted by both these MC generators are compared to the measured values. SHERPA is also used to derive correction factors used in the data analysis while PYTHIA is used to assess some modelling uncertainties.

SHERPA is used in the ME + PS prescription [27] to generate events containing a photon and a parton, with up to three additional partons. All photon emissions are effectively simulated by the combination of the tree-level matrix elements including additional partons and the parton shower [28]. Collinear divergences from the photon are regularized by requiring a minimum angular separation of $\Delta R = \sqrt{(\Delta\eta)^2 + (\Delta\phi)^2} = 0.3$ between the photon and any parton. PYTHIA is used to generate $2 \rightarrow 2$ events containing either a photon and a parton or two partons, where photons in the latter case are produced in the initial- and final-state radiation. The non-perturbative QCD models used for the parton shower, the hadronization and the hadron decays are different between SHERPA [29,30] and PYTHIA [31,32]. Both generators also include the effects of the underlying event. For the event generation with SHERPA, the five-flavour CT10 PDF set [33] is used in conjunction with dedicated parton shower tuning developed by the SHERPA authors. For the event generation with PYTHIA, the five-flavour LO CTEQ6L1 PDF set [34] is used with the AU2 set of tuned MC parameters [35]. In the calculation of the matrix element, SHERPA uses massive quarks, thus its calculations are in a massive 5F

² ATLAS uses a right-handed coordinate system with its origin at the nominal interaction point (IP) in the centre of the detector and the z -axis along the beam pipe. The x -axis points from the IP to the centre of the LHC ring and the y -axis points upward. Cylindrical coordinates (r, ϕ) are used in the transverse plane, ϕ being the azimuthal angle around the z -axis. The pseudorapidity is defined in terms of the polar angle θ as $\eta = -\ln \tan(\theta/2)$. The rapidity is defined as $y = (1/2) \cdot \ln((E + p_z)/(E - p_z))$.

scheme, while PYTHIA uses massless quarks, thus its calculations are in a standard 5F scheme. Both generators use massive b - and c -quarks in the parton showers. A GEANT4 simulation [36] of the ATLAS detector [37] is used to simulate the interactions between the particles and the detector. During the simulation, the signal events are overlaid with multiple pp collisions generated with the soft QCD processes of PYTHIA using the A2 set of tuned MC parameters [35] and the MSTW2008LO PDF set [38]. The resulting events are scaled to the integrated luminosity measured in the data. They are also weighted to reproduce the observed distribution in data of the number of reconstructed primary vertices and the size of the luminous region along the beam axis.

In addition, NLO pQCD particle-level predictions calculated using MADGRAPH5_aMC@NLO 2.3.3 [39] in the 5F scheme, interfaced to PYTHIA 8.212 [40] in the NLO + PS prescription, are used to interpret the measurement. For the $\gamma + b$ cross section, the 4F scheme is also considered. In the 5F scheme, events containing a photon and a jet are generated. After hadronization, only events with a jet containing a HF hadron are considered. In the 4F scheme, b -quarks are pair-produced from a gluon, hence events containing a photon and two b -quarks are generated. In contrast to the 5F scheme, all generated events are considered as they all contain at least one b -quark at parton level. In both schemes, the photon collinear divergences are regularized in the matrix element by requiring the photons to pass a Frixione isolation cut [41]: $E_T^{\text{iso}}(\delta) < \epsilon E_T^\gamma ((1 - \cos \delta)/(1 - \cos \delta_0))^n$ with parameters $\delta_0 = 0.4$, $n = 1$ and $\epsilon = 1$, where $E_T^{\text{iso}}(\delta)$ is the sum of the transverse energies of the particles around the photon up to an angular separation of δ in the η - ϕ space. The renormalization and factorization scales, μ_R and μ_F respectively, are chosen to be equal to the transverse mass of the clustered jets, obtained after all final-state particles from the matrix element are k_t -clustered [42] into jets. This choice follows the recommendations in Ref. [39] when interfacing the MADGRAPH5_aMC@NLO calculations to PYTHIA. The $\gamma + b$ predictions use the NNPDF3.0nlo³ 4F and 5F PDF sets [43], while the $\gamma + c$ predictions use NNPDF3.1nlo [44] and CT14nnlo [45]. The NNPDF3.1nlo sets include a set with a charm contribution fitted to data in the global PDF fit, equivalent to intrinsic charm contributing 0.26% of the proton momentum, and another with only perturbative charm. CT14nnlo provides two sets using the BHPS model [46] that include intrinsic charm contributions [47]: one with 0.6% of the proton momentum assigned to intrinsic charm, BHPS1, and one with 2.1%, BHPS2. The PDF sets include the running of the strong coupling constant, using a value at the energy scale of the mass of the Z boson of $\alpha_s(M_Z) = 0.118$. This treatment of α_s is used in both the PDFs and the matrix elements. The electromagnetic coupling constant is set to $\alpha = 1/137$ and its running is not included in the calculations [48].

Three types of uncertainties are considered in the NLO predictions. The scale uncertainty is assessed by multiplying or dividing by a factor of two μ_R and μ_F , separately and simultaneously. The envelope of the deviations from the nominal prediction is taken as the uncertainty. The uncertainty in the PDF sets is propagated to the cross sections using the prescribed eigenvector reduction approach for the CT14nnlo sets, which gives an uncertainty at the 90% confidence level. For the NNPDF3.0nlo and NNPDF3.1nlo PDF sets, the PDF uncertainty is assessed through the use of PDF replicas. The uncertainty due to the α_s value used in the predictions is assessed by varying up or down its value at the energy scale of the mass of the Z boson by 0.002 simultaneously in the matrix el-

ement and the PDF sets, resulting in an uncertainty in the cross sections at the 90% confidence level. In all cases, the uncertainties are reported at the 68% confidence level in the comparisons to data. The total theoretical uncertainty in the NLO predictions is the sum in quadrature of these three uncertainties. The scale uncertainty dominates the total uncertainty in the cross sections. The total uncertainty decreases with E_T^γ for the $\gamma + b$ and $\gamma + c$ cross sections, from around 25% to around 15% in the measured range. These uncertainties are also evaluated for the ratio of the cross section in the central photon pseudorapidity region to that in the forward region by separately propagating each uncertainty variation to the ratio, assuming full correlations between the two regions. The uncertainties are then assessed in a similar way as those in the cross sections. The total uncertainty in the cross-section ratios is nearly constant with E_T^γ and is about 5%. The scale uncertainty dominates the total uncertainty in the cross-section ratios, except in the case of the predictions using the fitted charm PDF set from NNPDF3.1nlo, for which the PDF uncertainty dominates. The total uncertainty in the cross-section ratios using this fitted charm PDF increases with E_T^γ , from about 5% at 25 GeV to about 15% at 350 GeV. No uncertainties are assessed for the LO predictions as the scale uncertainties are expected to be large and unreliable.

4. Event selection and calibration

This measurement makes use of the full dataset of pp collisions at a centre-of-mass energy of 8 TeV, recorded by the ATLAS detector in 2012. Only events taken during stable beam conditions when the ATLAS detector operation satisfied data-quality conditions are considered. Single-photon triggers with E_T^γ thresholds of 20, 40, 60, 80, 100 and 120 GeV, which have efficiencies measured to be greater than 99% with respect to the offline selection requirements, were used to record events. Below 125 GeV, each bin of the measurement is populated by a single trigger, while the remaining bins are all populated by the highest threshold trigger. Due to their higher rates and considering the available bandwidth, all but the 120 GeV trigger were prescaled, such that only some of the events satisfying the trigger requirement were recorded. Events recorded by a prescaled trigger are weighted by the ratio of the unrescaled recorded luminosity to the recorded luminosity of the respective trigger. The integrated luminosity of the data ranges from $4.58 \pm 0.09 \text{ pb}^{-1}$ for the 20 GeV trigger to $20.2 \pm 0.4 \text{ fb}^{-1}$ for the unrescaled 120 GeV trigger [49].

Events are required to have a hard reconstructed primary vertex consistent with the nominal interaction point and at least two associated tracks with transverse momentum, p_T , greater than 400 MeV. In events where more than a single vertex satisfies these criteria, the vertex with the highest $\sum p_T^2$ of associated tracks is considered as the hard vertex. The dataset exhibits an average of 19 pp interactions per bunch crossing, where the interactions not associated to the hard vertex are referred to as *pile-up*, an effect that is taken into account in the reconstruction. Effects related to events containing more than one hard vertex are estimated to be negligible, below the percent level, and are not considered.

Detector-level photon candidates are built from ECAL cell clusters with transverse energies greater than 2.5 GeV. They fall into two categories: unconverted and converted photons. Unconverted photons have no tracks associated with the cluster. Converted photons have associated tracks that are consistent with the signature of a photon interacting upstream. The overall photon reconstruction efficiency is 96% for prompt photons with $E_T^\gamma > 25 \text{ GeV}$ [50]. Converted and unconverted photons are calibrated separately, making use of both the calorimeter and the tracking information to correct the calorimeter response for upstream energy losses and leakage [51]. In the simulation, only detector-level photons that

³ NNPDF3.1nlo PDF sets with a 4F description of the proton were not available when this analysis was conducted. The PDF sets with a 5F description of the proton were found to produce consistent results between NNPDF3.0nlo and NNPDF3.1nlo.

match a particle-level prompt photon using a cone of $\Delta R = 0.2$ are considered. Detector-level photon candidates are subject to a two-stage shower-shape-based identification criterion. The first stage scrutinizes the leakage into the hadronic calorimeter, the lateral size and shape of the cluster in the second ECAL layer and the shower width in the first ECAL strip layer [50]. The second stage imposes additional criteria that are sensitive to the lateral shape of the shower in the ECAL strip layers, providing discrimination against neutral hadron decays into pairs of photons. This stage can be inverted to populate background enriched sideband regions. These two stages, which together are referred to as the *tight* criteria, are used in previous ATLAS prompt-photon analyses [4–11]. In the simulation, the distributions of the shower-shape variables used for photon identification are corrected to reproduce those observed in the data. Further, event weights are applied to simulated events whose leading photon satisfies the tight selection criteria such that the identification efficiency matches that of the data for both the converted and unconverted photons. These event weights are typically within 3% of unity.

Both the detector-level and particle-level photon candidates are required to exhibit an isolated signal, a requirement that targets prompt-photon production and discriminates against jets misidentified as photons. This criterion is imposed through the definition of the calorimeter isolation variable E_T^{iso} . This variable is defined at the detector level as the sum of the transverse energies recorded in clusters within a distance of $\Delta R = 0.4$ around the photon, excluding the contributions in a fixed-size window centred on the photon candidate of size 0.125×0.1715 in $\Delta\eta \times \Delta\phi$. The variable is then corrected for contributions from the pile-up and the underlying-event [7]. In the simulations, corrections are also applied to account for mismodelling of the mean and the spread of the detector-level E_T^{iso} distribution. These corrections are derived by matching the simulated E_T^{iso} distribution to the signal photon E_T^{iso} distribution extracted from data using a data-driven template fit. In the simulation, the particle-level E_T^{iso} is calculated by adding the transverse energy of all particles with a lifetime greater than 10 ps within a distance of $\Delta R = 0.4$ around the photon. Muons and neutrinos, however, are excluded since they deposit little or no energy in the calorimeter. The E_T^{iso} is then corrected for the energy density of the underlying event [52]. A sliding E_T^{iso} requirement is used to impose the isolation criterion at both the detector level and the particle level: $E_T^{\text{iso}} < 4.8 \text{ GeV} + 0.0042 \times E_T^\gamma$. The E_T^γ dependent nature of the requirement improves the acceptance of high- E_T^γ signal photons, yielding a roughly constant 92% signal efficiency. The efficiency for isolated detector-level unconverted (converted) photons in the data to satisfy the tight criteria is approximately 75% (75%) for an E_T^γ of 25 GeV and 95% (98%) for 400 GeV [50]. The E_T^{iso} requirement is inverted with a 2 GeV gap, $E_T^{\text{iso}} > (4.8 + 2) \text{ GeV} + 0.0042 \times E_T^\gamma$, to populate regions used for the photon background sideband subtraction. The 2 GeV gap is used to reduce the amount of signal in the sideband regions.

Detector-level jets are built using the anti- k_t algorithm [53], implemented in the FastJet package [54], taking as input calibrated topological clusters [55] in the calorimeter and a parameter of $R = 0.4$. The jets undergo a five-stage sequential calibration [56]. This calibration includes corrections based on the cluster shape and location, the jet area and pile-up [52], the response of simulated particle-level jets, the combined shower-structure and tracking information and finally the data-driven γ + jet, Z + jet and multijet p_T -balance of the energy scale [57]. Detector-level jets are required to satisfy quality criteria that ensure they are not affected by, or are the result of, detector defects and noise, cosmic rays or non-collision beam-related backgrounds [57,58]. To reduce the impact of jets coming from pile-up interactions, detector-level

jets with $p_T^{\text{jet}} < 50 \text{ GeV}$ and $|\eta^{\text{jet}}| < 2.4$ are also required to have at least 50% of the momentum of associated tracks to originate from the hard vertex [59]. Simulated particle-level jets used in the analysis are built using the anti- k_t algorithm taking as input all particles with a lifetime greater than 10 ps and a radius parameter of $R = 0.4$.

Simulated particle-level and detector-level jets are assigned a flavour based on the following hadron matching scheme. If a b -hadron with $p_T > 5 \text{ GeV}$ is found within $\Delta R = 0.3$ of a jet then it is considered to be a b -jet. If a jet that is not a b -jet is found to have a c -hadron with $p_T > 5 \text{ GeV}$ within $\Delta R = 0.3$ then it is considered to be a c -jet. If a jet that is not a b - or a c -jet is found to have a τ -lepton with $p_T > 5 \text{ GeV}$ within $\Delta R = 0.3$ then it is considered to be a τ -jet. If a jet is found to be neither a b -jet, a c -jet nor a τ -jet it is considered to be a light jet. The contribution of τ -jets in the measurement is negligible.

At the detector level, only the highest- E_T (leading) photon that satisfies the first stage of the photon identification criteria is considered. The photon candidate is then required to have $E_T^\gamma > 25 \text{ GeV}$ and $|\eta^\gamma| < 2.37$, excluding the transition region between the barrel and endcap ECAL modules $1.37 < |\eta^\gamma| < 1.56$. The photon candidate must then satisfy the second stage of the identification criteria. If it fails, it is instead used to populate regions used for the photon background sideband subtraction. The photon candidate must then satisfy the E_T^{iso} criterion. If it fails, but satisfies the inverted E_T^{iso} criterion, it is instead used to populate regions used for the photon background sideband subtraction. Next, only the leading jet with $\Delta R > 0.4$ from the photon candidate is considered. This jet is required to have $p_T^{\text{jet}} > 20 \text{ GeV}$, $|\eta^{\text{jet}}| < 2.5$ and to be separated from the photon candidate by $\Delta R > 1$. This last angular separation requirement ensures that the measured signals of the leading jet and the leading photon do not overlap.

At the particle level, only the leading photon is considered. The fiducial requirements imposed at particle level are similar to those used at the detector level, but using the jet rapidity instead of its pseudorapidity, and are summarized in Table 1.

Detector-level jets are assigned a b -tagging discriminant value by the MV1c algorithm. The MV1c algorithm is a neural network that takes as input the discriminants of three tagging algorithms, analogous to the MV1 algorithm [60], but is trained to identify b -jets with enhanced rejection of c -jets. The three tagging algorithms input to the MV1c tagger are based on different aspects of jet tracking information that are sensitive to the presence of secondary vertices originating from HF decays: the IP3D algorithm is sensitive to the displacement of the tracks associated to the jet from the primary vertex, the SV1 algorithm reconstructs secondary vertices and the JetFitter algorithm is sensitive to secondary and tertiary vertices that are kinematically consistent with the decay chain of a b - or c -hadron. The MV1c tagger discriminant distribution is divided into five bins delimited by four cuts corresponding to the b -jet identification efficiencies in simulated top quark pair ($t\bar{t}$) events of 80%, 70%, 60% and 50%, and bounded by the trivial 100% and 0% cut values. The discriminant distribution in the simulation is calibrated using event weights according to the jet flavour and kinematics, such that the overall efficiency of each cut value in the simulation matches that of the data. This calibration considers the correlations between the discriminant bins and has been used in a prior ATLAS measurement [61]. The efficiency of these cuts in simulated events satisfying the γ + jet selection used for this measurement is typically 2–5% lower than that measured in the $t\bar{t}$ calibration analysis. For the event weights, since they are ratios, this difference is mostly cancelled. No statistically significant difference is expected between the event weights in γ + jet and in $t\bar{t}$. These event weights deviate from unity by up to 30%.

Table 1

Particle-level requirements defining the fiducial region. The determination of the jet flavour and the calculation of E_T^{iso} are described in the text.

| Particle-level selection | Leading γ | Leading jet with $\Delta R^{\gamma\text{-jet}} > 0.4$ |
|--------------------------|---|---|
| Transverse momentum | $E_T^\gamma > 25 \text{ GeV}$ | $p_T^{\text{jet}} > 20 \text{ GeV}$ |
| Rapidity | $ \eta^\gamma < 1.37 \text{ or } 1.56 < \eta^\gamma < 2.37$ | $ y^{\text{jet}} < 2.5$ |
| Isolation | $E_T^{\text{iso}} < 4.8 \text{ GeV} + 0.0042 \times E_T^\gamma$ | — |
| Angular separation | $\sqrt{(\Delta\eta)^2 + (\Delta\phi)^2} > 1$ | |

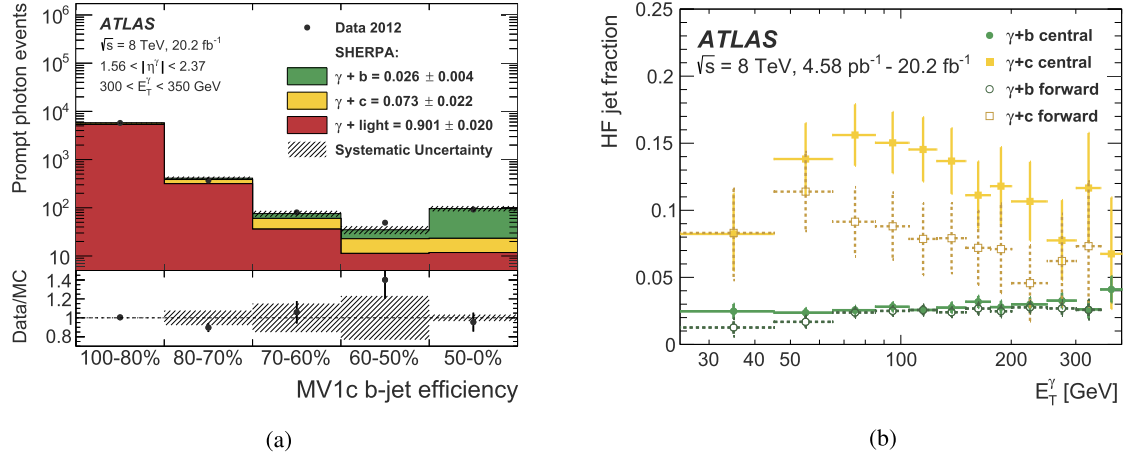


Fig. 1. (a) Example of a template fit to the MV1c tagger discriminant distribution used to measure the $\gamma + b$ and $\gamma + c$ fractions. The data yield is shown after subtraction of background photons. The error bars on the data correspond to the statistical uncertainty. The systematic uncertainty band takes into account the uncertainty correlations between the data and the MC templates. The numbers in the legend are the fractions of each template after the fit and their statistical uncertainties. (b) The heavy-flavour jet fractions obtained from the template fits as a function of the photon transverse energy, E_T^γ . The fractions are relative to the yield of selected $\gamma + \text{jet}$ data events after subtraction of background photons. The error bars correspond to the total uncertainty, including the statistical uncertainty and the complete set of systematic uncertainties. The central and forward regions are defined respectively as $|\eta^\gamma| < 1.37$ and $1.56 < |\eta^\gamma| < 2.37$. (For interpretation of the references to color in this figure legend, the reader is referred to the web version of this article.)

Separate b -, c - and light-jet calibrations are used to correct the efficiency of the discriminant cuts to better match the data. The b -jet calibration [62] uses an unbinned maximum-likelihood fit of simulated templates to extract the b -jet tagging efficiency distribution in data using a $t\bar{t}$ selection, which has a high b -jet purity. The fit considers the individual probability for each jet in a given event to be tagged, thereby exploiting per-event jet-flavour correlations. The c -jet calibration [63] uses a sample of reconstructed $D^{\pm\pm}$ mesons to extract the c -jet tagging efficiency by fitting simultaneously the $D^{\pm\pm}$ yield with and without applying a cut on the MV1c discriminant. As b -hadrons can also produce $D^{\pm\pm}$, a fit of the D^0 pseudo-proper lifetime is used to subtract the b -jet background. The inclusive c -jet tagging efficiency is then derived using existing dedicated decay measurements [64] and simulations based on EvtGEN [65] to extrapolate it from the measured $D^{\pm\pm}$ c -jet efficiency. Light jets can be tagged as b -jets mainly due to the finite tracking resolution. The light-jet calibration [63] involves inverting the sign of some of the criteria imposed on the impact parameter and the decay-length significance in the MV1c algorithm. The resulting discriminant distribution for all flavours is similar to that of the nominal MV1c discriminant distribution for light jets. Consequently, the jet tagging efficiency obtained using this method is taken as the light-jet tagging efficiency after correcting it for the effects of HF jets, long-lived particles and material interactions.

5. Signal extraction

A data-driven two-dimensional sideband technique [4,6–10] is applied to estimate and subtract photon background contamination from the data yield in each MV1c tagger discriminant bin, in every bin of the measurement. By this means, any correlation between jets misidentified as photons and the flavour of the accompanying

jet is taken into account. The technique relies on the use of three background-dominated control regions: two of them created by individually inverting separate aspects of the signal photon selection criteria and a third region created by inverting these two aspects simultaneously. The first aspect is the inversion of the second stage of the photon identification criteria based on shower shapes. The second aspect is the inversion of the E_T^{iso} selection requirement. Both of these aspects provide discrimination against jets faking photons and photons arising from hadron decays. The three background regions in the data are then used to estimate the prompt photon yield in the signal region, taking into account the estimated leakage of signal into these regions using the simulations. The procedure hinges on the assumption that the two inverted aspects of the selection criteria are uncorrelated for background events. Deviations from this assumption are small and are taken into account as an uncertainty. The photon purity, i.e. the fraction of signal photons, is typically 55% in the lowest bin of E_T^γ , rising steadily to greater than 95% around 400 GeV. The largest correlation between the photon purity and the MV1c discriminant is observed in the 25–45 GeV bin of E_T^γ in the central region where the photon purity exhibits a relative increase of roughly 15% from the 100–80% MV1c b -jet efficiency bin to the 50–0% bin.

Following the photon background subtraction, the MV1c tagger distribution of the signal photon yield is used to extract the b -jet and c -jet fractions in each bin of the measurement. Simulated discriminant shapes for b -jets, c -jets and light jets, which are corrected using factors derived from the aforementioned tagging calibration analyses, are used to perform a template fit. The shape uncertainty in the simulated templates is derived from the uncertainties in the tagging calibration, taking into account correlations between the discriminant bins. The template fit is performed as a binned maximum-likelihood fit. Fig. 1(a) shows the template fit for

the 300–350 GeV bin of E_T^γ in the forward region, which is particularly sensitive to intrinsic charm. The quality of this fit is similar to that of the others. The general features are that light jets populate the high b -jet efficiency side of the discriminant, b -jets populate the low b -jet efficiency side and c -jets lie between the two. Since the jet-flavour fractions are measured simultaneously, they are correlated in each bin of the measurement. Fig. 1(b) shows the measured b - and c -jet fractions for central and forward photons. The fraction of c -jets displays a maximum between 50 and 80 GeV while that of b -jets displays a slight monotonic increase. These features are predicted in the particle-level simulations.

6. Cross-section measurement procedure

The following equation outlines the procedure, making use of the SHERPA simulation, used to compute the cross section from the data yield:

$$\left(\frac{d\sigma^{\gamma+\text{HF-jet}}}{dE_T^\gamma} \right)_i = \frac{1}{(\Delta E_T^\gamma)_i} \frac{1}{(\mathcal{L}_{\text{int}}^{\text{trig}})_i} \frac{1}{\epsilon_i^{\text{trig}}} C_i f_i^{\text{HF-jet}} \sum_{j \in \text{MV1c}} p_{ij}^\gamma N_{ij}^{\text{Data}}.$$

The left side of this equation is the measured cross section corrected back to the particle level in bin i of E_T^γ , $(\Delta E_T^\gamma)_i$ is the bin width, $(\mathcal{L}_{\text{int}}^{\text{trig}})_i$ is the integrated luminosity of the trigger, ϵ_i^{trig} is the trigger efficiency, C_i is the particle-level correction factor, $f_i^{\text{HF-jet}}$ is the measured HF-jet fraction, p_{ij}^γ is the measured signal-photon purity in a tagger discriminant bin j and N_{ij}^{Data} is the yield of selected γ + jet data events. The particle-level correction factor accounts for detector effects, including the detector resolution and the signal reconstruction efficiency, using the one-dimensional bin-by-bin approach, yielding a measurement that is directly comparable to other experimental results and theoretical predictions. The bin-by-bin approach, used in previous ATLAS photon results [4,6–10], uses factors defined as the ratio of the particle-level to the detector-level E_T^γ distributions derived using the simulation for each bin of the measurement:

$$C_i = \frac{N_i^{\text{particle}, \gamma+\text{HF-jet}}}{N_i^{\text{detector}, \gamma+\text{HF-jet}}}.$$

The accuracy of this approach relies on the detector-level bin-migration effects being well described by the simulation since correlations between adjacent bins are neglected. As the cross sections are measured differentially with respect to E_T^γ , this condition is met since the E_T^γ resolution is much smaller than the bin width. In the central region, migrations are less than 5%, while in the forward region they are less than 10%. The values of the correction factors decrease with E_T^γ , driven by the improving photon identification efficiency, from typically 1.9 (1.7) at 25 GeV to 1.2 (1.2) at 400 GeV for $\gamma + b$ ($\gamma + c$) events. They do not have a strong dependence on $|\eta^\gamma|$.

7. Measurement uncertainties

Uncertainties affecting the measurement which originate from the finite numbers of data and MC events are considered together with systematic uncertainties related to the detector calibration and analysis techniques. The bootstrap resampling technique [66] is used to assess the statistical uncertainties by creating an ensemble of statistically equivalent measurements using event weights, randomly chosen for each event from a Poisson distribution with a mean of one, applied to either the data or MC events. The 68% confidence interval of the distribution of these measurements is

taken as the statistical uncertainty. The systematic uncertainties are derived by varying a parameter in the simulated events, repeating the complete analysis with this varied parameter and taking the difference between the new measured value and the nominal measurement as the uncertainty. The bootstrap resampling technique is then used to evaluate the statistical uncertainty in each systematic variation. Variations that are not statistically significant undergo a bin-merging procedure over an increasing number of E_T^γ bins to improve their significance. Following this procedure, only statistically significant variations are considered as systematic uncertainties. This procedure, however, gives rise to an interplay between the MC statistical uncertainty and the systematic uncertainties.

Sources related to the detector calibration include the photon energy scale and resolution [51], the photon identification efficiency [50], the jet energy scale and resolution [57], the inefficiency of the pile-up jet removal cut [59] and the MV1c tagger discriminant for the three jet flavours [62,63]. The energy scale and resolution of the photon and the jet have several uncertainty components that encompass both the imperfect knowledge of the detector response and the analysis techniques used to derive the calibration. The calibration is varied according to its uncertainties to assess the impact on the measurement. The calibrations of the photon identification efficiency and of the MV1c tagger discriminant have uncertainties related to the analysis techniques in which they were derived. For the case of the MV1c discriminant, the uncertainties are mostly related to the modelling of the track multiplicity and the misidentification of the hadron flavours. These factors are varied according to their uncertainties. However, some of their uncertainty components, such as those of the jet energy scale and resolution, are correlated with those of this measurement. As such, these components are varied coherently both in the discriminant calibration and in this analysis. To assess the uncertainty due to the pile-up jet removal cut, the 50% requirement on track momentum from the hard vertex is varied to 53% and 47%. The magnitude of the variation is motivated by the cut efficiency difference between the data and the simulation.

The uncertainties related to the analysis techniques are similar to those in the ATLAS inclusive photon and $\gamma + \text{jet}$ analyses at 8 TeV [8,9]. Specifically, the assumption that the photon background regions are uncorrelated in the two-dimensional sideband method is assessed by varying the correlation by 10%. The magnitude of this variation corresponds to the size of the measured correlation in control regions of the data. The two definitions of the background regions in the sideband method are varied as follows. The photon identification reversal is varied by adding, or by removing, an identification criterion based on the first layer of the calorimeter. The inverted photon isolation energy cut is increased and decreased by 2 GeV, motivated by the difference seen in the isolation energy resolution between data and the simulations. An uncertainty related to the photon isolation energy corrections is obtained by varying them according to the differences seen between SHERPA and PYTHIA. A prompt-photon modelling uncertainty is assessed by varying the relative fraction of hard-scatter photons and radiated photons generated in PYTHIA. Similarly, the change in the measurement when using simulated samples from PYTHIA instead of SHERPA is taken as an uncertainty, assessing the differences between the non-perturbative QCD models used by the generators. Possible migration effects in the bin-by-bin particle-level correction factors are also taken as an uncertainty.

The uncertainties in the cross-section ratios are obtained by propagating the individual systematic variations of the central and forward cross sections to the ratio and taking the resulting variations as the uncertainties. As most systematic uncertainties are positively correlated between these two pseudorapidity regions,

Table 2

Range of the size of the relative uncertainties in the measured cross sections along E_T^γ for the different uncertainty sources. The central region refers to the cross sections in the range $|\eta^\gamma| < 1.37$, the forward region refers to the cross sections in the range $1.56 < |\eta^\gamma| < 2.37$ and the ratio refers to the ratio of the cross section in the central region to that in the forward region. The systematic variations must be statistically significant to be considered as systematic uncertainties. Uncertainties with values listed as < 0.1 are not statistically significant.

| Uncertainty source | Uncertainty [%] | | | | | |
|----------------------------------|-----------------|---------|---------|--------------|---------|---------|
| | $\gamma + b$ | | | $\gamma + c$ | | |
| | Central | Forward | Ratio | Central | Forward | Ratio |
| MC statistical uncertainty | 1.9–6.4 | 3.1–14 | 3.6–17 | 2.5–24 | 6.0–33 | 6.1–39 |
| Photon energy scale | 0.2–2.5 | 0.7–5.3 | 0.9–1.9 | 0.2–1.0 | 0.0–0.2 | 0.5 |
| Photon identification efficiency | 0.2–1.2 | 0.4–1.8 | 0.1–0.5 | 0.2–1.3 | 0.4–1.7 | 0.1–0.5 |
| Jet energy scale | 0.6–4.8 | 0.7–4.6 | 0.1–0.2 | 0.2–2.3 | 0.2–2.8 | 0.1–0.5 |
| Jet energy resolution | 0.0–2.4 | 0.0–1.0 | 0.0–0.1 | 0.0–16 | 0.2–5.7 | 0.4–2.5 |
| b -jet tagging efficiency | 2.4–17 | 2.5–15 | 0.1–0.6 | 0.4–12 | 0.5–8.3 | 0.2–2.3 |
| c -jet tagging efficiency | 5.7–18 | 5.3–11 | 2.3–6.9 | 6.0–18 | 6.4–18 | 0.4–2.7 |
| Light-jet tagging efficiency | 4.9–15 | 6.1–31 | 1.6–8.3 | 12–46 | 21–57 | 8.4–28 |
| Sideband definition | 0.2–3.0 | 0.2–2.9 | 0.1–0.8 | 0.2–3.4 | 0.2–1.2 | 0.1–0.6 |
| Sideband correlation | 0.2–4.5 | 0.4–13 | 0.2–10 | 0.2–4.2 | 0.5–5.2 | 0.3–1.2 |
| Prompt-photon modelling | 2.2–2.5 | 2.4 | 4.2–6.7 | 1.5–2.8 | < 0.1 | < 0.1 |
| Non-perturbative QCD models | 2.3 | 7.3 | 11 | < 0.1 | < 0.1 | < 0.1 |
| Particle-level migration effects | 0.8–2.9 | 0.4 | 1.2–4.3 | 0.9–3.1 | < 0.1 | 0.6–3.0 |
| Luminosity | 1.9 | 1.9 | 0 | 1.9 | 1.9 | 0 |
| Total systematic uncertainty | 12–25 | 13–38 | 14–22 | 15–56 | 25–61 | 11–48 |
| Data statistical uncertainty | 1.5–13 | 2.1–37 | 2.5–58 | 1.1–27 | 2.9–33 | 3.2–47 |
| Total uncertainty | 13–27 | 14–54 | 14–62 | 15–62 | 26–66 | 14–66 |

Table 3

Measured values for the $\gamma + b$ and $\gamma + c$ differential cross sections, and their ratios, in the central and forward regions defined respectively as $|\eta^\gamma| < 1.37$ and $1.56 < |\eta^\gamma| < 2.37$. They are accompanied by their total measurement uncertainties.

| E_T^γ bin [GeV] | 25–45 | 45–65 | 65–85 | 85–105 | 105–125 | 125–150 | 150–175 | 175–200 | 200–250 | 250–300 | 300–350 | 350–400 |
|---|---------------------|----------------------|------------------------|------------------------|------------------------|------------------------|------------------------|----------------------|---------------------|---------------------|---------------------|---------------------|
| $\frac{d\sigma}{dE_T^\gamma}$ [pb/GeV] | $\times 10^0$ | $\times 10^0$ | $\times 10^{-1}$ | $\times 10^{-1}$ | $\times 10^{-2}$ | $\times 10^{-2}$ | $\times 10^{-2}$ | $\times 10^{-3}$ | $\times 10^{-3}$ | $\times 10^{-4}$ | $\times 10^{-4}$ | $\times 10^{-4}$ |
| $\gamma + b$ central | 32^{+7}_{-7} | $4.6^{+0.7}_{-0.7}$ | $11.5^{+1.5}_{-1.5}$ | $4.0^{+0.5}_{-0.5}$ | $14.7^{+2.2}_{-2.2}$ | $6.8^{+1.0}_{-1.0}$ | $3.5^{+0.5}_{-0.5}$ | $14.9^{+2.6}_{-2.7}$ | $6.8^{+1.2}_{-1.2}$ | 26^{+5}_{-5} | $8.3^{+2.1}_{-2.2}$ | $6.0^{+1.5}_{-1.4}$ |
| $\gamma + b$ forward | 9^{+5}_{-5} | $1.7^{+0.5}_{-0.4}$ | $5.5^{+0.9}_{-0.9}$ | $1.86^{+0.27}_{-0.27}$ | $7.4^{+1.1}_{-1.1}$ | $2.9^{+0.4}_{-0.4}$ | $1.38^{+0.22}_{-0.23}$ | $5.9^{+1.0}_{-1.0}$ | $2.5^{+0.4}_{-0.4}$ | $6.9^{+1.5}_{-1.4}$ | $2.1^{+0.6}_{-0.6}$ | – |
| $\gamma + c$ central | 92^{+35}_{-31} | 24^{+5}_{-5} | 65^{+10}_{-10} | $20.4^{+3.2}_{-3.1}$ | 80^{+13}_{-13} | 32^{+6}_{-6} | $11.8^{+2.7}_{-2.6}$ | 61^{+15}_{-15} | 23^{+6}_{-6} | 59^{+23}_{-23} | 36^{+13}_{-13} | 9^{+6}_{-6} |
| $\gamma + c$ forward | 49^{+20}_{-21} | $10.1^{+2.7}_{-2.6}$ | 19^{+6}_{-6} | $6.2^{+1.8}_{-1.8}$ | 22^{+7}_{-7} | $9.3^{+3.1}_{-3.1}$ | $3.5^{+1.3}_{-1.3}$ | 16^{+8}_{-8} | $3.9^{+2.4}_{-2.4}$ | 15^{+9}_{-8} | 6^{+4}_{-4} | – |
| $\sigma_{\text{central}}^{\gamma+b}/\sigma_{\text{forward}}^{\gamma+b}$ | $3.8^{+2.3}_{-1.3}$ | $2.7^{+0.7}_{-0.6}$ | $2.09^{+0.34}_{-0.33}$ | $2.17^{+0.35}_{-0.34}$ | $1.99^{+0.32}_{-0.31}$ | $2.31^{+0.33}_{-0.33}$ | $2.5^{+0.4}_{-0.4}$ | $2.6^{+0.4}_{-0.4}$ | $2.7^{+0.4}_{-0.4}$ | $3.7^{+0.7}_{-0.7}$ | $3.9^{+1.2}_{-1.0}$ | – |
| $\sigma_{\text{central}}^{\gamma+c}/\sigma_{\text{forward}}^{\gamma+c}$ | $1.9^{+0.9}_{-0.5}$ | $2.4^{+0.5}_{-0.4}$ | $3.3^{+0.5}_{-0.5}$ | $3.3^{+0.7}_{-0.5}$ | $3.7^{+0.9}_{-0.7}$ | $3.5^{+0.8}_{-0.5}$ | $3.4^{+0.9}_{-0.6}$ | $3.7^{+1.4}_{-1.0}$ | $5.9^{+2.2}_{-1.5}$ | $3.8^{+1.7}_{-1.2}$ | 6^{+4}_{-3} | – |

their effect on the ratios is smaller than on the cross sections. However, some components of the photon energy scale and of the light-jet tagging efficiency uncertainties are uncorrelated between the two regions. As the two regions considered are exclusive in $|\eta^\gamma|$, the data and MC statistical uncertainties in the ratio exceeds those in the cross sections.

The ranges of the size of the relative uncertainties in the measurement as a function of E_T^γ due to the various sources are provided in Table 2. The dominant uncertainties are due to the finite number of data events and the calibration of the MV1c tagger discriminant. This latter source of uncertainty primarily impacts the measurement through the HF jet fraction determined in the MV1c template fit. Uncertainties arising from the photon energy resolution, the data-driven photon isolation energy corrections and the pile-up jet removal cut are negligible and not listed in Table 2, nor are they considered further. The remaining uncertainties are added in quadrature to give the total uncertainty. The total uncertainty is largest at low and high E_T^γ , reaching a minimum at about 100 GeV. At higher E_T^γ values than those measured, the total relative uncertainty becomes excessively large and the MV1c template fit becomes unstable, curtailing the reach of the measurement. The total relative uncertainty is larger in the forward region than in the central region due to the higher data and MC statistical uncertainties. The $\gamma + c$ measurement is affected by larger relative uncertainties than the $\gamma + b$ measurement since the MV1c tagger discriminates better b -jets than c -jets.

8. Results

The values for the measured differential $\gamma + b$ and $\gamma + c$ cross sections and their ratios are given in Table 3. These values are plotted in Fig. 2 for the cross sections and in Fig. 3 for the ratios, with the relevant theory predictions. In general, considering the LO predictions in pQCD, those from SHERPA agree well with the measured values and provide a better description of the data than those from PYTHIA.

Comparisons of the $\gamma + b$ measurement to NLO + PS predictions from MADGRAPH5_aMC@NLO in both the 5F and 4F schemes are shown in Figs. 2(a) and 2(b), for the central and forward regions respectively. At low E_T^γ , both the 4F and 5F predictions agree with the data. Above 125 GeV, however, the 4F predictions underestimate the data. This is consistent with the expectation that 4F is better suited for energies close to the b -quark mass. The 5F scheme describes the data better than the 4F scheme at high E_T^γ , with a good description for $E_T^\gamma < 200$ GeV. However, the 5F scheme underestimates the data at higher E_T^γ values, by up to a factor of two. This is where the gluon-splitting contribution is expected to become more significant relative to the Compton contribution, as the latter depends on the b -quark PDF which falls steeply as a function of Bjorken- x , and thus E_T^γ . Since the gluon-splitting contribution appears only at tree level in the 5F NLO predictions, this indicates that higher-order calculations would seemingly be needed for a better description of the data in that high E_T^γ region. As shown in

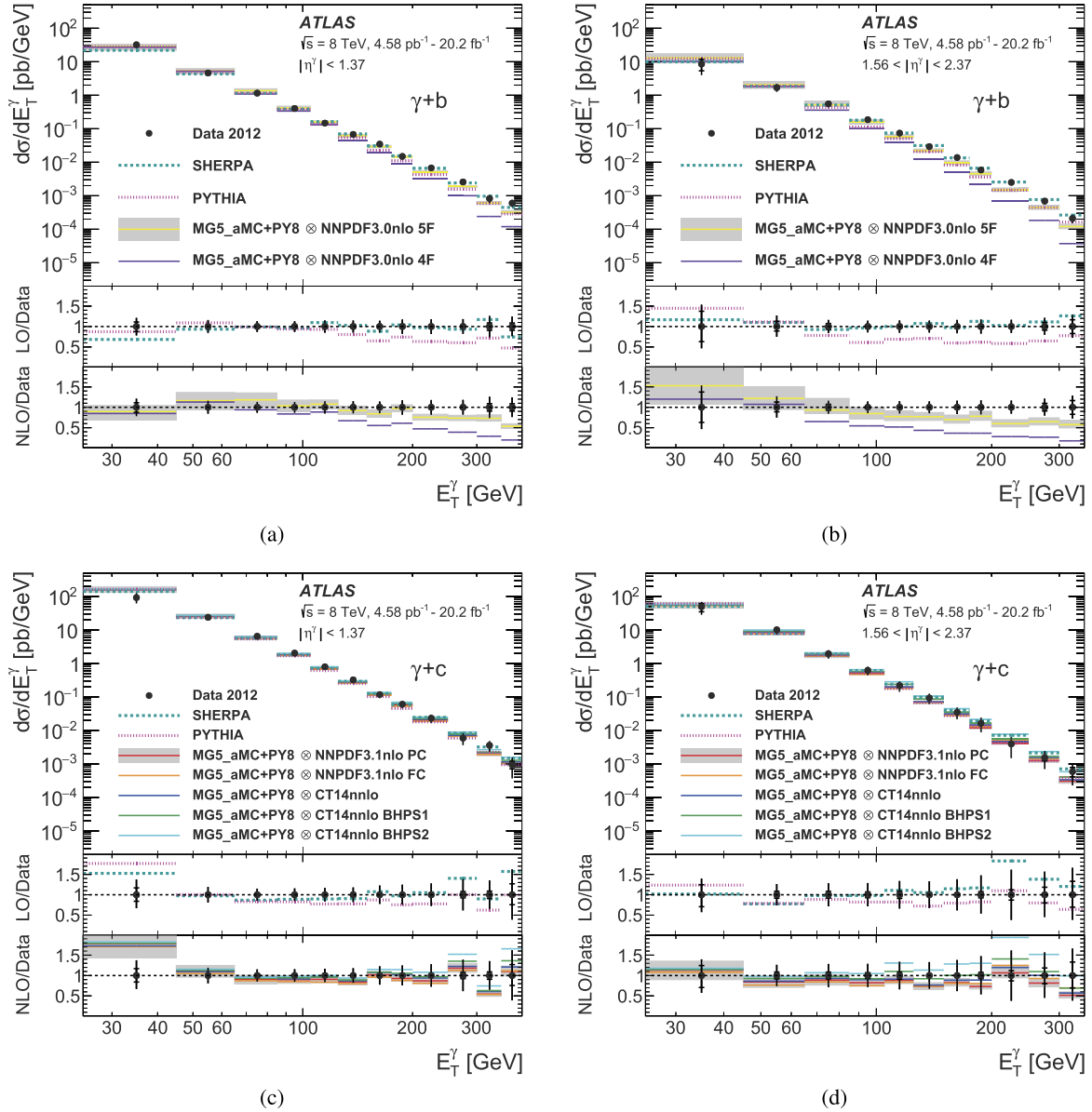


Fig. 2. Differential cross sections as a function of the photon transverse energy, E_T^γ , for (a) $\gamma + b$ in the central region, (b) $\gamma + b$ in the forward region, (c) $\gamma + c$ in the central region and (d) $\gamma + c$ in the forward region. The statistical uncertainty is represented by the complete length of the error bars. The MG5_aMC as PY8 label in the legend refers to the MADGRAPH5_aMC@NLO calculations interfaced to PYTHIA. The 5F and 4F labels in the legend refer to PDF sets with five quark flavours and four quark flavours respectively. The PC and FC labels in the legend refer to perturbative charm and fitted charm PDF sets respectively. All of the predictions for $\gamma + c$ use PDF sets with five quarks. The theoretical uncertainty in the MADGRAPH5_aMC@NLO predictions is displayed for a single PDF set since it is similar for each of the PDF sets. The SHERPA and PYTHIA cross sections are not normalized to data and no uncertainties are provided for them. (For interpretation of the references to color in this figure legend, the reader is referred to the web version of this article.)

Fig. 3(a), the 4F and 5F NLO predictions for the cross-section ratios consistently overestimate the data for $E_T^\gamma > 65$ GeV; the 5F predictions are at the edge of agreement with the measured values within uncertainties. SHERPA, which generates additional partons in the matrix element and uses a massive 5F scheme, provides a better description of the measured cross sections and cross-section ratios than MADGRAPH5_aMC@NLO in either the 5F or 4F scheme.

In comparison to the Compton contribution to the $\gamma + b$ cross section, the Compton contribution to the $\gamma + c$ cross section is larger. This is due to the larger values of both the PDF and absolute electric charge of the c -quark, compared to those of the b -quark. The gluon-splitting processes, which contribute equally to the $\gamma + b$ and $\gamma + c$ cross sections in the 5F scheme, are thus less important for $\gamma + c$ than for $\gamma + b$, considering the larger Compton

contribution to the former. The gluon-splitting contribution is expected to become important at E_T^γ values around 700 GeV, beyond the range of this measurement. Comparisons of the $\gamma + c$ measurement to NLO + PS predictions from MADGRAPH5_aMC@NLO in the 5F scheme using NNPDF3.1nlo and CT14nnlo are shown in Figs. 2(c) and 2(d), respectively for the central and forward regions. The predictions are found to agree with the data within the uncertainties across the entire E_T^γ range. However, those using the BHPS or the fitted charm PDF sets predict higher cross-section values in the forward region at high E_T^γ , above 105 GeV, than those using the nominal PDF sets. Correspondingly, the predicted values for the cross-section ratios, shown in Fig. 3(b), are smaller for the predictions using the BHPS or the fitted charm sets than for those using the nominal sets. This is the expected behaviour of the intrinsic

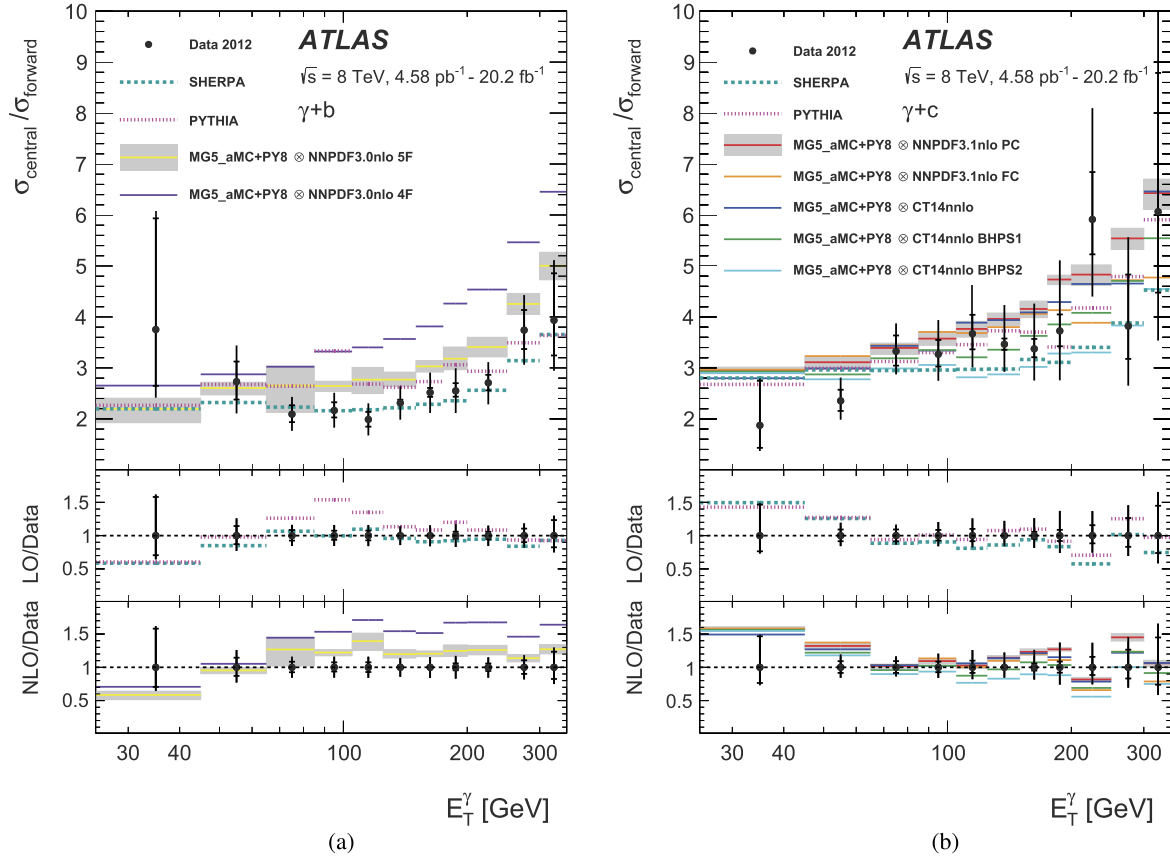


Fig. 3. Cross-section ratios of the central region, $|\eta^\gamma| < 1.37$, to the forward region, $1.56 < |\eta^\gamma| < 2.37$, as a function of the photon transverse energy, E_T^γ , for (a) $\gamma + b$ and (b) $\gamma + c$. The statistical uncertainty is represented by horizontal marks on the error bars of the data points, while the total measurement uncertainty is represented by the complete length of the error bars. The MG5_aMC + PY8 label in the legend refers to the MADGRAPH5_aMC@NLO calculations interfaced to PYTHIA. The 5F and 4F labels in the legend refer to PDF sets with five quark flavours and four quark flavours respectively. The PC and FC labels in the legend refer to perturbative charm and fitted charm PDF sets respectively. All of the predictions for $\gamma + c$ use PDF sets with five quarks. The theoretical uncertainty in the MADGRAPH5_aMC@NLO predictions is displayed for a single PDF set since it is similar for each of the PDF sets, except for NNPDF3.1nlo FC for which the total uncertainty is similar to that in NNPDF3.1nlo PC at a value of 25 GeV in E_T^γ , but rises steadily relative to it to be a factor of three larger at 350 GeV. No uncertainties are provided for SHERPA and PYTHIA. (For interpretation of the references to color in this figure legend, the reader is referred to the web version of this article.)

charm contributions from these PDF sets in the theory predictions. The predictions with the BHPS2 PDF set deviate the most from those using the nominal PDF sets, by about a factor 1.5, while those using the BHPS1 and the fitted charm PDF sets give intermediate values. The precision of the data is comparable to the size of these deviations in the predictions.

Although it is beyond the scope of this Letter, quantitative information about the level of agreement between the data and the theory predictions can be extracted by taking into account the correlations of the measurement uncertainties. Tabulated values of the measurement with full details about their uncertainties and their correlations are provided for this purpose in the Durham HEP database [67].

9. Conclusion

Differential cross sections as a function of E_T^γ for isolated prompt photons in association with a b -jet or a c -jet are measured with the ATLAS detector at the LHC using a dataset of pp collisions at $\sqrt{s} = 8$ TeV corresponding to an integrated luminosity of up to 20.2 fb^{-1} . The measured values are compared to LO calculations in pQCD from SHERPA and PYTHIA and to NLO calculations in pQCD from MADGRAPH5_aMC@NLO interfaced to PYTHIA. For the $\gamma + b$ final state, the best description of the data is provided by the SHERPA predictions, which include up to three additional partons

and are computed in the massive 5F scheme. The NLO predictions underestimate the data in the highest E_T^γ intervals measured. The 5F scheme of the theoretical calculations provides a better description of the data than the 4F scheme. For the $\gamma + c$ final state, which exhibits larger measurement uncertainties, all the predictions are in agreement with the data. Differences of about the size of the measurement uncertainties are seen between the predictions using PDF sets with intrinsic charm contributions and those without. These measured cross sections provide a test of pQCD calculations with heavy quarks and are sensitive to the b - and c -quark PDFs.

Acknowledgements

We thank CERN for the very successful operation of the LHC, as well as the support staff from our institutions without whom ATLAS could not be operated efficiently.

We acknowledge the support of ANPCyT, Argentina; YerPhI, Armenia; ARC, Australia; BMWFW and FWF, Austria; ANAS, Azerbaijan; SSTC, Belarus; CNPq and FAPESP, Brazil; NSERC, NRC and CFI, Canada; CERN; CONICYT, Chile; CAS, MOST and NSFC, China; COLCIENCIAS, Colombia; MSMT CR, MPO CR and VSC CR, Czech Republic; DNRF and DNSRC, Denmark; IN2P3-CNRS, CEA-DRF/IRFU, France; SRNSF, Georgia; BMBF, HGF, and MPG, Germany; GSRT, Greece; RGC, Hong Kong SAR, China; ISF, I-CORE and Benoziyo Center, Israel; INFN, Italy; MEXT and JSPS, Japan; CNRS, Mo-

rocco; NWO, Netherlands; RCN, Norway; MNiSW and NCN, Poland; FCT, Portugal; MNE/IFA, Romania; MES of Russia and NRC KI, Russian Federation; JINR; MESTD, Serbia; MSSR, Slovakia; ARRS and MIZŠ, Slovenia; DST/NRF, South Africa; MINECO, Spain; SRC and Wallenberg Foundation, Sweden; SERI, SNSF and Cantons of Bern and Geneva, Switzerland; MOST, Taiwan; TAEK, Turkey; STFC, United Kingdom; DOE and NSF, United States. In addition, individual groups and members have received support from BCKDF, the Canada Council, Canarie, CRC, Compute Canada, FQRNT, and the Ontario Innovation Trust, Canada; EPLANET, ERC, ERDF, FP7, Horizon 2020 and Marie Skłodowska-Curie Actions, European Union; Investissements d'Avenir Labex and Idex, ANR, Région Auvergne and Fondation Partager le Savoir, France; DFG and AvH Foundation, Germany; Herakleitos, Thales and Aristeia programmes co-financed by EU-ESF and the Greek NSRF; BSF, GIF and Minerva, Israel; BRF, Norway; CERCA Programme Generalitat de Catalunya, Generalitat Valenciana, Spain; the Royal Society and Leverhulme Trust, United Kingdom.

The crucial computing support from all WLCG partners is acknowledged gratefully, in particular from CERN, the ATLAS Tier-1 facilities at TRIUMF (Canada), NDGF (Denmark, Norway, Sweden), CC-IN2P3 (France), KIT/GridKA (Germany), INFN-CNAF (Italy), NL-T1 (Netherlands), PIC (Spain), ASGC (Taiwan), RAL (UK) and BNL (USA), the Tier-2 facilities worldwide and large non-WLCG resource providers. Major contributors of computing resources are listed in Ref. [68].

References

- [1] D0 Collaboration, Measurement of the photon + b -jet production differential cross section in $p\bar{p}$ collisions at $\sqrt{s} = 1.96$ TeV, Phys. Lett. B 714 (2012) 32, arXiv:1203.5865 [hep-ex].
- [2] D0 Collaboration, Measurement of the differential γ + c -jet cross section and the ratio of differential γ + c and γ + b cross sections in $p\bar{p}$ collisions at $\sqrt{s} = 1.96$ TeV, Phys. Lett. B 719 (2013) 354, arXiv:1210.5033 [hep-ex].
- [3] CDF Collaboration, Measurement of the cross section for direct-photon production in association with a heavy quark in $p\bar{p}$ collisions at $\sqrt{s} = 1.96$ TeV, Phys. Rev. Lett. 111 (2013) 042003, arXiv:1303.6136 [hep-ex].
- [4] ATLAS Collaboration, Measurement of the production cross section of an isolated photon associated with jets in proton–proton collisions at $\sqrt{s} = 7$ TeV with the ATLAS detector, Phys. Rev. D 85 (2012) 092014, arXiv:1203.3161 [hep-ex].
- [5] ATLAS Collaboration, Measurement of isolated-photon pair production in pp collisions at $\sqrt{s} = 7$ TeV with the ATLAS detector, J. High Energy Phys. 01 (2013) 086, arXiv:1211.1913 [hep-ex].
- [6] ATLAS Collaboration, Dynamics of isolated-photon plus jet production in pp collisions at $\sqrt{s} = 7$ TeV with the ATLAS detector, Nucl. Phys. B 875 (2013) 483, arXiv:1307.6795 [hep-ex].
- [7] ATLAS Collaboration, Measurement of the inclusive isolated prompt photons cross section in pp collisions at $\sqrt{s} = 7$ TeV with the ATLAS detector using 4.6 fb^{-1} , Phys. Rev. D 89 (2014) 052004, arXiv:1311.1440 [hep-ex].
- [8] ATLAS Collaboration, Measurement of the inclusive isolated prompt photon cross section in pp collisions at $\sqrt{s} = 8$ TeV with the ATLAS detector, J. High Energy Phys. 08 (2016) 005, arXiv:1605.03495 [hep-ex].
- [9] ATLAS Collaboration, High- E_T isolated-photon plus jets production in pp collisions at $\sqrt{s} = 8$ TeV with the ATLAS detector, Nucl. Phys. B 918 (2017) 257, arXiv:1611.06586 [hep-ex].
- [10] ATLAS Collaboration, Measurement of the cross section for inclusive isolated-photon production in pp collisions at $\sqrt{s} = 13$ TeV using the ATLAS detector, Phys. Lett. B 770 (2017) 473, arXiv:1701.06882 [hep-ex].
- [11] ATLAS Collaboration, Measurements of integrated and differential cross sections for isolated photon pair production in pp collisions at $\sqrt{s} = 8$ TeV with the ATLAS detector, Phys. Rev. D 95 (2017) 112005, arXiv:1704.03839 [hep-ex].
- [12] CMS Collaboration, Measurement of the differential cross section for isolated prompt photon production in pp collisions at 7 TeV, Phys. Rev. D 84 (2011) 052011, arXiv:1108.2044 [hep-ex].
- [13] CMS Collaboration, Rapidity distributions in exclusive Z + jet and γ + jet events in pp collisions at $\sqrt{s} = 7$ TeV, Phys. Rev. D 88 (2013) 112009, arXiv:1310.3082 [hep-ex].
- [14] CMS Collaboration, Measurement of the triple-differential cross section for photon + jets production in proton–proton collisions at $\sqrt{s} = 7$ TeV, J. High Energy Phys. 06 (2014) 009, arXiv:1311.6141 [hep-ex].
- [15] CMS Collaboration, Measurement of differential cross sections for the production of a pair of isolated photons in pp collisions at $\sqrt{s} = 7$ TeV, Eur. Phys. J. C 74 (2014) 3129, arXiv:1405.7225 [hep-ex].
- [16] CMS Collaboration, Comparison of the $Z/\gamma^* + \text{jets}$ to $\gamma + \text{jets}$ cross sections in pp collisions at $\sqrt{s} = 8$ TeV, J. High Energy Phys. 10 (2015) 128, arXiv:1505.06520 [hep-ex]; J. High Energy Phys. 04 (2016) 010 (Erratum).
- [17] J.L. Diaz-Cruz, H.-J. He, C.-P. Yuan, Soft supersymmetry breaking, scalar top-charm mixing and Higgs signatures, Phys. Lett. B 530 (2002) 179, arXiv:hep-ph/0103178.
- [18] J.R. Incandela, A. Quadt, W. Wagner, D. Wicke, Status and prospects of top-quark physics, Prog. Part. Nucl. Phys. 63 (2009) 239, arXiv:0904.2499 [hep-ex].
- [19] J.R. Andersen, et al., Handbook of LHC Higgs Cross Sections: 3. Higgs Properties, arXiv:1307.1347 [hep-ph], 2013.
- [20] ATLAS Collaboration, Search for scalar charm quark pair production in pp collisions at $\sqrt{s} = 8$ TeV with the ATLAS detector, Phys. Rev. Lett. 114 (2015) 161801, arXiv:1501.01325 [hep-ex].
- [21] ATLAS Collaboration, ATLAS Run 1 searches for direct pair production of third-generation squarks at the Large Hadron Collider, Eur. Phys. J. C 75 (2015) 510, arXiv:1506.08616 [hep-ex]; Eur. Phys. J. C 76 (2016) 153 (Erratum).
- [22] V.A. Bednyakov, M.A. Demichev, G.I. Lykasov, T. Stavreva, M. Stockton, Searching for intrinsic charm in the proton at the LHC, Phys. Lett. B 728 (2014) 602, arXiv:1305.3548 [hep-ph].
- [23] F. Maltoni, G. Ridolfi, M. Ubiali, b -initiated processes at the LHC: a reappraisal, J. High Energy Phys. 07 (2012) 022, arXiv:1203.6393 [hep-ph]; J. High Energy Phys. 04 (2013) 095 (Erratum).
- [24] ATLAS Collaboration, The ATLAS experiment at the CERN Large Hadron collider, J. Instrum. 3 (2008) S08003.
- [25] T. Gleisberg, et al., Event generation with SHERPA 1.1, J. High Energy Phys. 02 (2009) 007, arXiv:0811.4622 [hep-ph].
- [26] T. Sjöstrand, S. Mrenna, P.Z. Skands, A brief introduction to PYTHIA 8.1, Comput. Phys. Commun. 178 (2008) 852, arXiv:0710.3820 [hep-ph].
- [27] S. Höche, F. Krauss, S. Schumann, F. Siegert, QCD matrix elements and truncated showers, J. High Energy Phys. 05 (2009) 053, arXiv:0903.1219 [hep-ph].
- [28] F. Siegert, A practical guide to event generation for prompt photon production with Sherpa, J. Phys. G 44 (2017) 044007, arXiv:1611.07226 [hep-ph].
- [29] S. Schumann, F. Krauss, A parton shower algorithm based on Catani–Seymour dipole factorisation, J. High Energy Phys. 03 (2008) 038, arXiv:0709.1027 [hep-ph].
- [30] J.-C. Winter, F. Krauss, G. Soff, A modified cluster-hadronisation model, Eur. Phys. J. C 36 (2004) 381, arXiv:hep-ph/0311085.
- [31] T. Sjöstrand, P.Z. Skands, Transverse-momentum-ordered showers and interleaved multiple interactions, Eur. Phys. J. C 39 (2005) 129, arXiv:hep-ph/0408302.
- [32] B. Andersson, G. Gustafson, G. Ingelman, T. Sjöstrand, Parton fragmentation and string dynamics, Phys. Rep. 97 (1983) 31.
- [33] H.-L. Lai, et al., New parton distributions for collider physics, Phys. Rev. D 82 (2010) 074024, arXiv:1007.2241 [hep-ph].
- [34] J. Pumplin, et al., New generation of parton distributions with uncertainties from global QCD analysis, J. High Energy Phys. 07 (2002) 012, arXiv:hep-ph/0201195.
- [35] ATLAS Collaboration, Summary of ATLAS Pythia 8 tunes, ATL-PHYS-PUB-2012-003, <https://cds.cern.ch/record/1474107>.
- [36] S. Agostinelli, et al., GEANT4 – a simulation toolkit, Nucl. Instrum. Methods, Sect. A 506 (2003) 250.
- [37] ATLAS Collaboration, The ATLAS simulation infrastructure, Eur. Phys. J. C 70 (2010) 823, arXiv:1005.4568 [physics.ins-det].
- [38] A.D. Martin, W.J. Stirling, R.S. Thorne, G. Watt, Parton distributions for the LHC, Eur. Phys. J. C 63 (2009) 189, arXiv:0901.0002 [hep-ph].
- [39] J. Alwall, et al., The automated computation of tree-level and next-to-leading order differential cross sections, and their matching to parton shower simulations, J. High Energy Phys. 07 (2014) 079, arXiv:1405.0301 [hep-ph].
- [40] T. Sjöstrand, et al., An introduction to PYTHIA 8.2, Comput. Phys. Commun. 191 (2015) 159, arXiv:1410.3012 [hep-ph].
- [41] S. Frixione, Isolated photons in perturbative QCD, Phys. Lett. B 429 (1998) 369, arXiv:hep-ph/9801442.
- [42] J. Alwall, et al., Comparative study of various algorithms for the merging of parton showers and matrix elements in hadronic collisions, Eur. Phys. J. C 53 (2008) 473, arXiv:0706.2569 [hep-ph].
- [43] NNPDF Collaboration, Parton distributions for the LHC Run II, J. High Energy Phys. 04 (2015) 040, arXiv:1410.8849 [hep-ph].
- [44] NNPDF Collaboration, Parton distributions from high-precision collider data, arXiv:1706.00428 [hep-ph], 2017.
- [45] S. Dulat, et al., New parton distribution functions from a global analysis of quantum chromodynamics, Phys. Rev. D 93 (2016) 033006, arXiv:1506.07443 [hep-ph].
- [46] S.J. Brodsky, P. Hoyer, C. Peterson, N. Sakai, The intrinsic charm of the proton, Phys. Lett. B 93 (1980) 451.
- [47] T.-J. Hou, et al., CT14 intrinsic charm parton distribution functions from CTEQ-TEA global analysis, arXiv:1707.00657 [hep-ph], 2017.

- [48] A. Czarnecki, W.J. Marciano, Electroweak radiative corrections to $b \rightarrow s\gamma$, *Phys. Rev. Lett.* **81** (1998) 277, arXiv:hep-ph/9804252.
- [49] ATLAS Collaboration, Luminosity determination in pp collisions at $\sqrt{s} = 8$ TeV using the ATLAS detector at the LHC, *Eur. Phys. J. C* **76** (2016) 653, arXiv:1608.03953 [hep-ex].
- [50] ATLAS Collaboration, Measurement of the photon identification efficiencies with the ATLAS detector using LHC Run-1 data, *Eur. Phys. J. C* **76** (2016) 666, arXiv:1606.01813 [hep-ex].
- [51] ATLAS Collaboration, Electron and photon energy calibration with the ATLAS detector using LHC Run 1 data, *Eur. Phys. J. C* **74** (2014) 3071, arXiv:1407.5063 [hep-ex].
- [52] M. Cacciari, G.P. Salam, Pileup subtraction using jet areas, *Phys. Lett. B* **659** (2008) 119, arXiv:0707.1378 [hep-ph].
- [53] M. Cacciari, G.P. Salam, G. Soyez, The anti- k_t jet clustering algorithm, *J. High Energy Phys.* **04** (2008) 063, arXiv:0802.1189 [hep-ph].
- [54] M. Cacciari, G.P. Salam, G. Soyez, FastJet User Manual, *Eur. Phys. J. C* **72** (2012) 1896, arXiv:1111.6097 [hep-ph].
- [55] ATLAS Collaboration, Topological cell clustering in the ATLAS calorimeters and its performance in LHC Run 1, *Eur. Phys. J. C* **77** (2017) 490, arXiv:1603.02934 [hep-ex].
- [56] ATLAS Collaboration, Jet global sequential corrections with the ATLAS detector in proton–proton collisions at $\sqrt{s} = 8$ TeV, ATLAS-CONF-2015-002, <https://cds.cern.ch/record/2001682>.
- [57] ATLAS Collaboration, Jet energy measurement and its systematic uncertainty in proton–proton collisions at $\sqrt{s} = 7$ TeV with the ATLAS detector, *Eur. Phys. J. C* **75** (2015) 17, arXiv:1406.0076 [hep-ex].
- [58] ATLAS Collaboration, Jet energy measurement with the ATLAS detector in proton–proton collisions at $\sqrt{s} = 7$ TeV, *Eur. Phys. J. C* **73** (2013) 2304, arXiv:1112.6426 [hep-ex].
- [59] ATLAS Collaboration, Performance of pile-up mitigation techniques for jets in pp collisions at $\sqrt{s} = 8$ TeV using the ATLAS detector, *Eur. Phys. J. C* **76** (2016) 581, arXiv:1510.03823 [hep-ex].
- [60] ATLAS Collaboration, Performance of b -jet identification in the ATLAS experiment, *J. Instrum.* **11** (2016) P04008, arXiv:1512.01094 [hep-ex].
- [61] ATLAS Collaboration, Measurements of fiducial cross-sections for $t\bar{t}$ production with one or two additional b -jets in pp collisions at $\sqrt{s} = 8$ TeV using the ATLAS detector, *Eur. Phys. J. C* **76** (2016) 11, arXiv:1508.06868 [hep-ex].
- [62] ATLAS Collaboration, Calibration of b -tagging using dileptonic top pair events in a combinatorial likelihood approach with the ATLAS experiment, ATLAS-CONF-2014-004, <https://cds.cern.ch/record/1664335>.
- [63] ATLAS Collaboration, Calibration of the performance of b -tagging for c and light-flavour jets in the 2012 ATLAS data, ATLAS-CONF-2014-046, <https://cds.cern.ch/record/1741020>.
- [64] C. Patrignani, et al., Review of Particle Physics, *Chin. Phys. C* **40** (2016) 100001, and 2017 update.
- [65] D.J. Lange, The EvtGen particle decay simulation package, *Nucl. Instrum. Methods, Sect. A* **462** (2001) 152.
- [66] G. Bohm, G. Zech, Introduction to Statistics and Data Analysis for Physicists, third revised edition, Verlag Deutsches Elektronen-Synchrotron, ISBN 978-3-945931-13-4, 2017.
- [67] A complete set of tables with the full results are available at the Durham Hep-Data repository, <https://hepdata.net>.
- [68] ATLAS Collaboration, ATLAS computing acknowledgements 2016–2017, ATLAS-PUB-2016-002, <https://cds.cern.ch/record/2202407>.

The ATLAS Collaboration

M. Aaboud^{137d}, G. Aad⁸⁸, B. Abbott¹¹⁵, O. Abidinov^{12,*}, B. Abeloos¹¹⁹, S.H. Abidi¹⁶¹, O.S. AbouZeid¹³⁹, N.L. Abraham¹⁵¹, H. Abramowicz¹⁵⁵, H. Abreu¹⁵⁴, R. Abreu¹¹⁸, Y. Abulaiti^{148a,148b}, B.S. Acharya^{167a,167b,a}, S. Adachi¹⁵⁷, L. Adamczyk^{41a}, J. Adelman¹¹⁰, M. Adersberger¹⁰², T. Adye¹³³, A.A. Affolder¹³⁹, Y. Afik¹⁵⁴, C. Agheorghiesei^{28c}, J.A. Aguilar-Saavedra^{128a,128f}, S.P. Ahlen²⁴, F. Ahmadov^{68,b}, G. Aielli^{135a,135b}, S. Akatsuka⁷¹, H. Akerstedt^{148a,148b}, T.P.A. Åkesson⁸⁴, E. Akilli⁵², A.V. Akimov⁹⁸, G.L. Alberghi^{22a,22b}, J. Albert¹⁷², P. Albicocco⁵⁰, M.J. Alconada Verzini⁷⁴, S.C. Alderweireldt¹⁰⁸, M. Aleksa³², I.N. Aleksandrov⁶⁸, C. Alexa^{28b}, G. Alexander¹⁵⁵, T. Alexopoulos¹⁰, M. Alhroob¹¹⁵, B. Ali¹³⁰, M. Aliev^{76a,76b}, G. Alimonti^{94a}, J. Alison³³, S.P. Alkire³⁸, B.M.M. Allbrooke¹⁵¹, B.W. Allen¹¹⁸, P.P. Allport¹⁹, A. Aloisio^{106a,106b}, A. Alonso³⁹, F. Alonso⁷⁴, C. Alpigiani¹⁴⁰, A.A. Alshehri⁵⁶, M.I. Alstady⁸⁸, B. Alvarez Gonzalez³², D. Álvarez Piqueras¹⁷⁰, M.G. Alviggi^{106a,106b}, B.T. Amadio¹⁶, Y. Amaral Coutinho^{26a}, C. Amelung²⁵, D. Amidei⁹², S.P. Amor Dos Santos^{128a,128c}, S. Amoroso³², C. Anastopoulos¹⁴¹, L.S. Ancu⁵², N. Andari¹⁹, T. Andeen¹¹, C.F. Anders^{60b}, J.K. Anders⁷⁷, K.J. Anderson³³, A. Andreazza^{94a,94b}, V. Andrei^{60a}, S. Angelidakis³⁷, I. Angelozzi¹⁰⁹, A. Angerami³⁸, A.V. Anisenkov^{111,c}, N. Anjos¹³, A. Annovi^{126a}, C. Antel^{60a}, M. Antonelli⁵⁰, A. Antonov^{100,*}, D.J. Antrim¹⁶⁶, F. Anulli^{134a}, M. Aoki⁶⁹, L. Aperio Bella³², G. Arabidze⁹³, Y. Arai⁶⁹, J.P. Araque^{128a}, V. Araujo Ferraz^{26a}, A.T.H. Arce⁴⁸, R.E. Ardell⁸⁰, F.A. Arduh⁷⁴, J-F. Arguin⁹⁷, S. Argyropoulos⁶⁶, M. Arik^{20a}, A.J. Armbruster³², L.J. Armitage⁷⁹, O. Arnaez¹⁶¹, H. Arnold⁵¹, M. Arratia³⁰, O. Arslan²³, A. Artamonov^{99,*}, G. Artoni¹²², S. Artz⁸⁶, S. Asai¹⁵⁷, N. Asbah⁴⁵, A. Ashkenazi¹⁵⁵, L. Asquith¹⁵¹, K. Assamagan²⁷, R. Astalos^{146a}, M. Atkinson¹⁶⁹, N.B. Atlay¹⁴³, K. Augsten¹³⁰, G. Avolio³², B. Axen¹⁶, M.K. Ayoub^{35a}, G. Azuelos^{97,d}, A.E. Baas^{60a}, M.J. Baca¹⁹, H. Bachacou¹³⁸, K. Bachas^{76a,76b}, M. Backes¹²², P. Bagnaia^{134a,134b}, M. Bahmani⁴², H. Bahrasemani¹⁴⁴, J.T. Baines¹³³, M. Bajic³⁹, O.K. Baker¹⁷⁹, P.J. Bakker¹⁰⁹, E.M. Baldin^{111,c}, P. Balek¹⁷⁵, F. Balli¹³⁸, W.K. Balunas¹²⁴, E. Banas⁴², A. Bandyopadhyay²³, Sw. Banerjee^{176,e}, A.A.E. Bannoura¹⁷⁸, L. Barak¹⁵⁵, E.L. Barberio⁹¹, D. Barberis^{53a,53b}, M. Barbero⁸⁸, T. Barillari¹⁰³, M-S Barisits⁶⁵, J.T. Barkeloo¹¹⁸, T. Barklow¹⁴⁵, N. Barlow³⁰, S.L. Barnes^{36c}, B.M. Barnett¹³³, R.M. Barnett¹⁶, Z. Barnovska-Blenessy^{36a}, A. Baroncelli^{136a}, G. Barone²⁵, A.J. Barr¹²², L. Barranco Navarro¹⁷⁰, F. Barreiro⁸⁵, J. Barreiro Guimarães da Costa^{35a}, R. Bartoldus¹⁴⁵, A.E. Barton⁷⁵, P. Bartos^{146a}, A. Basalae¹²⁵, A. Bassalat^{119,f}, R.L. Bates⁵⁶, S.J. Batista¹⁶¹, J.R. Batley³⁰, M. Battaglia¹³⁹, M. Baue^{134a,134b}, F. Bauer¹³⁸, K.T. Bauer¹⁶⁶, H.S. Bawa^{145,g}, J.B. Beacham¹¹³, M.D. Beattie⁷⁵, T. Beau⁸³, P.H. Beauchemin¹⁶⁵, P. Bechtel²³, H.P. Beck^{18,h}, H.C. Beck⁵⁷, K. Becker¹²², M. Becker⁸⁶, C. Becot¹¹², A.J. Beddall^{20e}, A. Beddall^{20b}, V.A. Bednyakov⁶⁸, M. Bedognetti¹⁰⁹, C.P. Bee¹⁵⁰, T.A. Beermann³², M. Begalli^{26a}, M. Begel²⁷, J.K. Behr⁴⁵, A.S. Bell⁸¹,

G. Bella¹⁵⁵, L. Bellagamba^{22a}, A. Bellerive³¹, M. Bellomo¹⁵⁴, K. Belotskiy¹⁰⁰, O. Beltramello³², N.L. Belyaev¹⁰⁰, O. Benary^{155,*}, D. Benchekroun^{137a}, M. Bender¹⁰², N. Benekos¹⁰, Y. Benhammou¹⁵⁵, E. Benhar Noccioli¹⁷⁹, J. Benitez⁶⁶, D.P. Benjamin⁴⁸, M. Benoit⁵², J.R. Bensinger²⁵, S. Bentvelsen¹⁰⁹, L. Beresford¹²², M. Beretta⁵⁰, D. Berge¹⁰⁹, E. Bergeaas Kuutmann¹⁶⁸, N. Berger⁵, L.J. Bergsten²⁵, J. Beringer¹⁶, S. Berlendis⁵⁸, N.R. Bernard⁸⁹, G. Bernardi⁸³, C. Bernius¹⁴⁵, F.U. Bernlochner²³, T. Berry⁸⁰, P. Berta⁸⁶, C. Bertella^{35a}, G. Bertoli^{148a,148b}, I.A. Bertram⁷⁵, C. Bertsche⁴⁵, G.J. Besjes³⁹, O. Bessidskaia Bylund^{148a,148b}, M. Bessner⁴⁵, N. Besson¹³⁸, A. Bethani⁸⁷, S. Bethke¹⁰³, A. Betti²³, A.J. Bevan⁷⁹, J. Beyer¹⁰³, R.M. Bianchi¹²⁷, O. Biebel¹⁰², D. Biedermann¹⁷, R. Bielski⁸⁷, K. Bierwagen⁸⁶, N.V. Biesuz^{126a,126b}, M. Biglietti^{136a}, T.R.V. Billoud⁹⁷, H. Bilokon⁵⁰, M. Bindi⁵⁷, A. Bingul^{20b}, C. Bini^{134a,134b}, S. Biondi^{22a,22b}, T. Bisanz⁵⁷, C. Bittrich⁴⁷, D.M. Bjergaard⁴⁸, J.E. Black¹⁴⁵, K.M. Black²⁴, R.E. Blair⁶, T. Blazek^{146a}, I. Bloch⁴⁵, C. Blocker²⁵, A. Blue⁵⁶, U. Blumenschein⁷⁹, S. Blunier^{34a}, G.J. Bobbink¹⁰⁹, V.S. Bobrovnikov^{111,c}, S.S. Bocchetta⁸⁴, A. Bocci⁴⁸, C. Bock¹⁰², M. Boehler⁵¹, D. Boerner¹⁷⁸, D. Bogavac¹⁰², A.G. Bogdanchikov¹¹¹, C. Bohm^{148a}, V. Boisvert⁸⁰, P. Bokan^{168,i}, T. Bold^{41a}, A.S. Boldyrev¹⁰¹, A.E. Bolz^{60b}, M. Bomben⁸³, M. Bona⁷⁹, M. Boonekamp¹³⁸, A. Borisov¹³², G. Borissov⁷⁵, J. Bortfeldt³², D. Bortoletto¹²², V. Bortolotto^{62a}, D. Boscherini^{22a}, M. Bosman¹³, J.D. Bossio Sola²⁹, J. Boudreau¹²⁷, E.V. Bouhova-Thacker⁷⁵, D. Boumediene³⁷, C. Bourdarios¹¹⁹, S.K. Boutle⁵⁶, A. Boveia¹¹³, J. Boyd³², I.R. Boyko⁶⁸, A.J. Bozson⁸⁰, J. Bracinik¹⁹, A. Brandt⁸, G. Brandt⁵⁷, O. Brandt^{60a}, F. Braren⁴⁵, U. Bratzler¹⁵⁸, B. Brau⁸⁹, J.E. Brau¹¹⁸, W.D. Breaden Madden⁵⁶, K. Brendlinger⁴⁵, A.J. Brennan⁹¹, L. Brenner¹⁰⁹, R. Brenner¹⁶⁸, S. Bressler¹⁷⁵, D.L. Briglin¹⁹, T.M. Bristow⁴⁹, D. Britton⁵⁶, D. Britzger⁴⁵, F.M. Brochu³⁰, I. Brock²³, R. Brock⁹³, G. Brooijmans³⁸, T. Brooks⁸⁰, W.K. Brooks^{34b}, E. Brost¹¹⁰, J.H. Broughton¹⁹, P.A. Bruckman de Renstrom⁴², D. Bruncko^{146b}, A. Bruni^{22a}, G. Bruni^{22a}, L.S. Bruni¹⁰⁹, S. Bruno^{135a,135b}, B.H. Brunt³⁰, M. Bruschi^{22a}, N. Bruscino¹²⁷, P. Bryant³³, L. Bryngemark⁴⁵, T. Buanes¹⁵, Q. Buat¹⁴⁴, P. Buchholz¹⁴³, A.G. Buckley⁵⁶, I.A. Budagov⁶⁸, F. Buehrer⁵¹, M.K. Bugge¹²¹, O. Bulekov¹⁰⁰, D. Bullock⁸, T.J. Burch¹¹⁰, S. Burdin⁷⁷, C.D. Burgard¹⁰⁹, A.M. Burger⁵, B. Burghgrave¹¹⁰, K. Burka⁴², S. Burke¹³³, I. Burmeister⁴⁶, J.T.P. Burr¹²², D. Büscher⁵¹, V. Büscher⁸⁶, P. Bussey⁵⁶, J.M. Butler²⁴, C.M. Buttar⁵⁶, J.M. Butterworth⁸¹, P. Butti³², W. Buttinger²⁷, A. Buzatu¹⁵³, A.R. Buzykaev^{111,c}, C.-Q. Changqiao^{36a}, S. Cabrera Urbán¹⁷⁰, D. Caforio¹³⁰, H. Cai¹⁶⁹, V.M. Cairo^{40a,40b}, O. Cakir^{4a}, N. Calace⁵², P. Calafiura¹⁶, A. Calandri⁸⁸, G. Calderini⁸³, P. Calfayan⁶⁴, G. Callea^{40a,40b}, L.P. Caloba^{26a}, S. Calvente Lopez⁸⁵, D. Calvet³⁷, S. Calvet³⁷, T.P. Calvet⁸⁸, R. Camacho Toro³³, S. Camarda³², P. Camarri^{135a,135b}, D. Cameron¹²¹, R. Caminal Armadans¹⁶⁹, C. Camincher⁵⁸, S. Campana³², M. Campanelli⁸¹, A. Camplani^{94a,94b}, A. Campoverde¹⁴³, V. Canale^{106a,106b}, M. Cano Bret^{36c}, J. Cantero¹¹⁶, T. Cao¹⁵⁵, M.D.M. Capeans Garrido³², I. Caprini^{28b}, M. Caprini^{28b}, M. Capua^{40a,40b}, R.M. Carbone³⁸, R. Cardarelli^{135a}, F. Cardillo⁵¹, I. Carli¹³¹, T. Carli³², G. Carlino^{106a}, B.T. Carlson¹²⁷, L. Carminati^{94a,94b}, R.M.D. Carney^{148a,148b}, S. Caron¹⁰⁸, E. Carquin^{34b}, S. Carrá^{94a,94b}, G.D. Carrillo-Montoya³², D. Casadei¹⁹, M.P. Casado^{13,j}, A.F. Casha¹⁶¹, M. Casolino¹³, D.W. Casper¹⁶⁶, R. Castelijns¹⁰⁹, V. Castillo Gimenez¹⁷⁰, N.F. Castro^{128a,k}, A. Catinaccio³², J.R. Catmore¹²¹, A. Cattai³², J. Caudron²³, V. Cavaliere¹⁶⁹, E. Cavallaro¹³, D. Cavalli^{94a}, M. Cavalli-Sforza¹³, V. Cavasinni^{126a,126b}, E. Celebi^{20d}, F. Ceradini^{136a,136b}, L. Cerda Alberich¹⁷⁰, A.S. Cerqueira^{26b}, A. Cerri¹⁵¹, L. Cerrito^{135a,135b}, F. Cerutti¹⁶, A. Cervelli^{22a,22b}, S.A. Cetin^{20d}, A. Chafaq^{137a}, D. Chakraborty¹¹⁰, S.K. Chan⁵⁹, W.S. Chan¹⁰⁹, Y.L. Chan^{62a}, P. Chang¹⁶⁹, J.D. Chapman³⁰, D.G. Charlton¹⁹, C.C. Chau³¹, C.A. Chavez Barajas¹⁵¹, S. Che¹¹³, S. Cheatham^{167a,167c}, A. Chegwidden⁹³, S. Chekanov⁶, S.V. Chekulaev^{163a}, G.A. Chelkov^{68,l}, M.A. Chelstowska³², C. Chen^{36a}, C. Chen⁶⁷, H. Chen²⁷, J. Chen^{36a}, S. Chen^{35b}, S. Chen¹⁵⁷, X. Chen^{35c,m}, Y. Chen⁷⁰, H.C. Cheng⁹², H.J. Cheng^{35a,35d}, A. Cheplakov⁶⁸, E. Cheremushkina¹³², R. Cherkaoui El Moursli^{137e}, E. Cheu⁷, K. Cheung⁶³, L. Chevalier¹³⁸, V. Chiarella⁵⁰, G. Chiarelli^{126a}, G. Chiodini^{76a}, A.S. Chisholm³², A. Chitan^{28b}, Y.H. Chiu¹⁷², M.V. Chizhov⁶⁸, K. Choi⁶⁴, A.R. Chomont³⁷, S. Chouridou¹⁵⁶, Y.S. Chow^{62a}, V. Christodoulou⁸¹, M.C. Chu^{62a}, J. Chudoba¹²⁹, A.J. Chuinard⁹⁰, J.J. Chwastowski⁴², L. Chytka¹¹⁷, A.K. Ciftci^{4a}, D. Cinca⁴⁶, V. Cindro⁷⁸, I.A. Cioara²³, A. Ciocio¹⁶, F. Ciotto^{106a,106b}, Z.H. Citron¹⁷⁵, M. Citterio^{94a}, M. Ciubancan^{28b}, A. Clark⁵², M.R. Clark³⁸, P.J. Clark⁴⁹, R.N. Clarke¹⁶, C. Clement^{148a,148b}, Y. Coadou⁸⁸, M. Cobal^{167a,167c}, A. Coccaro⁵², J. Cochran⁶⁷, L. Colasurdo¹⁰⁸, B. Cole³⁸, A.P. Colijn¹⁰⁹, J. Collot⁵⁸, T. Colombo¹⁶⁶, P. Conde Muiño^{128a,128b}, E. Coniavitis⁵¹, S.H. Connell^{147b}, I.A. Connelly⁸⁷, S. Constantinescu^{28b}, G. Conti³², F. Conventi^{106a,n}, M. Cooke¹⁶, A.M. Cooper-Sarkar¹²², F. Cormier¹⁷¹,

K.J.R. Cormier¹⁶¹, M. Corradi^{134a,134b}, E.E. Corrigan⁸⁴, F. Corriveau^{90,o}, A. Cortes-Gonzalez³², G. Costa^{94a}, M.J. Costa¹⁷⁰, D. Costanzo¹⁴¹, G. Cottin³⁰, G. Cowan⁸⁰, B.E. Cox⁸⁷, K. Cranmer¹¹², S.J. Crawley⁵⁶, R.A. Creager¹²⁴, G. Cree³¹, S. Crépé-Renaudin⁵⁸, F. Crescioli⁸³, W.A. Cribbs^{148a,148b}, M. Cristinziani²³, V. Croft¹¹², G. Crosetti^{40a,40b}, A. Cueto⁸⁵, T. Cuhadar Donszelmann¹⁴¹, A.R. Cukierman¹⁴⁵, J. Cummings¹⁷⁹, M. Curatolo⁵⁰, J. Cúth⁸⁶, S. Czekierda⁴², P. Czodrowski³², G. D'amen^{22a,22b}, S. D'Auria⁵⁶, L. D'eraimo⁸³, M. D'Onofrio⁷⁷, M.J. Da Cunha Sargedas De Sousa^{128a,128b}, C. Da Via⁸⁷, W. Dabrowski^{41a}, T. Dado^{146a}, T. Dai⁹², O. Dale¹⁵, F. Dallaire⁹⁷, C. Dallapiccola⁸⁹, M. Dam³⁹, J.R. Dandoy¹²⁴, M.F. Daneri²⁹, N.P. Dang¹⁷⁶, A.C. Daniells¹⁹, N.S. Dann⁸⁷, M. Danninger¹⁷¹, M. Dano Hoffmann¹³⁸, V. Dao¹⁵⁰, G. Darbo^{53a}, S. Darmora⁸, J. Dassoulas³, A. Dattagupta¹¹⁸, T. Daubney⁴⁵, W. Davey²³, C. David⁴⁵, T. Davidek¹³¹, D.R. Davis⁴⁸, P. Davison⁸¹, E. Dawe⁹¹, I. Dawson¹⁴¹, K. De⁸, R. de Asmundis^{106a}, A. De Benedetti¹¹⁵, S. De Castro^{22a,22b}, S. De Cecco⁸³, N. De Groot¹⁰⁸, P. de Jong¹⁰⁹, H. De la Torre⁹³, F. De Lorenzi⁶⁷, A. De Maria⁵⁷, D. De Pedis^{134a}, A. De Salvo^{134a}, U. De Sanctis^{135a,135b}, A. De Santo¹⁵¹, K. De Vasconcelos Corga⁸⁸, J.B. De Vivie De Regie¹¹⁹, R. Debbe²⁷, C. Debenedetti¹³⁹, D.V. Dedovich⁶⁸, N. Dehghanian³, I. Deigaard¹⁰⁹, M. Del Gaudio^{40a,40b}, J. Del Peso⁸⁵, D. Delgove¹¹⁹, F. Deliot¹³⁸, C.M. Delitzsch⁷, A. Dell'Acqua³², L. Dell'Asta²⁴, M. Dell'Orso^{126a,126b}, M. Della Pietra^{106a,106b}, D. della Volpe⁵², M. Delmastro⁵, C. Delporte¹¹⁹, P.A. Delsart⁵⁸, D.A. DeMarco¹⁶¹, S. Demers¹⁷⁹, M. Demichev⁶⁸, A. Demilly⁸³, S.P. Denisov¹³², D. Denysiuk¹³⁸, D. Derendarz⁴², J.E. Derkaoui^{137d}, F. Derue⁸³, P. Dervan⁷⁷, K. Desch²³, C. Deterre⁴⁵, K. Dette¹⁶¹, M.R. Devesa²⁹, P.O. Deviveiros³², A. Dewhurst¹³³, S. Dhaliwal²⁵, F.A. Di Bello⁵², A. Di Ciaccio^{135a,135b}, L. Di Ciaccio⁵, W.K. Di Clemente¹²⁴, C. Di Donato^{106a,106b}, A. Di Girolamo³², B. Di Girolamo³², B. Di Micco^{136a,136b}, R. Di Nardo³², K.F. Di Petrillo⁵⁹, A. Di Simone⁵¹, R. Di Sipio¹⁶¹, D. Di Valentino³¹, C. Diaconu⁸⁸, M. Diamond¹⁶¹, F.A. Dias³⁹, M.A. Diaz^{34a}, J. Dickinson¹⁶, E.B. Diehl⁹², J. Dietrich¹⁷, S. Díez Cornell⁴⁵, A. Dimitrievska¹⁴, J. Dingfelder²³, P. Dita^{28b}, S. Dita^{28b}, F. Dittus³², F. Djama⁸⁸, T. Djobava^{54b}, J.I. Djuvsland^{60a}, M.A.B. do Vale^{26c}, M. Dobre^{28b}, D. Dodsworth²⁵, C. Doglioni⁸⁴, J. Dolejsi¹³¹, Z. Dolezal¹³¹, M. Donadelli^{26d}, S. Donati^{126a,126b}, J. Donini³⁷, J. Dopke¹³³, A. Doria^{106a}, M.T. Dova⁷⁴, A.T. Doyle⁵⁶, E. Drechsler⁵⁷, M. Dris¹⁰, Y. Du^{36b}, J. Duarte-Campderros¹⁵⁵, F. Dubinin⁹⁸, A. Dubreuil⁵², E. Duchovni¹⁷⁵, G. Duckeck¹⁰², A. Ducourthial⁸³, O.A. Ducu^{97,p}, D. Duda¹⁰⁹, A. Dudarev³², A. Chr. Dudder⁸⁶, E.M. Duffield¹⁶, L. Dufлот¹¹⁹, M. Dührssen³², C. Dulsen¹⁷⁸, M. Dumancic¹⁷⁵, A.E. Dumitriu^{28b}, A.K. Duncan⁵⁶, M. Dunford^{60a}, A. Duperrin⁸⁸, H. Duran Yildiz^{4a}, M. Düren⁵⁵, A. Durglishvili^{54b}, D. Duschinger⁴⁷, B. Dutta⁴⁵, D. Duvnjak¹, M. Dyndal⁴⁵, B.S. Dziedzic⁴², C. Eckardt⁴⁵, K.M. Ecker¹⁰³, R.C. Edgar⁹², T. Eifert³², G. Eigen¹⁵, K. Einsweiler¹⁶, T. Ekelof¹⁶⁸, M. El Kacimi^{137c}, R. El Kosseifi⁸⁸, V. Ellajosyula⁸⁸, M. Ellert¹⁶⁸, S. Elles⁵, F. Ellinghaus¹⁷⁸, A.A. Elliot¹⁷², N. Ellis³², J. Elmsheuser²⁷, M. Elsing³², D. Emelianov¹³³, Y. Enari¹⁵⁷, J.S. Ennis¹⁷³, M.B. Epland⁴⁸, J. Erdmann⁴⁶, A. Ereditato¹⁸, M. Ernst²⁷, S. Errede¹⁶⁹, M. Escalier¹¹⁹, C. Escobar¹⁷⁰, B. Esposito⁵⁰, O. Estrada Pastor¹⁷⁰, A.I. Etienne¹³⁸, E. Etzion¹⁵⁵, H. Evans⁶⁴, A. Ezhilov¹²⁵, M. Ezzi^{137e}, F. Fabbri^{22a,22b}, L. Fabbri^{22a,22b}, V. Fabiani¹⁰⁸, G. Facini⁸¹, R.M. Fakhruddinov¹³², S. Falciano^{134a}, R.J. Falla⁸¹, J. Faltova³², Y. Fang^{35a}, M. Fanti^{94a,94b}, A. Farbin⁸, A. Farilla^{136a}, E.M. Farina^{123a,123b}, T. Farooque⁹³, S. Farrell¹⁶, S.M. Farrington¹⁷³, P. Farthouat³², F. Fassi^{137e}, P. Fassnacht³², D. Fassouliotis⁹, M. Faucci Giannelli⁴⁹, A. Favareto^{53a,53b}, W.J. Fawcett¹²², L. Fayard¹¹⁹, O.L. Fedin^{125,q}, W. Fedorko¹⁷¹, S. Feigl¹²¹, L. Feligioni⁸⁸, C. Feng^{36b}, E.J. Feng³², M. Feng⁴⁸, M.J. Fenton⁵⁶, A.B. Fenyuk¹³², L. Feremenga⁸, P. Fernandez Martinez¹⁷⁰, J. Ferrando⁴⁵, A. Ferrari¹⁶⁸, P. Ferrari¹⁰⁹, R. Ferrari^{123a}, D.E. Ferreira de Lima^{60b}, A. Ferrer¹⁷⁰, D. Ferrere⁵², C. Ferretti⁹², F. Fiedler⁸⁶, A. Filipčič⁷⁸, M. Filipuzzi⁴⁵, F. Filthaut¹⁰⁸, M. Fincke-Keeler¹⁷², K.D. Finelli²⁴, M.C.N. Fiolhais^{128a,128c,r}, L. Fiorini¹⁷⁰, A. Fischer², C. Fischer¹³, J. Fischer¹⁷⁸, W.C. Fisher⁹³, N. Flaschel⁴⁵, I. Fleck¹⁴³, P. Fleischmann⁹², R.R.M. Fletcher¹²⁴, T. Flick¹⁷⁸, B.M. Flierl¹⁰², L.R. Flores Castillo^{62a}, M.J. Flowerdew¹⁰³, G.T. Forcolin⁸⁷, A. Formica¹³⁸, F.A. Förster¹³, A. Forti⁸⁷, A.G. Foster¹⁹, D. Fournier¹¹⁹, H. Fox⁷⁵, S. Fracchia¹⁴¹, P. Francavilla^{126a,126b}, M. Franchini^{22a,22b}, S. Franchino^{60a}, D. Francis³², L. Franconi¹²¹, M. Franklin⁵⁹, M. Frate¹⁶⁶, M. Fraternali^{123a,123b}, D. Freeborn⁸¹, S.M. Fressard-Batraneanu³², B. Freund⁹⁷, D. Froidevaux³², J.A. Frost¹²², C. Fukunaga¹⁵⁸, T. Fusayasu¹⁰⁴, J. Fuster¹⁷⁰, O. Gabizon¹⁵⁴, A. Gabrielli^{22a,22b}, A. Gabrielli¹⁶, G.P. Gach^{41a}, S. Gadatsch³², S. Gadomski⁸⁰, G. Gagliardi^{53a,53b}, L.G. Gagnon⁹⁷, C. Galea¹⁰⁸, B. Galhardo^{128a,128c}, E.J. Gallas¹²², B.J. Gallop¹³³, P. Gallus¹³⁰, G. Galster³⁹,

K.K. Gan¹¹³, S. Ganguly³⁷, Y. Gao⁷⁷, Y.S. Gao^{145,g}, F.M. Garay Walls^{34a}, C. García¹⁷⁰, J.E. García Navarro¹⁷⁰, J.A. García Pascual^{35a}, M. Garcia-Sciveres¹⁶, R.W. Gardner³³, N. Garelli¹⁴⁵, V. Garonne¹²¹, A. Gascon Bravo⁴⁵, K. Gasnikova⁴⁵, C. Gatti⁵⁰, A. Gaudiello^{53a,53b}, G. Gaudio^{123a}, I.L. Gavrilenko⁹⁸, C. Gay¹⁷¹, G. Gaycken²³, E.N. Gazis¹⁰, C.N.P. Gee¹³³, J. Geisen⁵⁷, M. Geisen⁸⁶, M.P. Geisler^{60a}, K. Gellerstedt^{148a,148b}, C. Gemme^{53a}, M.H. Genest⁵⁸, C. Geng⁹², S. Gentile^{134a,134b}, C. Gentsos¹⁵⁶, S. George⁸⁰, D. Gerbaudo¹³, G. Geßner⁴⁶, S. Ghasemi¹⁴³, M. Ghneimat²³, B. Giacobbe^{22a}, S. Giagu^{134a,134b}, N. Giangiacomi^{22a,22b}, P. Giannetti^{126a}, S.M. Gibson⁸⁰, M. Gignac¹⁷¹, M. Gilchriese¹⁶, D. Gillberg³¹, G. Gilles¹⁷⁸, D.M. Gingrich^{3,d}, M.P. Giordani^{167a,167c}, F.M. Giorgi^{22a}, P.F. Giraud¹³⁸, P. Giromini⁵⁹, G. Giugliarelli^{167a,167c}, D. Giugni^{94a}, F. Giuliani¹²², C. Giuliani¹⁰³, M. Giulini^{60b}, B.K. Gjelsten¹²¹, S. Gkaitatzis¹⁵⁶, I. Gkialas^{9,s}, E.L. Gkougkousis¹³, P. Gkoutoumis¹⁰, L.K. Gladilin¹⁰¹, C. Glasman⁸⁵, J. Glatzer¹³, P.C.F. Glaysher⁴⁵, A. Glazov⁴⁵, M. Goblirsch-Kolb²⁵, J. Godlewski⁴², S. Goldfarb⁹¹, T. Golling⁵², D. Golubkov¹³², A. Gomes^{128a,128b,128d}, R. Gonçalo^{128a}, R. Goncalves Gama^{26a}, J. Goncalves Pinto Firmino Da Costa¹³⁸, G. Gonella⁵¹, L. Gonella¹⁹, A. Gongadze⁶⁸, F. Gonnella¹⁹, J.L. Gonski⁵⁹, S. González de la Hoz¹⁷⁰, S. Gonzalez-Sevilla⁵², L. Goossens³², P.A. Gorbounov⁹⁹, H.A. Gordon²⁷, B. Gorini³², E. Gorini^{76a,76b}, A. Gorišek⁷⁸, A.T. Goshaw⁴⁸, C. Gössling⁴⁶, M.I. Gostkin⁶⁸, C.A. Gottardo²³, C.R. Goudet¹¹⁹, D. Goujdami^{137c}, A.G. Goussiou¹⁴⁰, N. Govender^{147b,t}, E. Gozani¹⁵⁴, I. Grabowska-Bold^{41a}, P.O.J. Gradin¹⁶⁸, E.C. Graham⁷⁷, J. Gramling¹⁶⁶, E. Gramstad¹²¹, S. Grancagnolo¹⁷, V. Gratchev¹²⁵, P.M. Gravila^{28f}, C. Gray⁵⁶, H.M. Gray¹⁶, Z.D. Greenwood^{82,u}, C. Grefe²³, K. Gregersen⁸¹, I.M. Gregor⁴⁵, P. Grenier¹⁴⁵, K. Grevtsov⁵, J. Griffiths⁸, A.A. Grillo¹³⁹, K. Grimm⁷⁵, S. Grinstein^{13,v}, Ph. Gris³⁷, J.-F. Grivaz¹¹⁹, S. Groh⁸⁶, E. Gross¹⁷⁵, J. Grosse-Knetter⁵⁷, G.C. Grossi⁸², Z.J. Grout⁸¹, A. Grummer¹⁰⁷, L. Guan⁹², W. Guan¹⁷⁶, J. Guenther³², F. Guescini^{163a}, D. Guest¹⁶⁶, O. Gueta¹⁵⁵, B. Gui¹¹³, E. Guido^{53a,53b}, T. Guillemin⁵, S. Guindon³², U. Gul⁵⁶, C. Gumpert³², J. Guo^{36c}, W. Guo⁹², Y. Guo^{36a,w}, R. Gupta⁴³, S. Gurbuz^{20a}, G. Gustavino¹¹⁵, B.J. Gutelman¹⁵⁴, P. Gutierrez¹¹⁵, N.G. Gutierrez Ortiz⁸¹, C. Gutsche⁸¹, C. Guyot¹³⁸, M.P. Guzik^{41a}, C. Gwenlan¹²², C.B. Gwilliam⁷⁷, A. Haas¹¹², C. Haber¹⁶, H.K. Hadavand⁸, N. Haddad^{137e}, A. Hadeef⁸⁸, S. Hageböck²³, M. Hagihara¹⁶⁴, H. Hakobyan^{180,*}, M. Haleem⁴⁵, J. Haley¹¹⁶, G. Halladjian⁹³, G.D. Hallowell⁸⁸, K. Hamacher¹⁷⁸, P. Hamal¹¹⁷, K. Hamano¹⁷², A. Hamilton^{147a}, G.N. Hamity¹⁴¹, P.G. Hamnett⁴⁵, K. Han^{36a,x}, L. Han^{36a}, S. Han^{35a,35d}, K. Hanagaki^{69,y}, K. Hanawa¹⁵⁷, M. Hance¹³⁹, D.M. Handl¹⁰², B. Haney¹²⁴, P. Hanke^{60a}, J.B. Hansen³⁹, J.D. Hansen³⁹, M.C. Hansen²³, P.H. Hansen³⁹, K. Hara¹⁶⁴, A.S. Hard¹⁷⁶, T. Harenberg¹⁷⁸, F. Hariri¹¹⁹, S. Harkusha⁹⁵, P.F. Harrison¹⁷³, N.M. Hartmann¹⁰², Y. Hasegawa¹⁴², A. Hasib⁴⁹, S. Hassani¹³⁸, S. Haug¹⁸, R. Hauser⁹³, L. Hauswald⁴⁷, L.B. Havener³⁸, M. Havranek¹³⁰, C.M. Hawkes¹⁹, R.J. Hawking³², D. Hayden⁹³, C.P. Hays¹²², J.M. Hays⁷⁹, H.S. Hayward⁷⁷, S.J. Haywood¹³³, T. Heck⁸⁶, V. Hedberg⁸⁴, L. Heelan⁸, S. Heer²³, K.K. Heidegger⁵¹, S. Heim⁴⁵, T. Heim¹⁶, B. Heinemann^{45,z}, J.J. Heinrich¹⁰², L. Heinrich¹¹², C. Heinz⁵⁵, J. Hejbal¹²⁹, L. Helary³², A. Held¹⁷¹, S. Hellman^{148a,148b}, C. Helsens³², R.C.W. Henderson⁷⁵, Y. Heng¹⁷⁶, S. Henkelmann¹⁷¹, A.M. Henriques Correia³², S. Henrot-Versille¹¹⁹, G.H. Herbert¹⁷, H. Herde²⁵, V. Herget¹⁷⁷, Y. Hernández Jiménez^{147c}, H. Herr⁸⁶, G. Herten⁵¹, R. Hertenberger¹⁰², L. Hervas³², T.C. Herwig¹²⁴, G.G. Hesketh⁸¹, N.P. Hessey^{163a}, J.W. Hetherly⁴³, S. Higashino⁶⁹, E. Higón-Rodríguez¹⁷⁰, K. Hildebrand³³, E. Hill¹⁷², J.C. Hill³⁰, K.H. Hiller⁴⁵, S.J. Hillier¹⁹, M. Hils⁴⁷, I. Hinchliffe¹⁶, M. Hirose⁵¹, D. Hirschbuehl¹⁷⁸, B. Hiti⁷⁸, O. Hladik¹²⁹, D.R. Hlaluku^{147c}, X. Hoad⁴⁹, J. Hobbs¹⁵⁰, N. Hod^{163a}, M.C. Hodgkinson¹⁴¹, P. Hodgson¹⁴¹, A. Hoecker³², M.R. Hoferkamp¹⁰⁷, F. Hoenig¹⁰², D. Hohn²³, T.R. Holmes³³, M. Holzbock¹⁰², M. Homann⁴⁶, S. Honda¹⁶⁴, T. Honda⁶⁹, T.M. Hong¹²⁷, B.H. Hooberman¹⁶⁹, W.H. Hopkins¹¹⁸, Y. Horii¹⁰⁵, A.J. Horton¹⁴⁴, J.-Y. Hostachy⁵⁸, A. Hostiuc¹⁴⁰, S. Hou¹⁵³, A. Hoummada^{137a}, J. Howarth⁸⁷, J. Hoya⁷⁴, M. Hrabovsky¹¹⁷, J. Hrdinka³², I. Hristova¹⁷, J. Hrivnac¹¹⁹, T. Hryn'ova⁵, A. Hrynevich⁹⁶, P.J. Hsu⁶³, S.-C. Hsu¹⁴⁰, Q. Hu²⁷, S. Hu^{36c}, Y. Huang^{35a}, Z. Hubacek¹³⁰, F. Hubaut⁸⁸, F. Huegging²³, T.B. Huffman¹²², E.W. Hughes³⁸, M. Huhtinen³², R.F.H. Hunter³¹, P. Huo¹⁵⁰, N. Huseynov^{68,b}, J. Huston⁹³, J. Huth⁵⁹, R. Hyneman⁹², G. Iacobucci⁵², G. Iakovidis²⁷, I. Ibragimov¹⁴³, L. Iconomidou-Fayard¹¹⁹, Z. Idrissi^{137e}, P. Iengo³², O. Igonkina^{109,aa}, T. Iizawa¹⁷⁴, Y. Ikegami⁶⁹, M. Ikeno⁶⁹, Y. Ilchenko^{11,ab}, D. Iliadis¹⁵⁶, N. Ilic¹⁴⁵, F. Iltzsche⁴⁷, G. Introzzi^{123a,123b}, P. Ioannou^{9,*}, M. Iodice^{136a}, K. Iordanidou³⁸, V. Ippolito⁵⁹, M.F. Isacson¹⁶⁸, N. Ishijima¹²⁰, M. Ishino¹⁵⁷, M. Ishitsuka¹⁵⁹, C. Issever¹²², S. Istin^{20a}, F. Ito¹⁶⁴, J.M. Iturbe Ponce^{62a}, R. Iuppa^{162a,162b}, H. Iwasaki⁶⁹, J.M. Izen⁴⁴, V. Izzo^{106a}, S. Jabbar³, P. Jackson¹, R.M. Jacobs²³, V. Jain²,

K.B. Jakobi⁸⁶, K. Jakobs⁵¹, S. Jakobsen⁶⁵, T. Jakoubek¹²⁹, D.O. Jamin¹¹⁶, D.K. Jana⁸², R. Jansky⁵², J. Janssen²³, M. Janus⁵⁷, P.A. Janus^{41a}, G. Jarlskog⁸⁴, N. Javadov^{68,b}, T. Javůrek⁵¹, M. Javurkova⁵¹, F. Jeanneau¹³⁸, L. Jeanty¹⁶, J. Jejelava^{54a,ac}, A. Jelinskas¹⁷³, P. Jenni^{51,ad}, C. Jeske¹⁷³, S. Jézéquel⁵, H. Ji¹⁷⁶, J. Jia¹⁵⁰, H. Jiang⁶⁷, Y. Jiang^{36a}, Z. Jiang¹⁴⁵, S. Jiggins⁸¹, J. Jimenez Pena¹⁷⁰, S. Jin^{35b}, A. Jinaru^{28b}, O. Jinnouchi¹⁵⁹, H. Jivan^{147c}, P. Johansson¹⁴¹, K.A. Johns⁷, C.A. Johnson⁶⁴, W.J. Johnson¹⁴⁰, K. Jon-And^{148a,148b}, R.W.L. Jones⁷⁵, S.D. Jones¹⁵¹, S. Jones⁷, T.J. Jones⁷⁷, J. Jongmanns^{60a}, P.M. Jorge^{128a,128b}, J. Jovicevic^{163a}, X. Ju¹⁷⁶, A. Juste Rozas^{13,v}, M.K. Köhler¹⁷⁵, A. Kaczmarska⁴², M. Kado¹¹⁹, H. Kagan¹¹³, M. Kagan¹⁴⁵, S.J. Kahn⁸⁸, T. Kaji¹⁷⁴, E. Kajomovitz¹⁵⁴, C.W. Kalderon⁸⁴, A. Kaluza⁸⁶, S. Kama⁴³, A. Kamenshchikov¹³², N. Kanaya¹⁵⁷, L. Kanjir⁷⁸, V.A. Kantserov¹⁰⁰, J. Kanzaki⁶⁹, B. Kaplan¹¹², L.S. Kaplan¹⁷⁶, D. Kar^{147c}, K. Karakostas¹⁰, N. Karastathis¹⁰, M.J. Kareem^{163b}, E. Karentzos¹⁰, S.N. Karpov⁶⁸, Z.M. Karpova⁶⁸, V. Kartvelishvili⁷⁵, A.N. Karyukhin¹³², K. Kasahara¹⁶⁴, L. Kashif¹⁷⁶, R.D. Kass¹¹³, A. Kastanas¹⁴⁹, Y. Kataoka¹⁵⁷, C. Kato¹⁵⁷, A. Katre⁵², J. Katzy⁴⁵, K. Kawade⁷⁰, K. Kawagoe⁷³, T. Kawamoto¹⁵⁷, G. Kawamura⁵⁷, E.F. Kay⁷⁷, V.F. Kazanin^{111,c}, R. Keeler¹⁷², R. Kehoe⁴³, J.S. Keller³¹, E. Kellermann⁸⁴, J.J. Kempster⁸⁰, J. Kendrick¹⁹, H. Keoshkerian¹⁶¹, O. Kepka¹²⁹, B.P. Kerševan⁷⁸, S. Kersten¹⁷⁸, R.A. Keyes⁹⁰, M. Khader¹⁶⁹, F. Khalil-zada¹², A. Khanov¹¹⁶, A.G. Kharlamov^{111,c}, T. Kharlamova^{111,c}, A. Khodinov¹⁶⁰, T.J. Khoo⁵², V. Khovanskiy^{99,*}, E. Khramov⁶⁸, J. Khubua^{54b,ae}, S. Kido⁷⁰, C.R. Kilby⁸⁰, H.Y. Kim⁸, S.H. Kim¹⁶⁴, Y.K. Kim³³, N. Kimura¹⁵⁶, O.M. Kind¹⁷, B.T. King⁷⁷, D. Kirchmeier⁴⁷, J. Kirk¹³³, A.E. Kiryunin¹⁰³, T. Kishimoto¹⁵⁷, D. Kisieleska^{41a}, V. Kitali⁴⁵, O. Kivernyk⁵, E. Kladiva^{146b}, T. Klapdor-Kleingrothaus⁵¹, M.H. Klein⁹², M. Klein⁷⁷, U. Klein⁷⁷, K. Kleinknecht⁸⁶, P. Klimek¹¹⁰, A. Klimentov²⁷, R. Klingenberg^{46,*}, T. Klingl²³, T. Klioutchnikova³², F.F. Klitzner¹⁰², E.-E. Kluge^{60a}, P. Kluit¹⁰⁹, S. Kluth¹⁰³, E. Kneringer⁶⁵, E.B.F.G. Knoops⁸⁸, A. Knue¹⁰³, A. Kobayashi¹⁵⁷, D. Kobayashi⁷³, T. Kobayashi¹⁵⁷, M. Kobel⁴⁷, M. Kocian¹⁴⁵, P. Kodys¹³¹, T. Koffas³¹, E. Koffeman¹⁰⁹, N.M. Köhler¹⁰³, T. Koi¹⁴⁵, M. Kolb^{60b}, I. Koletsou⁵, T. Kondo⁶⁹, N. Kondrashova^{36c}, K. Köneke⁵¹, A.C. König¹⁰⁸, T. Kono^{69,af}, R. Konoplich^{112,ag}, N. Konstantinidis⁸¹, B. Konya⁸⁴, R. Kopeliansky⁶⁴, S. Koperny^{41a}, K. Korcyl⁴², K. Kordas¹⁵⁶, A. Korn⁸¹, I. Korolkov¹³, E.V. Korolkova¹⁴¹, O. Kortner¹⁰³, S. Kortner¹⁰³, T. Kosek¹³¹, V.V. Kostyukhin²³, A. Kotwal⁴⁸, A. Koulouris¹⁰, A. Kourkoulouli-Charalampidi^{123a,123b}, C. Kourkoulouli⁹, E. Kourlitis¹⁴¹, V. Kouskoura²⁷, A.B. Kowalewska⁴², R. Kowalewski¹⁷², T.Z. Kowalski^{41a}, C. Kozakai¹⁵⁷, W. Kozanecki¹³⁸, A.S. Kozhin¹³², V.A. Kramarenko¹⁰¹, G. Kramberger⁷⁸, D. Krasnopevtsev¹⁰⁰, M.W. Krasny⁸³, A. Krasznahorkay³², D. Krauss¹⁰³, J.A. Kremer^{41a}, J. Kretschmar⁷⁷, K. Kreutzfeldt⁵⁵, P. Krieger¹⁶¹, K. Krizka¹⁶, K. Kroeninger⁴⁶, H. Kroha¹⁰³, J. Kroll¹²⁹, J. Kroll¹²⁴, J. Kroseberg²³, J. Krstic¹⁴, U. Kruchonak⁶⁸, H. Krüger²³, N. Krumnack⁶⁷, M.C. Kruse⁴⁸, T. Kubota⁹¹, H. Kucuk⁸¹, S. Kuday^{4b}, J.T. Kuechler¹⁷⁸, S. Kuehn³², A. Kugel^{60a}, F. Kuger¹⁷⁷, T. Kuhl⁴⁵, V. Kukhtin⁶⁸, R. Kukla⁸⁸, Y. Kulchitsky⁹⁵, S. Kuleshov^{34b}, Y.P. Kulinich¹⁶⁹, M. Kuna¹¹, T. Kunigo⁷¹, A. Kupco¹²⁹, T. Kupfer⁴⁶, O. Kuprash¹⁵⁵, H. Kurashige⁷⁰, L.L. Kurchaninov^{163a}, Y.A. Kurochkin⁹⁵, M.G. Kurth^{35a,35d}, E.S. Kuwertz¹⁷², M. Kuze¹⁵⁹, J. Kvita¹¹⁷, T. Kwan¹⁷², D. Kyriazopoulos¹⁴¹, A. La Rosa¹⁰³, J.L. La Rosa Navarro^{26d}, L. La Rotonda^{40a,40b}, F. La Ruffa^{40a,40b}, C. Lacasta¹⁷⁰, F. Lacava^{134a,134b}, J. Lacey⁴⁵, D.P.J. Lack⁸⁷, H. Lacker¹⁷, D. Lacour⁸³, E. Ladygin⁶⁸, R. Lafaye⁵, B. Laforge⁸³, S. Lai⁵⁷, S. Lammers⁶⁴, W. Lampl⁷, E. Lançon²⁷, U. Landgraf⁵¹, M.P.J. Landon⁷⁹, M.C. Lanfermann⁵², V.S. Lang⁴⁵, J.C. Lange¹³, R.J. Langenberg³², A.J. Lankford¹⁶⁶, F. Lanni²⁷, K. Lantzsch²³, A. Lanza^{123a}, A. Lapertosa^{53a,53b}, S. Laplace⁸³, J.F. Laporte¹³⁸, T. Lari^{94a}, F. Lasagni Manghi^{22a,22b}, M. Lassnig³², T.S. Lau^{62a}, P. Laurelli⁵⁰, W. Lavrijsen¹⁶, A.T. Law¹³⁹, P. Laycock⁷⁷, T. Lazovich⁵⁹, M. Lazzaroni^{94a,94b}, B. Le⁹¹, O. Le Dortz⁸³, E. Le Guirriec⁸⁸, E.P. Le Quilleuc¹³⁸, M. LeBlanc⁷, T. LeCompte⁶, F. Ledroit-Guillon⁵⁸, C.A. Lee²⁷, G.R. Lee^{34a}, S.C. Lee¹⁵³, L. Lee⁵⁹, B. Lefebvre⁹⁰, G. Lefebvre⁸³, M. Lefebvre¹⁷², F. Legger¹⁰², C. Leggett¹⁶, G. Lehmann Miotto³², X. Lei⁷, W.A. Leight⁴⁵, M.A.L. Leite^{26d}, R. Leitner¹³¹, D. Lellouch¹⁷⁵, B. Lemmer⁵⁷, K.J.C. Leney⁸¹, T. Lenz²³, B. Lenzi³², R. Leone⁷, S. Leone^{126a}, C. Leonidopoulos⁴⁹, G. Lerner¹⁵¹, C. Leroy⁹⁷, R. Les¹⁶¹, A.A.J. Lesage¹³⁸, C.G. Lester³⁰, M. Levchenko¹²⁵, J. Levêque⁵, D. Levin⁹², L.J. Levinson¹⁷⁵, M. Levy¹⁹, D. Lewis⁷⁹, B. Li^{36a,w}, H. Li¹⁵⁰, L. Li^{36c}, Q. Li^{35a,35d}, Q. Li^{36a}, S. Li⁴⁸, X. Li^{36c}, Y. Li¹⁴³, Z. Liang^{35a}, B. Liberti^{135a}, A. Liblong¹⁶¹, K. Lie^{62c}, W. Liebig¹⁵, A. Limosani¹⁵², C.Y. Lin³⁰, K. Lin⁹³, S.C. Lin¹⁸², T.H. Lin⁸⁶, R.A. Linck⁶⁴, B.E. Lindquist¹⁵⁰, A.E. Lioni⁵², E. Lipeles¹²⁴, A. Lipniacka¹⁵, M. Lisovsky^{60b}, T.M. Liss^{169,ah}, A. Lister¹⁷¹, A.M. Litke¹³⁹, B. Liu⁶⁷, H. Liu⁹², H. Liu²⁷, J.K.K. Liu¹²², J. Liu^{36b}, J.B. Liu^{36a}, K. Liu⁸⁸, L. Liu¹⁶⁹, M. Liu^{36a}, Y.L. Liu^{36a}, Y. Liu^{36a}, M. Livan^{123a,123b}, A. Lleres⁵⁸, J. Llorente Merino^{35a},

S.L. Lloyd⁷⁹, C.Y. Lo^{62b}, F. Lo Sterzo⁴³, E.M. Lobodzinska⁴⁵, P. Loch⁷, F.K. Loebinger⁸⁷, A. Loesle⁵¹, K.M. Loew²⁵, T. Lohse¹⁷, K. Lohwasser¹⁴¹, M. Lokajicek¹²⁹, B.A. Long²⁴, J.D. Long¹⁶⁹, R.E. Long⁷⁵, L. Longo^{76a,76b}, K.A. Looper¹¹³, J.A. Lopez^{34b}, I. Lopez Paz¹³, A. Lopez Solis⁸³, J. Lorenz¹⁰², N. Lorenzo Martinez⁵, M. Losada²¹, P.J. Lösel¹⁰², X. Lou^{35a}, A. Lounis¹¹⁹, J. Love⁶, P.A. Love⁷⁵, H. Lu^{62a}, N. Lu⁹², Y.J. Lu⁶³, H.J. Lubatti¹⁴⁰, C. Luci^{134a,134b}, A. Lucotte⁵⁸, C. Luedtke⁵¹, F. Luehring⁶⁴, W. Lukas⁶⁵, L. Luminari^{134a}, B. Lund-Jensen¹⁴⁹, M.S. Lutz⁸⁹, P.M. Luzi⁸³, D. Lynn²⁷, R. Lysak¹²⁹, E. Lytken⁸⁴, F. Lyu^{35a}, V. Lyubushkin⁶⁸, H. Ma²⁷, L.L. Ma^{36b}, Y. Ma^{36b}, G. Maccarrone⁵⁰, A. Macchiolo¹⁰³, C.M. Macdonald¹⁴¹, B. Maček⁷⁸, J. Machado Miguens^{124,128b}, D. Madaffari¹⁷⁰, R. Madar³⁷, W.F. Mader⁴⁷, A. Madsen⁴⁵, N. Madysa⁴⁷, J. Maeda⁷⁰, S. Maeland¹⁵, T. Maeno²⁷, A.S. Maevskiy¹⁰¹, V. Magerl⁵¹, C. Maiani¹¹⁹, C. Maidantchik^{26a}, T. Maier¹⁰², A. Maio^{128a,128b,128d}, O. Majersky^{146a}, S. Majewski¹¹⁸, Y. Makida⁶⁹, N. Makovec¹¹⁹, B. Malaescu⁸³, Pa. Malecki⁴², V.P. Maleev¹²⁵, F. Malek⁵⁸, U. Mallik⁶⁶, D. Malon⁶, C. Malone³⁰, S. Maltezos¹⁰, S. Malyukov³², J. Mamuzic¹⁷⁰, G. Mancini⁵⁰, I. Mandić⁷⁸, J. Maneira^{128a,128b}, L. Manhaes de Andrade Filho^{26b}, J. Manjarres Ramos⁴⁷, K.H. Mankinen⁸⁴, A. Mann¹⁰², A. Manousos³², B. Mansoulie¹³⁸, J.D. Mansour^{35a}, R. Mantifel⁹⁰, M. Mantoani⁵⁷, S. Manzoni^{94a,94b}, L. Mapelli³², G. Marceca²⁹, L. March⁵², L. Marchese¹²², G. Marchiori⁸³, M. Marcisovsky¹²⁹, C.A. Marin Tobon³², M. Marjanovic³⁷, D.E. Marley⁹², F. Marroquim^{26a}, S.P. Marsden⁸⁷, Z. Marshall¹⁶, M.U.F. Martensson¹⁶⁸, S. Marti-Garcia¹⁷⁰, C.B. Martin¹¹³, T.A. Martin¹⁷³, V.J. Martin⁴⁹, B. Martin dit Latour¹⁵, M. Martinez^{13,v}, V.I. Martinez Outschoorn¹⁶⁹, S. Martin-Haugh¹³³, V.S. Martoiu^{28b}, A.C. Martyniuk⁸¹, A. Marzin³², L. Masetti⁸⁶, T. Mashimo¹⁵⁷, R. Mashinistov⁹⁸, J. Masik⁸⁷, A.L. Maslennikov^{111,c}, L.H. Mason⁹¹, L. Massa^{135a,135b}, P. Mastrandrea⁵, A. Mastroberardino^{40a,40b}, T. Masubuchi¹⁵⁷, P. Mättig¹⁷⁸, J. Maurer^{28b}, S.J. Maxfield⁷⁷, D.A. Maximov^{111,c}, R. Mazini¹⁵³, I. Maznas¹⁵⁶, S.M. Mazza^{94a,94b}, N.C. Mc Fadden¹⁰⁷, G. Mc Goldrick¹⁶¹, S.P. Mc Kee⁹², A. McCarn⁹², R.L. McCarthy¹⁵⁰, T.G. McCarthy¹⁰³, L.I. McClymont⁸¹, E.F. McDonald⁹¹, J.A. Mcfayden³², G. Mchedlidze⁵⁷, S.J. McMahon¹³³, P.C. McNamara⁹¹, C.J. McNicol¹⁷³, R.A. McPherson^{172,o}, S. Meehan¹⁴⁰, T.J. Megy⁵¹, S. Mehlhase¹⁰², A. Mehta⁷⁷, T. Meideck⁵⁸, K. Meier^{60a}, B. Meirose⁴⁴, D. Melini^{170,ai}, B.R. Mellado Garcia^{147c}, J.D. Mellenthin⁵⁷, M. Melo^{146a}, F. Meloni¹⁸, A. Melzer²³, S.B. Menary⁸⁷, L. Meng⁷⁷, X.T. Meng⁹², A. Mengarelli^{22a,22b}, S. Menke¹⁰³, E. Meoni^{40a,40b}, S. Mergelmeyer¹⁷, C. Merlassino¹⁸, P. Mermod⁵², L. Merola^{106a,106b}, C. Meroni^{94a}, F.S. Merritt³³, A. Messina^{134a,134b}, J. Metcalfe⁶, A.S. Mete¹⁶⁶, C. Meyer¹²⁴, J-P. Meyer¹³⁸, J. Meyer¹⁰⁹, H. Meyer Zu Theenhausen^{60a}, F. Miano¹⁵¹, R.P. Middleton¹³³, S. Miglioranza^{53a,53b}, L. Mijović⁴⁹, G. Mikenberg¹⁷⁵, M. Mikestikova¹²⁹, M. Mikuž⁷⁸, M. Milesi⁹¹, A. Milic¹⁶¹, D.A. Millar⁷⁹, D.W. Miller³³, C. Mills⁴⁹, A. Milov¹⁷⁵, D.A. Milstead^{148a,148b}, A.A. Minaenko¹³², Y. Minami¹⁵⁷, I.A. Minashvili^{54b}, A.I. Mincer¹¹², B. Mindur^{41a}, M. Mineev⁶⁸, Y. Minegishi¹⁵⁷, Y. Ming¹⁷⁶, L.M. Mir¹³, A. Mirto^{76a,76b}, K.P. Mistry¹²⁴, T. Mitani¹⁷⁴, J. Mitrevski¹⁰², V.A. Mitsou¹⁷⁰, A. Miucci¹⁸, P.S. Miyagawa¹⁴¹, A. Mizukami⁶⁹, J.U. Mjörnmark⁸⁴, T. Mkrtchyan¹⁸⁰, M. Mlynarikova¹³¹, T. Moa^{148a,148b}, K. Mochizuki⁹⁷, P. Mogg⁵¹, S. Mohapatra³⁸, S. Molander^{148a,148b}, R. Moles-Valls²³, M.C. Mondragon⁹³, K. Mönig⁴⁵, J. Monk³⁹, E. Monnier⁸⁸, A. Montalbano¹⁵⁰, J. Montejo Berlingen³², F. Monticelli⁷⁴, S. Monzani^{94a}, R.W. Moore³, N. Morange¹¹⁹, D. Moreno²¹, M. Moreno Llácer³², P. Morettini^{53a}, M. Morgenstern¹⁰⁹, S. Morgenstern³², D. Mori¹⁴⁴, T. Mori¹⁵⁷, M. Morii⁵⁹, M. Morinaga¹⁷⁴, V. Morisbak¹²¹, A.K. Morley³², G. Mornacchi³², J.D. Morris⁷⁹, L. Morvaj¹⁵⁰, P. Moschovakos¹⁰, M. Mosidze^{54b}, H.J. Moss¹⁴¹, J. Moss^{145,aj}, K. Motohashi¹⁵⁹, R. Mount¹⁴⁵, E. Mountricha²⁷, E.J.W. Moyse⁸⁹, S. Muanza⁸⁸, F. Mueller¹⁰³, J. Mueller¹²⁷, R.S.P. Mueller¹⁰², D. Muenstermann⁷⁵, P. Mullen⁵⁶, G.A. Mullier¹⁸, F.J. Munoz Sanchez⁸⁷, W.J. Murray^{173,133}, H. Musheghyan³², M. Muškinja⁷⁸, C. Mwewa^{147a}, A.G. Myagkov^{132,ak}, M. Myska¹³⁰, B.P. Nachman¹⁶, O. Nackenhorst⁵², K. Nagai¹²², R. Nagai^{69,af}, K. Nagano⁶⁹, Y. Nagasaka⁶¹, K. Nagata¹⁶⁴, M. Nagel⁵¹, E. Nagy⁸⁸, A.M. Nairz³², Y. Nakahama¹⁰⁵, K. Nakamura⁶⁹, T. Nakamura¹⁵⁷, I. Nakano¹¹⁴, R.F. Naranjo Garcia⁴⁵, R. Narayan¹¹, D.I. Narrias Villar^{60a}, I. Naryshkin¹²⁵, T. Naumann⁴⁵, G. Navarro²¹, R. Nayyar⁷, H.A. Neal⁹², P.Yu. Nechaeva⁹⁸, T.J. Neep¹³⁸, A. Negri^{123a,123b}, M. Negrini^{22a}, S. Nektarijevic¹⁰⁸, C. Nellist⁵⁷, A. Nelson¹⁶⁶, M.E. Nelson¹²², S. Nemecek¹²⁹, P. Nemethy¹¹², M. Nessi^{32,al}, M.S. Neubauer¹⁶⁹, M. Neumann¹⁷⁸, P.R. Newman¹⁹, T.Y. Ng^{62c}, Y.S. Ng¹⁷, T. Nguyen Manh⁹⁷, R.B. Nickerson¹²², R. Nicolaïdou¹³⁸, J. Nielsen¹³⁹, N. Nikiforou¹¹, V. Nikolaenko^{132,ak}, I. Nikolic-Audit⁸³, K. Nikolopoulos¹⁹, P. Nilsson²⁷, Y. Ninomiya⁶⁹, A. Nisati^{134a},

N. Nishu^{36c}, R. Nisius¹⁰³, I. Nitsche⁴⁶, T. Nitta¹⁷⁴, T. Nobe¹⁵⁷, Y. Noguchi⁷¹, M. Nomachi¹²⁰, I. Nomidis³¹, M.A. Nomura²⁷, T. Nooney⁷⁹, M. Nordberg³², N. Norjoharuddeen¹²², O. Novgorodova⁴⁷, M. Nozaki⁶⁹, L. Nozka¹¹⁷, K. Ntekas¹⁶⁶, E. Nurse⁸¹, F. Nuti⁹¹, K. O'Connor²⁵, D.C. O'Neil¹⁴⁴, A.A. O'Rourke⁴⁵, V. O'Shea⁵⁶, F.G. Oakham^{31,d}, H. Oberlack¹⁰³, T. Obermann²³, J. Ocariz⁸³, A. Ochi⁷⁰, I. Ochoa³⁸, J.P. Ochoa-Ricoux^{34a}, S. Oda⁷³, S. Odaka⁶⁹, A. Oh⁸⁷, S.H. Oh⁴⁸, C.C. Ohm¹⁴⁹, H. Ohman¹⁶⁸, H. Oide^{53a,53b}, H. Okawa¹⁶⁴, Y. Okumura¹⁵⁷, T. Okuyama⁶⁹, A. Olariu^{28b}, L.F. Oleiro Seabra^{128a}, S.A. Olivares Pino^{34a}, D. Oliveira Damazio²⁷, M.J.R. Olsson³³, A. Olszewski⁴², J. Olszowska⁴², A. Onofre^{128a,128e}, K. Onogi¹⁰⁵, P.U.E. Onyisi^{11,ab}, H. Oppen¹²¹, M.J. Oreglia³³, Y. Oren¹⁵⁵, D. Orestano^{136a,136b}, N. Orlando^{62b}, R.S. Orr¹⁶¹, B. Osculati^{53a,53b,*}, R. Ospanov^{36a}, G. Otero y Garzon²⁹, H. Otono⁷³, M. Ouchrif^{137d}, F. Ould-Saada¹²¹, A. Ouraou¹³⁸, K.P. Oussoren¹⁰⁹, Q. Ouyang^{35a}, M. Owen⁵⁶, R.E. Owen¹⁹, V.E. Ozcan^{20a}, N. Ozturk⁸, K. Pachal¹⁴⁴, A. Pacheco Pages¹³, L. Pacheco Rodriguez¹³⁸, C. Padilla Aranda¹³, S. Pagan Griso¹⁶, M. Paganini¹⁷⁹, F. Paige²⁷, G. Palacino⁶⁴, S. Palazzo^{40a,40b}, S. Palestini³², M. Palka^{41b}, D. Pallin³⁷, E. St. Panagiotopoulou¹⁰, I. Panagoulas¹⁰, C.E. Pandini⁵², J.G. Panduro Vazquez⁸⁰, P. Pani³², S. Panitkin²⁷, D. Pantea^{28b}, L. Paolozzi⁵², Th.D. Papadopoulos¹⁰, K. Papageorgiou^{9,s}, A. Paramonov⁶, D. Paredes Hernandez¹⁷⁹, A.J. Parker⁷⁵, M.A. Parker³⁰, K.A. Parker⁴⁵, F. Parodi^{53a,53b}, J.A. Parsons³⁸, U. Parzefall⁵¹, V.R. Pascuzzi¹⁶¹, J.M. Pasner¹³⁹, E. Pasqualucci^{134a}, S. Passaggio^{53a}, Fr. Pastore⁸⁰, S. Patariaia⁸⁶, J.R. Pater⁸⁷, T. Pauly³², B. Pearson¹⁰³, S. Pedraza Lopez¹⁷⁰, R. Pedro^{128a,128b}, S.V. Peleganchuk^{111,c}, O. Penc¹²⁹, C. Peng^{35a,35d}, H. Peng^{36a}, J. Penwell⁶⁴, B.S. Peralva^{26b}, M.M. Perego¹³⁸, D.V. Perepelitsa²⁷, F. Peri¹⁷, L. Perini^{94a,94b}, H. Pernegger³², S. Perrella^{106a,106b}, R. Peschke⁴⁵, V.D. Peshekhonov^{68,*}, K. Peters⁴⁵, R.F.Y. Peters⁸⁷, B.A. Petersen³², T.C. Petersen³⁹, E. Petit⁵⁸, A. Petridis¹, C. Petridou¹⁵⁶, P. Petroff¹¹⁹, E. Petrolo^{134a}, M. Petrov¹²², F. Petrucci^{136a,136b}, N.E. Pettersson⁸⁹, A. Peyaud¹³⁸, R. Pezoa^{34b}, F.H. Phillips⁹³, P.W. Phillips¹³³, G. Piacquadio¹⁵⁰, E. Pianori¹⁷³, A. Picazio⁸⁹, M.A. Pickering¹²², R. Piegaia²⁹, J.E. Pilcher³³, A.D. Pilkington⁸⁷, M. Pinamonti^{135a,135b}, J.L. Pinfold³, H. Pirumov⁴⁵, M. Pitt¹⁷⁵, L. Plazak^{146a}, M.-A. Pleier²⁷, V. Pleskot⁸⁶, E. Plotnikova⁶⁸, D. Pluth⁶⁷, P. Podberezko¹¹¹, R. Poettgen⁸⁴, R. Poggi^{123a,123b}, L. Poggioli¹¹⁹, I. Pogrebnnyak⁹³, D. Pohl²³, I. Pokharel⁵⁷, G. Polesello^{123a}, A. Poley⁴⁵, A. Policicchio^{40a,40b}, R. Polifka³², A. Polini^{22a}, C.S. Pollard⁵⁶, V. Polychronakos²⁷, K. Pommès³², D. Ponomarenko¹⁰⁰, L. Pontecorvo^{134a}, G.A. Popeneciu^{28d}, D.M. Portillo Quintero⁸³, S. Pospisil¹³⁰, K. Potamianos⁴⁵, I.N. Potrap⁶⁸, C.J. Potter³⁰, H. Potti¹¹, T. Poulsen⁸⁴, J. Poveda³², M.E. Pozo Astigarraga³², P. Pralavorio⁸⁸, A. Pranko¹⁶, S. Prell⁶⁷, D. Price⁸⁷, M. Primavera^{76a}, S. Prince⁹⁰, N. Proklova¹⁰⁰, K. Prokofiev^{62c}, F. Prokoshin^{34b}, S. Protopopescu²⁷, J. Proudfoot⁶, M. Przybycien^{41a}, A. Puri¹⁶⁹, P. Puzo¹¹⁹, J. Qian⁹², Y. Qin⁸⁷, A. Quadt⁵⁷, M. Queitsch-Maitland⁴⁵, D. Quilty⁵⁶, S. Raddum¹²¹, V. Radeka²⁷, V. Radescu¹²², S.K. Radhakrishnan¹⁵⁰, P. Radloff¹¹⁸, P. Rados⁹¹, F. Ragusa^{94a,94b}, G. Rahal¹⁸¹, J.A. Raine⁸⁷, S. Rajagopalan²⁷, C. Rangel-Smith¹⁶⁸, T. Rashid¹¹⁹, S. Raspopov⁵, M.G. Ratti^{94a,94b}, D.M. Rauch⁴⁵, F. Rauscher¹⁰², S. Rave⁸⁶, I. Ravinovich¹⁷⁵, J.H. Rawling⁸⁷, M. Raymond³², A.L. Read¹²¹, N.P. Readoff⁵⁸, M. Reale^{76a,76b}, D.M. Rebuszi^{123a,123b}, A. Redelbach¹⁷⁷, G. Redlinger²⁷, R. Reece¹³⁹, R.G. Reed^{147c}, K. Reeves⁴⁴, L. Rehnisch¹⁷, J. Reichert¹²⁴, A. Reiss⁸⁶, C. Rembser³², H. Ren^{35a,35d}, M. Rescigno^{134a}, S. Resconi^{94a}, E.D. Resseguie¹²⁴, S. Rettie¹⁷¹, E. Reynolds¹⁹, O.L. Rezanova^{111,c}, P. Reznicek¹³¹, R. Rezvani⁹⁷, R. Richter¹⁰³, S. Richter⁸¹, E. Richter-Was^{41b}, O. Ricken²³, M. Ridel⁸³, P. Rieck¹⁰³, C.J. Riegel¹⁷⁸, J. Rieger⁵⁷, O. Rifki¹¹⁵, M. Rijssenbeek¹⁵⁰, A. Rimoldi^{123a,123b}, M. Rimoldi¹⁸, L. Rinaldi^{22a}, G. Ripellino¹⁴⁹, B. Ristić³², E. Ritsch³², I. Riu¹³, F. Rizatdinova¹¹⁶, E. Rizvi⁷⁹, C. Rizzi¹³, R.T. Roberts⁸⁷, S.H. Robertson^{90,o}, A. Robichaud-Veronneau⁹⁰, D. Robinson³⁰, J.E.M. Robinson⁴⁵, A. Robson⁵⁶, E. Rocco⁸⁶, C. Roda^{126a,126b}, Y. Rodina^{88,am}, S. Rodriguez Bosca¹⁷⁰, A. Rodriguez Perez¹³, D. Rodriguez Rodriguez¹⁷⁰, S. Roe³², C.S. Rogan⁵⁹, O. Røhne¹²¹, J. Roloff⁵⁹, A. Romaniouk¹⁰⁰, M. Romano^{22a,22b}, S.M. Romano Saez³⁷, E. Romero Adam¹⁷⁰, N. Rompotis⁷⁷, M. Ronzani⁵¹, L. Roos⁸³, S. Rosati^{134a}, K. Rosbach⁵¹, P. Rose¹³⁹, N.-A. Rosien⁵⁷, E. Rossi^{106a,106b}, L.P. Rossi^{53a}, J.H.N. Rosten³⁰, R. Rosten¹⁴⁰, M. Rotaru^{28b}, J. Rothberg¹⁴⁰, D. Rousseau¹¹⁹, D. Roy^{147c}, A. Rozanov⁸⁸, Y. Rozen¹⁵⁴, X. Ruan^{147c}, F. Rubbo¹⁴⁵, F. Rühr⁵¹, A. Ruiz-Martinez³¹, Z. Rurikova⁵¹, N.A. Rusakovich⁶⁸, H.L. Russell⁹⁰, J.P. Rutherford⁷, N. Ruthmann³², E.M. Rüttinger⁴⁵, Y.F. Ryabov¹²⁵, M. Rybar¹⁶⁹, G. Rybkin¹¹⁹, S. Ryu⁶, A. Ryzhov¹³², G.F. Rzehorz⁵⁷, A.F. Saavedra¹⁵², G. Sabato¹⁰⁹, S. Sacerdoti²⁹, H.F.-W. Sadrozinski¹³⁹, R. Sadykov⁶⁸, F. Safai Tehrani^{134a}, P. Saha¹¹⁰, M. Sahinsoy^{60a}, M. Saimpert⁴⁵, M. Saito¹⁵⁷, T. Saito¹⁵⁷, H. Sakamoto¹⁵⁷,

Y. Sakurai ¹⁷⁴, G. Salamanna ^{136a,136b}, J.E. Salazar Loyola ^{34b}, D. Salek ¹⁰⁹, P.H. Sales De Bruin ¹⁶⁸, D. Saliagic ¹⁰³, A. Salnikov ¹⁴⁵, J. Salt ¹⁷⁰, D. Salvatore ^{40a,40b}, F. Salvatore ¹⁵¹, A. Salvucci ^{62a,62b,62c}, A. Salzburger ³², D. Sammel ⁵¹, D. Sampsonidis ¹⁵⁶, D. Sampsonidou ¹⁵⁶, J. Sánchez ¹⁷⁰, A. Sanchez Pineda ^{167a,167c}, H. Sandaker ¹²¹, R.L. Sandbach ⁷⁹, C.O. Sander ⁴⁵, M. Sandhoff ¹⁷⁸, C. Sandoval ²¹, D.P.C. Sankey ¹³³, M. Sannino ^{53a,53b}, Y. Sano ¹⁰⁵, A. Sansoni ⁵⁰, C. Santoni ³⁷, H. Santos ^{128a}, I. Santoyo Castillo ¹⁵¹, A. Saponov ⁶⁸, J.G. Saraiva ^{128a,128d}, O. Sasaki ⁶⁹, K. Sato ¹⁶⁴, E. Sauvan ⁵, G. Savage ⁸⁰, P. Savard ^{161,d}, N. Savic ¹⁰³, C. Sawyer ¹³³, L. Sawyer ^{82,u}, C. Sbarra ^{22a}, A. Sbrizzi ^{22a,22b}, T. Scanlon ⁸¹, D.A. Scannicchio ¹⁶⁶, J. Schaarschmidt ¹⁴⁰, P. Schacht ¹⁰³, B.M. Schachtner ¹⁰², D. Schaefer ³³, L. Schaefer ¹²⁴, J. Schaeffer ⁸⁶, S. Schaepe ³², S. Schaezel ^{60b}, U. Schäfer ⁸⁶, A.C. Schaffer ¹¹⁹, D. Schaile ¹⁰², R.D. Schamberger ¹⁵⁰, V.A. Schegelsky ¹²⁵, D. Scheirich ¹³¹, F. Schenck ¹⁷, M. Schernau ¹⁶⁶, C. Schiavi ^{53a,53b}, S. Schier ¹³⁹, L.K. Schildgen ²³, C. Schillo ⁵¹, M. Schioppa ^{40a,40b}, S. Schlenker ³², K.R. Schmidt-Sommerfeld ¹⁰³, K. Schmieden ³², C. Schmitt ⁸⁶, S. Schmitt ⁴⁵, S. Schmitz ⁸⁶, U. Schnoor ⁵¹, L. Schoeffel ¹³⁸, A. Schoening ^{60b}, B.D. Schoenrock ⁹³, E. Schopf ²³, M. Schott ⁸⁶, J.F.P. Schouwenberg ¹⁰⁸, J. Schovancova ³², S. Schramm ⁵², N. Schuh ⁸⁶, A. Schulte ⁸⁶, M.J. Schultens ²³, H.-C. Schultz-Coulon ^{60a}, M. Schumacher ⁵¹, B.A. Schumm ¹³⁹, Ph. Schune ¹³⁸, A. Schwartzman ¹⁴⁵, T.A. Schwarz ⁹², H. Schweiger ⁸⁷, Ph. Schwemling ¹³⁸, R. Schwenhorst ⁹³, J. Schwindling ¹³⁸, A. Sciandra ²³, G. Sciolla ²⁵, M. Scornajenghi ^{40a,40b}, F. Scuri ^{126a}, F. Scutti ⁹¹, J. Searcy ⁹², P. Seema ²³, S.C. Seidel ¹⁰⁷, A. Seiden ¹³⁹, J.M. Seixas ^{26a}, G. Sekhniaidze ^{106a}, K. Sekhon ⁹², S.J. Sekula ⁴³, N. Semprini-Cesari ^{22a,22b}, S. Senkin ³⁷, C. Serfon ¹²¹, L. Serin ¹¹⁹, L. Serkin ^{167a,167b}, M. Sessa ^{136a,136b}, R. Seuster ¹⁷², H. Severini ¹¹⁵, T. Šfiligoi ⁷⁸, F. Sforza ¹⁶⁵, A. Sfyrila ⁵², E. Shabalina ⁵⁷, N.W. Shaikh ^{148a,148b}, L.Y. Shan ^{35a}, R. Shang ¹⁶⁹, J.T. Shank ²⁴, M. Shapiro ¹⁶, P.B. Shatalov ⁹⁹, K. Shaw ^{167a,167b}, S.M. Shaw ⁸⁷, A. Shcherbakova ^{148a,148b}, C.Y. Shehu ¹⁵¹, Y. Shen ¹¹⁵, N. Sherafati ³¹, A.D. Sherman ²⁴, P. Sherwood ⁸¹, L. Shi ^{153,an}, S. Shimizu ⁷⁰, C.O. Shimmin ¹⁷⁹, M. Shimojima ¹⁰⁴, I.P.J. Shipsey ¹²², S. Shirabe ⁷³, M. Shiyakova ^{68,ao}, J. Shlomi ¹⁷⁵, A. Shmeleva ⁹⁸, D. Shoaleh Saadi ⁹⁷, M.J. Shochet ³³, S. Shojaii ^{94a,94b}, D.R. Shope ¹¹⁵, S. Shrestha ¹¹³, E. Shulga ¹⁰⁰, M.A. Shupe ⁷, P. Sicho ¹²⁹, A.M. Sickles ¹⁶⁹, P.E. Sidebo ¹⁴⁹, E. Sideras Haddad ^{147c}, O. Sidiropoulou ¹⁷⁷, A. Sidoti ^{22a,22b}, F. Siegert ⁴⁷, Dj. Sijacki ¹⁴, J. Silva ^{128a,128d}, S.B. Silverstein ^{148a}, V. Simak ¹³⁰, L. Simic ⁶⁸, S. Simion ¹¹⁹, E. Simioni ⁸⁶, B. Simmons ⁸¹, M. Simon ⁸⁶, P. Sinervo ¹⁶¹, N.B. Sinev ¹¹⁸, M. Sioli ^{22a,22b}, G. Siragusa ¹⁷⁷, I. Siral ⁹², S.Yu. Sivoklov ¹⁰¹, J. Sjölín ^{148a,148b}, M.B. Skinner ⁷⁵, P. Skubic ¹¹⁵, M. Slater ¹⁹, T. Slavicek ¹³⁰, M. Slawinska ⁴², K. Sliwa ¹⁶⁵, R. Slovak ¹³¹, V. Smakhtin ¹⁷⁵, B.H. Smart ⁵, J. Smiesko ^{146a}, N. Smirnov ¹⁰⁰, S.Yu. Smirnov ¹⁰⁰, Y. Smirnov ¹⁰⁰, L.N. Smirnova ^{101,ap}, O. Smirnova ⁸⁴, J.W. Smith ⁵⁷, M.N.K. Smith ³⁸, R.W. Smith ³⁸, M. Smizanska ⁷⁵, K. Smolek ¹³⁰, A.A. Snesarev ⁹⁸, I.M. Snyder ¹¹⁸, S. Snyder ²⁷, R. Sobie ^{172,o}, F. Socher ⁴⁷, A. Soffer ¹⁵⁵, A. Søgaard ⁴⁹, D.A. Soh ¹⁵³, G. Sokhrannyi ⁷⁸, C.A. Solans Sanchez ³², M. Solar ¹³⁰, E.Yu. Soldatov ¹⁰⁰, U. Soldevila ¹⁷⁰, A.A. Solodkov ¹³², A. Soloshenko ⁶⁸, O.V. Solovyanov ¹³², V. Solovyev ¹²⁵, P. Sommer ¹⁴¹, H. Son ¹⁶⁵, A. Sopczak ¹³⁰, D. Sosa ^{60b}, C.L. Sotiropoulou ^{126a,126b}, S. Sottocornola ^{123a,123b}, R. Soualah ^{167a,167c}, A.M. Soukharev ^{111,c}, D. South ⁴⁵, B.C. Sowden ⁸⁰, S. Spagnolo ^{76a,76b}, M. Spalla ^{126a,126b}, M. Spangenberg ¹⁷³, F. Spanò ⁸⁰, D. Sperlich ¹⁷, F. Spettel ¹⁰³, T.M. Spieker ^{60a}, R. Spighi ^{22a}, G. Spigo ³², L.A. Spiller ⁹¹, M. Spousta ¹³¹, R.D. St. Denis ^{56,*}, A. Stabile ^{94a,94b}, R. Stamen ^{60a}, S. Stamm ¹⁷, E. Stanecka ⁴², R.W. Stanek ⁶, C. Stanescu ^{136a}, M.M. Stanitzki ⁴⁵, B.S. Stapf ¹⁰⁹, S. Stapnes ¹²¹, E.A. Starchenko ¹³², G.H. Stark ³³, J. Stark ⁵⁸, S.H. Stark ³⁹, P. Staroba ¹²⁹, P. Starovoitov ^{60a}, S. Stärz ³², R. Staszewski ⁴², M. Stegler ⁴⁵, P. Steinberg ²⁷, B. Stelzer ¹⁴⁴, H.J. Stelzer ³², O. Stelzer-Chilton ^{163a}, H. Stenzel ⁵⁵, T.J. Stevenson ⁷⁹, G.A. Stewart ⁵⁶, M.C. Stockton ¹¹⁸, M. Stoebe ⁹⁰, G. Stoica ^{28b}, P. Stolte ⁵⁷, S. Stonjek ¹⁰³, A.R. Stradling ⁸, A. Straessner ⁴⁷, M.E. Stramaglia ¹⁸, J. Strandberg ¹⁴⁹, S. Strandberg ^{148a,148b}, M. Strauss ¹¹⁵, P. Strizenec ^{146b}, R. Ströhmer ¹⁷⁷, D.M. Strom ¹¹⁸, R. Stroynowski ⁴³, A. Strubig ⁴⁹, S.A. Stucci ²⁷, B. Stugu ¹⁵, N.A. Styles ⁴⁵, D. Su ¹⁴⁵, J. Su ¹²⁷, S. Suchek ^{60a}, Y. Sugaya ¹²⁰, M. Suk ¹³⁰, V.V. Sulín ⁹⁸, DMS Sultan ^{162a,162b}, S. Sultansoy ^{4c}, T. Sumida ⁷¹, S. Sun ⁵⁹, X. Sun ³, K. Suruliz ¹⁵¹, C.J.E. Suster ¹⁵², M.R. Sutton ¹⁵¹, S. Suzuki ⁶⁹, M. Svatos ¹²⁹, M. Swiatkowski ³³, S.P. Swift ², I. Sykora ^{146a}, T. Sykora ¹³¹, D. Ta ⁵¹, K. Tackmann ⁴⁵, J. Taenzer ¹⁵⁵, A. Taffard ¹⁶⁶, R. Tafirout ^{163a}, E. Tahirovic ⁷⁹, N. Taiblum ¹⁵⁵, H. Takai ²⁷, R. Takashima ⁷², E.H. Takasugi ¹⁰³, K. Takeda ⁷⁰, T. Takeshita ¹⁴², Y. Takubo ⁶⁹, M. Talby ⁸⁸, A.A. Talyshev ^{111,c}, J. Tanaka ¹⁵⁷, M. Tanaka ¹⁵⁹, R. Tanaka ¹¹⁹, R. Tanioka ⁷⁰, B.B. Tannenwald ¹¹³, S. Tapia Araya ^{34b}, S. Tapprogge ⁸⁶, S. Tarem ¹⁵⁴, G.F. Tartarelli ^{94a}, P. Tas ¹³¹, M. Tasevsky ¹²⁹, T. Tashiro ⁷¹, E. Tassi ^{40a,40b}, A. Tavares Delgado ^{128a,128b}, Y. Tayalati ^{137e}, A.C. Taylor ¹⁰⁷, A.J. Taylor ⁴⁹, G.N. Taylor ⁹¹,

P.T.E. Taylor⁹¹, W. Taylor^{163b}, P. Teixeira-Dias⁸⁰, D. Temple¹⁴⁴, H. Ten Kate³², P.K. Teng¹⁵³, J.J. Teoh¹²⁰, F. Tepel¹⁷⁸, S. Terada⁶⁹, K. Terashi¹⁵⁷, J. Terron⁸⁵, S. Terzo¹³, M. Testa⁵⁰, R.J. Teuscher^{161,o}, S.J. Thais¹⁷⁹, T. Theveneaux-Pelzer⁸⁸, F. Thiele³⁹, J.P. Thomas¹⁹, J. Thomas-Wilsker⁸⁰, P.D. Thompson¹⁹, A.S. Thompson⁵⁶, L.A. Thomsen¹⁷⁹, E. Thomson¹²⁴, Y. Tian³⁸, M.J. Tibbetts¹⁶, R.E. Ticse Torres⁵⁷, V.O. Tikhomirov^{98,aq}, Yu.A. Tikhonov^{111,c}, S. Timoshenko¹⁰⁰, P. Tipton¹⁷⁹, S. Tisserant⁸⁸, K. Todome¹⁵⁹, S. Todorova-Nova⁵, S. Todt⁴⁷, J. Tojo⁷³, S. Tokár^{146a}, K. Tokushuku⁶⁹, E. Tolley¹¹³, L. Tomlinson⁸⁷, M. Tomoto¹⁰⁵, L. Tompkins^{145,ar}, K. Toms¹⁰⁷, B. Tong⁵⁹, P. Tornambe⁵¹, E. Torrence¹¹⁸, H. Torres⁴⁷, E. Torró Pastor¹⁴⁰, J. Toth^{88,as}, F. Touchard⁸⁸, D.R. Tovey¹⁴¹, C.J. Treado¹¹², T. Trefzger¹⁷⁷, F. Tresoldi¹⁵¹, A. Tricoli²⁷, I.M. Trigger^{163a}, S. Trincaz-Duvoid⁸³, M.F. Tripiana¹³, W. Trischuk¹⁶¹, B. Trocme⁵⁸, A. Trofymov⁴⁵, C. Troncon^{94a}, M. Trovatelli¹⁷², L. Truong^{147b}, M. Trzebinski⁴², A. Trzupek⁴², K.W. Tsang^{62a}, J.C.-L. Tseng¹²², P.V. Tsiareshka⁹⁵, N. Tsirintanis⁹, S. Tsiskaridze¹³, V. Tsiskaridze⁵¹, E.G. Tskhadadze^{54a}, I.I. Tsukerman⁹⁹, V. Tsulaia¹⁶, S. Tsuno⁶⁹, D. Tsybychev¹⁵⁰, Y. Tu^{62b}, A. Tudorache^{28b}, V. Tudorache^{28b}, T.T. Tulbure^{28a}, A.N. Tuna⁵⁹, S. Turchikhin⁶⁸, D. Turgeman¹⁷⁵, I. Turk Cakir^{4b,at}, R. Turra^{94a}, P.M. Tuts³⁸, G. Ucchielli^{22a,22b}, I. Ueda⁶⁹, M. Ughetto^{148a,148b}, F. Ukegawa¹⁶⁴, G. Unal³², A. Undrus²⁷, G. Unel¹⁶⁶, F.C. Ungaro⁹¹, Y. Unno⁶⁹, K. Uno¹⁵⁷, J. Urban^{146b}, P. Urquijo⁹¹, P. Urrejola⁸⁶, G. Usai⁸, J. Usui⁶⁹, L. Vacavant⁸⁸, V. Vacek¹³⁰, B. Vachon⁹⁰, K.O.H. Vadla¹²¹, A. Vaidya⁸¹, C. Valderanis¹⁰², E. Valdes Santurio^{148a,148b}, M. Valente⁵², S. Valentinetti^{22a,22b}, A. Valero¹⁷⁰, L. Valéry¹³, A. Vallier⁵, J.A. Valls Ferrer¹⁷⁰, W. Van Den Wollenberg¹⁰⁹, H. van der Graaf¹⁰⁹, P. van Gemmeren⁶, J. Van Nieuwkoop¹⁴⁴, I. van Vulpen¹⁰⁹, M.C. van Woerden¹⁰⁹, M. Vanadia^{135a,135b}, W. Vandelli³², A. Vaniachine¹⁶⁰, P. Vankov¹⁰⁹, G. Vardanyan¹⁸⁰, R. Vari^{134a}, E.W. Varnes⁷, C. Varni^{53a,53b}, T. Varol⁴³, D. Varouchas¹¹⁹, A. Vartapetian⁸, K.E. Varvell¹⁵², J.G. Vasquez¹⁷⁹, G.A. Vasquez^{34b}, F. Vazeille³⁷, D. Vazquez Furelos¹³, T. Vazquez Schroeder⁹⁰, J. Veatch⁵⁷, V. Veeraraghavan⁷, L.M. Veloce¹⁶¹, F. Veloso^{128a,128c}, S. Veneziano^{134a}, A. Ventura^{76a,76b}, M. Venturi¹⁷², N. Venturi³², V. Vercesi^{123a}, M. Verducci^{136a,136b}, W. Verkerke¹⁰⁹, A.T. Vermeulen¹⁰⁹, J.C. Vermeulen¹⁰⁹, M.C. Vetterli^{144,d}, N. Viaux Maira^{34b}, O. Viazlo⁸⁴, I. Vichou^{169,*}, T. Vickey¹⁴¹, O.E. Vickey Boeriu¹⁴¹, G.H.A. Viehhauser¹²², S. Viel¹⁶, L. Vigani¹²², M. Villa^{22a,22b}, M. Villaplana Perez^{94a,94b}, E. Vilucchi⁵⁰, M.G. Vincter³¹, V.B. Vinogradov⁶⁸, A. Vishwakarma⁴⁵, C. Vittori^{22a,22b}, I. Vivarelli¹⁵¹, S. Vlachos¹⁰, M. Vogel¹⁷⁸, P. Vokac¹³⁰, G. Volpi¹³, S.E. von Buddenbrock^{147c}, H. von der Schmitt¹⁰³, E. von Toerne²³, V. Vorobel¹³¹, K. Vorobev¹⁰⁰, M. Vos¹⁷⁰, R. Voss³², J.H. Vosseveld⁷⁷, N. Vranjes¹⁴, M. Vranjes Milosavljevic¹⁴, V. Vrba¹³⁰, M. Vreeswijk¹⁰⁹, R. Vuillermet³², I. Vukotic³³, P. Wagner²³, W. Wagner¹⁷⁸, J. Wagner-Kuhr¹⁰², H. Wahlberg⁷⁴, S. Wahrmund⁴⁷, K. Wakamiya⁷⁰, J. Walder⁷⁵, R. Walker¹⁰², W. Walkowiak¹⁴³, V. Wallangen^{148a,148b}, C. Wang^{35b}, C. Wang^{36b,au}, F. Wang¹⁷⁶, H. Wang¹⁶, H. Wang³, J. Wang⁴⁵, J. Wang¹⁵², Q. Wang¹¹⁵, R.-J. Wang⁸³, R. Wang⁶, S.M. Wang¹⁵³, T. Wang³⁸, W. Wang^{153,av}, W. Wang^{36a,aw}, Z. Wang^{36c}, C. Wanotayaroj⁴⁵, A. Warburton⁹⁰, C.P. Ward³⁰, D.R. Wardrope⁸¹, A. Washbrook⁴⁹, P.M. Watkins¹⁹, A.T. Watson¹⁹, M.F. Watson¹⁹, G. Watts¹⁴⁰, S. Watts⁸⁷, B.M. Waugh⁸¹, A.F. Webb¹¹, S. Webb⁸⁶, M.S. Weber¹⁸, S.M. Weber^{60a}, S.W. Weber¹⁷⁷, S.A. Weber³¹, J.S. Webster⁶, A.R. Weidberg¹²², B. Weinert⁶⁴, J. Weingarten⁵⁷, M. Weirich⁸⁶, C. Weiser⁵¹, P.S. Wells³², T. Wenaus²⁷, T. Wengler³², S. Wenig³², N. Wermes²³, M.D. Werner⁶⁷, P. Werner³², M. Wessels^{60a}, T.D. Weston¹⁸, K. Whalen¹¹⁸, N.L. Whallon¹⁴⁰, A.M. Wharton⁷⁵, A.S. White⁹², A. White⁸, M.J. White¹, R. White^{34b}, D. Whiteson¹⁶⁶, B.W. Whitmore⁷⁵, F.J. Wickens¹³³, W. Wiedenmann¹⁷⁶, M. Wielers¹³³, C. Wigglesworth³⁹, L.A.M. Wiik-Fuchs⁵¹, A. Wildauer¹⁰³, F. Wilk⁸⁷, H.G. Wilkens³², H.H. Williams¹²⁴, S. Williams¹⁰⁹, C. Willis⁹³, S. Willocq⁸⁹, J.A. Wilson¹⁹, I. Wingerter-Seez⁵, E. Winkels¹⁵¹, F. Winklmeier¹¹⁸, O.J. Winston¹⁵¹, B.T. Winter²³, M. Wittgen¹⁴⁵, M. Wobisch^{82,u}, A. Wolf⁸⁶, T.M.H. Wolf¹⁰⁹, R. Wolff⁸⁸, M.W. Wolter⁴², H. Wolters^{128a,128c}, V.W.S. Wong¹⁷¹, N.L. Woods¹³⁹, S.D. Worm¹⁹, B.K. Wosiek⁴², J. Wotschack³², K.W. Wozniak⁴², M. Wu³³, S.L. Wu¹⁷⁶, X. Wu⁵², Y. Wu⁹², T.R. Wyatt⁸⁷, B.M. Wynne⁴⁹, S. Xella³⁹, Z. Xi⁹², L. Xia^{35c}, D. Xu^{35a}, L. Xu²⁷, T. Xu¹³⁸, W. Xu⁹², B. Yabsley¹⁵², S. Yacoob^{147a}, D. Yamaguchi¹⁵⁹, Y. Yamaguchi¹⁵⁹, A. Yamamoto⁶⁹, S. Yamamoto¹⁵⁷, T. Yamanaka¹⁵⁷, F. Yamane⁷⁰, M. Yamatani¹⁵⁷, T. Yamazaki¹⁵⁷, Y. Yamazaki⁷⁰, Z. Yan²⁴, H. Yang^{36c}, H. Yang¹⁶, Y. Yang¹⁵³, Z. Yang¹⁵, W.-M. Yao¹⁶, Y.C. Yap⁴⁵, Y. Yasu⁶⁹, E. Yatsenko⁵, K.H. Yau Wong²³, J. Ye⁴³, S. Ye²⁷, I. Yeletskikh⁶⁸, E. Yigitbasi²⁴, E. Yildirim⁸⁶, K. Yorita¹⁷⁴, K. Yoshihara¹²⁴, C. Young¹⁴⁵, C.J.S. Young³², J. Yu⁸, J. Yu⁶⁷, S.P.Y. Yuen²³, I. Yusuff^{30,ax}, B. Zabinski⁴², G. Zacharis¹⁰, R. Zaidan¹³,

A.M. Zaitsev^{132,ak}, N. Zakharchuk⁴⁵, J. Zalieckas¹⁵, A. Zaman¹⁵⁰, S. Zambito⁵⁹, D. Zanzi⁹¹,
 C. Zeitnitz¹⁷⁸, G. Zemaityte¹²², A. Zemla^{41a}, J.C. Zeng¹⁶⁹, Q. Zeng¹⁴⁵, O. Zenin¹³², T. Ženiš^{146a},
 D. Zerwas¹¹⁹, D. Zhang^{36b}, D. Zhang⁹², F. Zhang¹⁷⁶, G. Zhang^{36a,aw}, H. Zhang¹¹⁹, J. Zhang⁶, L. Zhang⁵¹,
 L. Zhang^{36a}, M. Zhang¹⁶⁹, P. Zhang^{35b}, R. Zhang²³, R. Zhang^{36a,au}, X. Zhang^{36b}, Y. Zhang^{35a,35d},
 Z. Zhang¹¹⁹, X. Zhao⁴³, Y. Zhao^{36b,x}, Z. Zhao^{36a}, A. Zhemchugov⁶⁸, B. Zhou⁹², C. Zhou¹⁷⁶, L. Zhou⁴³,
 M. Zhou^{35a,35d}, M. Zhou¹⁵⁰, N. Zhou^{36c}, Y. Zhou⁷, C.G. Zhu^{36b}, H. Zhu^{35a}, J. Zhu⁹², Y. Zhu^{36a},
 X. Zhuang^{35a}, K. Zhukov⁹⁸, A. Zibell¹⁷⁷, D. Zieminska⁶⁴, N.I. Zimine⁶⁸, C. Zimmermann⁸⁶,
 S. Zimmermann⁵¹, Z. Zinonos¹⁰³, M. Zinser⁸⁶, M. Ziolkowski¹⁴³, L. Živković¹⁴, G. Zobernig¹⁷⁶,
 A. Zoccoli^{22a,22b}, R. Zou³³, M. zur Nedden¹⁷, L. Zwalinski³²

¹ Department of Physics, University of Adelaide, Adelaide, Australia

² Physics Department, SUNY Albany, Albany, NY, United States

³ Department of Physics, University of Alberta, Edmonton, AB, Canada

⁴ (a) Department of Physics, Ankara University, Ankara; (b) Istanbul Aydin University, Istanbul; (c) Division of Physics, TOBB University of Economics and Technology, Ankara, Turkey

⁵ LAPP, CNRS/IN2P3 and Université Savoie Mont Blanc, Annecy-le-Vieux, France

⁶ High Energy Physics Division, Argonne National Laboratory, Argonne, IL, United States

⁷ Department of Physics, University of Arizona, Tucson, AZ, United States

⁸ Department of Physics, The University of Texas at Arlington, Arlington, TX, United States

⁹ Physics Department, National and Kapodistrian University of Athens, Athens, Greece

¹⁰ Physics Department, National Technical University of Athens, Zografou, Greece

¹¹ Department of Physics, The University of Texas at Austin, Austin, TX, United States

¹² Institute of Physics, Azerbaijan Academy of Sciences, Baku, Azerbaijan

¹³ Institut de Física d'Altes Energies (IFAE), The Barcelona Institute of Science and Technology, Barcelona, Spain

¹⁴ Institute of Physics, University of Belgrade, Belgrade, Serbia

¹⁵ Department for Physics and Technology, University of Bergen, Bergen, Norway

¹⁶ Physics Division, Lawrence Berkeley National Laboratory and University of California, Berkeley, CA, United States

¹⁷ Department of Physics, Humboldt University, Berlin, Germany

¹⁸ Albert Einstein Center for Fundamental Physics and Laboratory for High Energy Physics, University of Bern, Bern, Switzerland

¹⁹ School of Physics and Astronomy, University of Birmingham, Birmingham, United Kingdom

²⁰ (a) Department of Physics, Bogazici University, Istanbul; (b) Department of Physics Engineering, Gaziantep University, Gaziantep; (d) Istanbul Bilgi University, Faculty of Engineering and

Natural Sciences, Istanbul; (e) Bahcesehir University, Faculty of Engineering and Natural Sciences, Istanbul, Turkey

²¹ Centro de Investigaciones, Universidad Antonio Narino, Bogota, Colombia

²² (a) INFN Sezione di Bologna; (b) Dipartimento di Fisica e Astronomia, Università di Bologna, Bologna, Italy

²³ Physikalisches Institut, University of Bonn, Bonn, Germany

²⁴ Department of Physics, Boston University, Boston, MA, United States

²⁵ Department of Physics, Brandeis University, Waltham, MA, United States

²⁶ (a) Universidade Federal do Rio De Janeiro COPPE/EE/IF, Rio de Janeiro; (b) Electrical Circuits Department, Federal University of Juiz de Fora (UFJF), Juiz de Fora; (c) Federal University of

Sao Joao del Rei (UFSJ), Sao Joao del Rei; (d) Instituto de Fisica, Universidade de Sao Paulo, Sao Paulo, Brazil

²⁷ Physics Department, Brookhaven National Laboratory, Upton, NY, United States

²⁸ (a) Transilvania University of Brasov, Brasov; (b) Horia Hulubei National Institute of Physics and Nuclear Engineering, Bucharest; (c) Department of Physics, Alexandru Ioan Cuza

University of Iasi, Iasi; (d) National Institute for Research and Development of Isotopic and Molecular Technologies, Physics Department, Cluj Napoca; (e) University Politehnica Bucharest,

Bucharest; (f) West University in Timisoara, Timisoara, Romania

²⁹ Departamento de Fisica, Universidad de Buenos Aires, Buenos Aires, Argentina

³⁰ Cavendish Laboratory, University of Cambridge, Cambridge, United Kingdom

³¹ Department of Physics, Carleton University, Ottawa, ON, Canada

³² CERN, Geneva, Switzerland

³³ Enrico Fermi Institute, University of Chicago, Chicago, IL, United States

³⁴ (a) Departamento de Fisica, Pontificia Universidad Católica de Chile, Santiago; (b) Departamento de Fisica, Universidad Técnica Federico Santa María, Valparaíso, Chile

³⁵ (a) Institute of High Energy Physics, Chinese Academy of Sciences, Beijing; (b) Department of Physics, Nanjing University, Jiangsu; (c) Physics Department, Tsinghua University, Beijing

100084; (d) University of Chinese Academy of Science (UCAS), Beijing, China

³⁶ (a) Department of Modern Physics and State Key Laboratory of Particle Detection and Electronics, University of Science and Technology of China, Anhui; (b) School of Physics, Shandong

University, Shandong; (c) Department of Physics and Astronomy, Key Laboratory for Particle Physics, Astrophysics and Cosmology, Ministry of Education; Shanghai Key Laboratory for

Particle Physics and Cosmology, Shanghai Jiao Tong University, Tsung-Dao Lee Institute, China

³⁷ Université Clermont Auvergne, CNRS/IN2P3, LPC, Clermont-Ferrand, France

³⁸ Nevis Laboratory, Columbia University, Irvington, NY, United States

³⁹ Niels Bohr Institute, University of Copenhagen, Copenhagen, Denmark

⁴⁰ (a) INFN Gruppo Collegato di Cosenza, Laboratori Nazionali di Frascati; (b) Dipartimento di Fisica, Università della Calabria, Rende, Italy

⁴¹ (a) AGH University of Science and Technology, Faculty of Physics and Applied Computer Science, Krakow; (b) Marian Smoluchowski Institute of Physics, Jagiellonian University, Krakow,

Poland

⁴² Institute of Nuclear Physics Polish Academy of Sciences, Krakow, Poland

⁴³ Physics Department, Southern Methodist University, Dallas, TX, United States

⁴⁴ Physics Department, University of Texas at Dallas, Richardson, TX, United States

⁴⁵ DESY, Hamburg and Zeuthen, Germany

⁴⁶ Lehrstuhl für Experimentelle Physik IV, Technische Universität Dortmund, Dortmund, Germany

⁴⁷ Institut für Kern- und Teilchenphysik, Technische Universität Dresden, Dresden, Germany

⁴⁸ Department of Physics, Duke University, Durham, NC, United States

⁴⁹ SUPA - School of Physics and Astronomy, University of Edinburgh, Edinburgh, United Kingdom

⁵⁰ INFN e Laboratori Nazionali di Frascati, Frascati, Italy

⁵¹ Fakultät für Mathematik und Physik, Albert-Ludwigs-Universität, Freiburg, Germany

⁵² Département de Physique Nucleaire et Corpusculaire, Université de Genève, Geneva, Switzerland

⁵³ (a) INFN Sezione di Genova; (b) Dipartimento di Fisica, Università di Genova, Genova, Italy

⁵⁴ (a) E. Andronikashvili Institute of Physics, Iv. Javakishvili Tbilisi State University, Tbilisi; (b) High Energy Physics Institute, Tbilisi State University, Tbilisi, Georgia

⁵⁵ II Physikalisches Institut, Justus-Liebig-Universität Giessen, Giessen, Germany

⁵⁶ SUPA - School of Physics and Astronomy, University of Glasgow, Glasgow, United Kingdom

⁵⁷ II Physikalisches Institut, Georg-August-Universität, Göttingen, Germany

- ⁵⁸ Laboratoire de Physique Subatomique et de Cosmologie, Université Grenoble-Alpes, CNRS/IN2P3, Grenoble, France
- ⁵⁹ Laboratory for Particle Physics and Cosmology, Harvard University, Cambridge, MA, United States
- ⁶⁰ ^(a) Kirchhoff-Institut für Physik, Ruprecht-Karls-Universität Heidelberg, Heidelberg; ^(b) Physikalisches Institut, Ruprecht-Karls-Universität Heidelberg, Heidelberg, Germany
- ⁶¹ Faculty of Applied Information Science, Hiroshima Institute of Technology, Hiroshima, Japan
- ⁶² ^(a) Department of Physics, The Chinese University of Hong Kong, Shatin, N.T.; ^(b) Department of Physics, The University of Hong Kong; ^(c) Department of Physics and Institute for Advanced Study, The Hong Kong University of Science and Technology, Clear Water Bay, Kowloon, Hong Kong, China
- ⁶³ Department of Physics, National Tsing Hua University, Hsinchu, Taiwan
- ⁶⁴ Department of Physics, Indiana University, Bloomington, IN, United States
- ⁶⁵ Institut für Astro- und Teilchenphysik, Leopold-Franzens-Universität, Innsbruck, Austria
- ⁶⁶ University of Iowa, Iowa City, IA, United States
- ⁶⁷ Department of Physics and Astronomy, Iowa State University, Ames, IA, United States
- ⁶⁸ Joint Institute for Nuclear Research, JINR Dubna, Dubna, Russia
- ⁶⁹ KEK, High Energy Accelerator Research Organization, Tsukuba, Japan
- ⁷⁰ Graduate School of Science, Kobe University, Kobe, Japan
- ⁷¹ Faculty of Science, Kyoto University, Kyoto, Japan
- ⁷² Kyoto University of Education, Kyoto, Japan
- ⁷³ Research Center for Advanced Particle Physics and Department of Physics, Kyushu University, Fukuoka, Japan
- ⁷⁴ Instituto de Física La Plata, Universidad Nacional de La Plata and CONICET, La Plata, Argentina
- ⁷⁵ Physics Department, Lancaster University, Lancaster, United Kingdom
- ⁷⁶ ^(a) INFN Sezione di Lecce; ^(b) Dipartimento di Matematica e Fisica, Università del Salento, Lecce, Italy
- ⁷⁷ Oliver Lodge Laboratory, University of Liverpool, Liverpool, United Kingdom
- ⁷⁸ Department of Experimental Particle Physics, Jožef Stefan Institute and Department of Physics, University of Ljubljana, Ljubljana, Slovenia
- ⁷⁹ School of Physics and Astronomy, Queen Mary University of London, London, United Kingdom
- ⁸⁰ Department of Physics, Royal Holloway University of London, Surrey, United Kingdom
- ⁸¹ Department of Physics and Astronomy, University College London, London, United Kingdom
- ⁸² Louisiana Tech University, Ruston, LA, United States
- ⁸³ Laboratoire de Physique Nucléaire et de Hautes Energies, UPMC and Université Paris-Diderot and CNRS/IN2P3, Paris, France
- ⁸⁴ Fysiska institutionen, Lunds universitet, Lund, Sweden
- ⁸⁵ Departamento de Física Teórica C-15, Universidad Autónoma de Madrid, Madrid, Spain
- ⁸⁶ Institut für Physik, Universität Mainz, Mainz, Germany
- ⁸⁷ School of Physics and Astronomy, University of Manchester, Manchester, United Kingdom
- ⁸⁸ CPPM, Aix-Marseille Université and CNRS/IN2P3, Marseille, France
- ⁸⁹ Department of Physics, University of Massachusetts, Amherst, MA, United States
- ⁹⁰ Department of Physics, McGill University, Montreal, QC, Canada
- ⁹¹ School of Physics, University of Melbourne, Victoria, Australia
- ⁹² Department of Physics, The University of Michigan, Ann Arbor, MI, United States
- ⁹³ Department of Physics and Astronomy, Michigan State University, East Lansing, MI, United States
- ⁹⁴ ^(a) INFN Sezione di Milano; ^(b) Dipartimento di Fisica, Università di Milano, Milano, Italy
- ⁹⁵ B.I. Stepanov Institute of Physics, National Academy of Sciences of Belarus, Minsk, Belarus
- ⁹⁶ Research Institute for Nuclear Problems of Byelorussian State University, Minsk, Belarus
- ⁹⁷ Group of Particle Physics, University of Montreal, Montreal, QC, Canada
- ⁹⁸ P.N. Lebedev Physical Institute of the Russian Academy of Sciences, Moscow, Russia
- ⁹⁹ Institute for Theoretical and Experimental Physics (ITEP), Moscow, Russia
- ¹⁰⁰ National Research Nuclear University MEPhI, Moscow, Russia
- ¹⁰¹ D.V. Skobeltsyn Institute of Nuclear Physics, M.V. Lomonosov Moscow State University, Moscow, Russia
- ¹⁰² Fakultät für Physik, Ludwig-Maximilians-Universität München, München, Germany
- ¹⁰³ Max-Planck-Institut für Physik (Werner-Heisenberg-Institut), München, Germany
- ¹⁰⁴ Nagasaki Institute of Applied Science, Nagasaki, Japan
- ¹⁰⁵ Graduate School of Science and Kobayashi-Maskawa Institute, Nagoya University, Nagoya, Japan
- ¹⁰⁶ ^(a) INFN Sezione di Napoli; ^(b) Dipartimento di Fisica, Università di Napoli, Napoli, Italy
- ¹⁰⁷ Department of Physics and Astronomy, University of New Mexico, Albuquerque, NM, United States
- ¹⁰⁸ Institute for Mathematics, Astrophysics and Particle Physics, Radboud University Nijmegen/Nikhef, Nijmegen, Netherlands
- ¹⁰⁹ Nikhef National Institute for Subatomic Physics and University of Amsterdam, Amsterdam, Netherlands
- ¹¹⁰ Department of Physics, Northern Illinois University, DeKalb, IL, United States
- ¹¹¹ Budker Institute of Nuclear Physics, SB RAS, Novosibirsk, Russia
- ¹¹² Department of Physics, New York University, New York, NY, United States
- ¹¹³ Ohio State University, Columbus, OH, United States
- ¹¹⁴ Faculty of Science, Okayama University, Okayama, Japan
- ¹¹⁵ Homer L. Dodge Department of Physics and Astronomy, University of Oklahoma, Norman, OK, United States
- ¹¹⁶ Department of Physics, Oklahoma State University, Stillwater, OK, United States
- ¹¹⁷ Palacký University, RCPTM, Olomouc, Czech Republic
- ¹¹⁸ Center for High Energy Physics, University of Oregon, Eugene, OR, United States
- ¹¹⁹ LAL, Univ. Paris-Sud, CNRS/IN2P3, Université Paris-Saclay, Orsay, France
- ¹²⁰ Graduate School of Science, Osaka University, Osaka, Japan
- ¹²¹ Department of Physics, University of Oslo, Oslo, Norway
- ¹²² Department of Physics, Oxford University, Oxford, United Kingdom
- ¹²³ ^(a) INFN Sezione di Pavia; ^(b) Dipartimento di Fisica, Università di Pavia, Pavia, Italy
- ¹²⁴ Department of Physics, University of Pennsylvania, Philadelphia, PA, United States
- ¹²⁵ National Research Centre "Kurchatov Institute" B.P. Konstantinov Petersburg Nuclear Physics Institute, St. Petersburg, Russia
- ¹²⁶ ^(a) INFN Sezione di Pisa; ^(b) Dipartimento di Fisica E. Fermi, Università di Pisa, Pisa, Italy
- ¹²⁷ Department of Physics and Astronomy, University of Pittsburgh, Pittsburgh, PA, United States
- ¹²⁸ ^(a) Laboratório de Instrumentação e Física Experimental de Partículas - LIP, Lisboa; ^(b) Faculdade de Ciências, Universidade de Lisboa, Lisboa; ^(c) Department of Physics, University of Coimbra, Coimbra; ^(d) Centro de Física Nuclear da Universidade de Lisboa, Lisboa; ^(e) Departamento de Física, Universidade do Minho, Braga; ^(f) Departamento de Física Teórica y del Cosmos, Universidad de Granada, Granada; ^(g) Dep Física and CEFITEC of Faculdade de Ciências e Tecnologia, Universidade Nova de Lisboa, Caparica, Portugal
- ¹²⁹ Institute of Physics, Academy of Sciences of the Czech Republic, Praha, Czech Republic
- ¹³⁰ Czech Technical University in Prague, Praha, Czech Republic
- ¹³¹ Charles University, Faculty of Mathematics and Physics, Prague, Czech Republic
- ¹³² State Research Center Institute for High Energy Physics (Protvino), NRC KI, Russia
- ¹³³ Particle Physics Department, Rutherford Appleton Laboratory, Didcot, United Kingdom

- ¹³⁴ ^(a) INFN Sezione di Roma; ^(b) Dipartimento di Fisica, Sapienza Università di Roma, Roma, Italy
- ¹³⁵ ^(a) INFN Sezione di Roma Tor Vergata; ^(b) Dipartimento di Fisica, Università di Roma Tor Vergata, Roma, Italy
- ¹³⁶ ^(a) INFN Sezione di Roma Tre; ^(b) Dipartimento di Matematica e Fisica, Università Roma Tre, Roma, Italy
- ¹³⁷ ^(a) Faculté des Sciences Ain Chock, Réseau Universitaire de Physique des Hautes Energies - Université Hassan II, Casablanca; ^(b) Centre National de l'Energie des Sciences Techniques Nucleaires, Rabat; ^(c) Faculté des Sciences Semlalia, Université Cadi Ayyad, LPHEA-Marrakech; ^(d) Faculté des Sciences, Université Mohamed Premier and LPTPM, Oujda; ^(e) Faculté des sciences, Université Mohammed V, Rabat, Morocco
- ¹³⁸ DSM/IRFU (Institut de Recherches sur les Lois Fondamentales de l'Univers), CEA Saclay (Commissariat à l'Energie Atomique et aux Energies Alternatives), Gif-sur-Yvette, France
- ¹³⁹ Santa Cruz Institute for Particle Physics, University of California Santa Cruz, Santa Cruz, CA, United States
- ¹⁴⁰ Department of Physics, University of Washington, Seattle, WA, United States
- ¹⁴¹ Department of Physics and Astronomy, University of Sheffield, Sheffield, United Kingdom
- ¹⁴² Department of Physics, Shinshu University, Nagano, Japan
- ¹⁴³ Department Physik, Universität Siegen, Siegen, Germany
- ¹⁴⁴ Department of Physics, Simon Fraser University, Burnaby, BC, Canada
- ¹⁴⁵ SLAC National Accelerator Laboratory, Stanford, CA, United States
- ¹⁴⁶ ^(a) Faculty of Mathematics, Physics & Informatics, Comenius University, Bratislava; ^(b) Department of Subnuclear Physics, Institute of Experimental Physics of the Slovak Academy of Sciences, Kosice, Slovak Republic
- ¹⁴⁷ ^(a) Department of Physics, University of Cape Town, Cape Town; ^(b) Department of Physics, University of Johannesburg, Johannesburg; ^(c) School of Physics, University of the Witwatersrand, Johannesburg, South Africa
- ¹⁴⁸ ^(a) Department of Physics, Stockholm University; ^(b) The Oskar Klein Centre, Stockholm, Sweden
- ¹⁴⁹ Physics Department, Royal Institute of Technology, Stockholm, Sweden
- ¹⁵⁰ Departments of Physics & Astronomy and Chemistry, Stony Brook University, Stony Brook, NY, United States
- ¹⁵¹ Department of Physics and Astronomy, University of Sussex, Brighton, United Kingdom
- ¹⁵² School of Physics, University of Sydney, Sydney, Australia
- ¹⁵³ Institute of Physics, Academia Sinica, Taipei, Taiwan
- ¹⁵⁴ Department of Physics, Technion: Israel Institute of Technology, Haifa, Israel
- ¹⁵⁵ Raymond and Beverly Sackler School of Physics and Astronomy, Tel Aviv University, Tel Aviv, Israel
- ¹⁵⁶ Department of Physics, Aristotle University of Thessaloniki, Thessaloniki, Greece
- ¹⁵⁷ International Center for Elementary Particle Physics and Department of Physics, The University of Tokyo, Tokyo, Japan
- ¹⁵⁸ Graduate School of Science and Technology, Tokyo Metropolitan University, Tokyo, Japan
- ¹⁵⁹ Department of Physics, Tokyo Institute of Technology, Tokyo, Japan
- ¹⁶⁰ Tomsk State University, Tomsk, Russia
- ¹⁶¹ Department of Physics, University of Toronto, Toronto, ON, Canada
- ¹⁶² ^(a) INFN-TIFPA; ^(b) University of Trento, Trento, Italy
- ¹⁶³ ^(a) TRIUMF, Vancouver, BC; ^(b) Department of Physics and Astronomy, York University, Toronto, ON, Canada
- ¹⁶⁴ Faculty of Pure and Applied Sciences, and Center for Integrated Research in Fundamental Science and Engineering, University of Tsukuba, Tsukuba, Japan
- ¹⁶⁵ Department of Physics and Astronomy, Tufts University, Medford, MA, United States
- ¹⁶⁶ Department of Physics and Astronomy, University of California Irvine, Irvine, CA, United States
- ¹⁶⁷ ^(a) INFN Gruppo Collegato di Udine, Sezione di Trieste, Udine; ^(b) ICTP, Trieste; ^(c) Dipartimento di Chimica, Fisica e Ambiente, Università di Udine, Udine, Italy
- ¹⁶⁸ Department of Physics and Astronomy, University of Uppsala, Uppsala, Sweden
- ¹⁶⁹ Department of Physics, University of Illinois, Urbana, IL, United States
- ¹⁷⁰ Instituto de Fisica Corpuscular (IFIC), Centro Mixto Universidad de Valencia - CSIC, Spain
- ¹⁷¹ Department of Physics, University of British Columbia, Vancouver, BC, Canada
- ¹⁷² Department of Physics and Astronomy, University of Victoria, Victoria, BC, Canada
- ¹⁷³ Department of Physics, University of Warwick, Coventry, United Kingdom
- ¹⁷⁴ Waseda University, Tokyo, Japan
- ¹⁷⁵ Department of Particle Physics, The Weizmann Institute of Science, Rehovot, Israel
- ¹⁷⁶ Department of Physics, University of Wisconsin, Madison, WI, United States
- ¹⁷⁷ Fakultät für Physik und Astronomie, Julius-Maximilians-Universität, Würzburg, Germany
- ¹⁷⁸ Fakultät für Mathematik und Naturwissenschaften, Fachgruppe Physik, Bergische Universität Wuppertal, Wuppertal, Germany
- ¹⁷⁹ Department of Physics, Yale University, New Haven, CT, United States
- ¹⁸⁰ Yerevan Physics Institute, Yerevan, Armenia
- ¹⁸¹ Centre de Calcul de l'Institut National de Physique Nucléaire et de Physique des Particules (IN2P3), Villeurbanne, France
- ¹⁸² Academia Sinica Grid Computing, Institute of Physics, Academia Sinica, Taipei, Taiwan

^a Also at Department of Physics, King's College London, London, United Kingdom.

^b Also at Institute of Physics, Azerbaijan Academy of Sciences, Baku, Azerbaijan.

^c Also at Novosibirsk State University, Novosibirsk, Russia.

^d Also at TRIUMF, Vancouver, BC, Canada.

^e Also at Department of Physics & Astronomy, University of Louisville, Louisville, KY, United States.

^f Also at Physics Department, An-Najah National University, Nablus, Palestine.

^g Also at Department of Physics, California State University, Fresno, CA, United States.

^h Also at Department of Physics, University of Fribourg, Fribourg, Switzerland.

ⁱ Also at II Physikalisches Institut, Georg-August-Universität, Göttingen, Germany.

^j Also at Departament de Física de la Universitat Autònoma de Barcelona, Barcelona, Spain.

^k Also at Departamento de Física e Astronomia, Faculdade de Ciências, Universidade do Porto, Portugal.

^l Also at Tomsk State University, Tomsk, and Moscow Institute of Physics and Technology State University, Dolgoprudny, Russia.

^m Also at The Collaborative Innovation Center of Quantum Matter (CICQM), Beijing, China.

ⁿ Also at Università di Napoli Parthenope, Napoli, Italy.

^o Also at Institute of Particle Physics (IPP), Canada.

^p Also at Horia Hulubei National Institute of Physics and Nuclear Engineering, Bucharest, Romania.

^q Also at Department of Physics, St. Petersburg State Polytechnical University, St. Petersburg, Russia.

^r Also at Borough of Manhattan Community College, City University of New York, New York City, United States.

^s Also at Department of Financial and Management Engineering, University of the Aegean, Chios, Greece.

^t Also at Centre for High Performance Computing, CSIR Campus, Rosebank, Cape Town, South Africa.

^u Also at Louisiana Tech University, Ruston, LA, United States.

^v Also at Institutio Catalana de Recerca i Estudis Avançats, ICREA, Barcelona, Spain.

^w Also at Department of Physics, The University of Michigan, Ann Arbor, MI, United States.

^x Also at LAL, Univ. Paris-Sud, CNRS/IN2P3, Université Paris-Saclay, Orsay, France.

^y Also at Graduate School of Science, Osaka University, Osaka, Japan.

^z Also at Fakultät für Mathematik und Physik, Albert-Ludwigs-Universität, Freiburg, Germany.

^{aa} Also at Institute for Mathematics, Astrophysics and Particle Physics, Radboud University Nijmegen/Nikhef, Nijmegen, Netherlands.

^{ab} Also at Department of Physics, The University of Texas at Austin, Austin, TX, United States.

^{ac} Also at Institute of Theoretical Physics, Ilia State University, Tbilisi, Georgia.

^{ad} Also at CERN, Geneva, Switzerland.

^{ae} Also at Georgian Technical University (GTU), Tbilisi, Georgia.

^{af} Also at Ochadai Academic Production, Ochanomizu University, Tokyo, Japan.

^{ag} Also at Manhattan College, New York, NY, United States.

^{ah} Also at The City College of New York, New York, NY, United States.

^{ai} Also at Departamento de Física Teórica y del Cosmos, Universidad de Granada, Granada, Portugal.

^{aj} Also at Department of Physics, California State University, Sacramento, CA, United States.

^{ak} Also at Moscow Institute of Physics and Technology State University, Dolgoprudny, Russia.

^{al} Also at Departement de Physique Nucleaire et Corpusculaire, Université de Genève, Geneva, Switzerland.

^{am} Also at Institut de Física d'Altes Energies (IFAE), The Barcelona Institute of Science and Technology, Barcelona, Spain.

^{an} Also at School of Physics, Sun Yat-sen University, Guangzhou, China.

^{ao} Also at Institute for Nuclear Research and Nuclear Energy (INRNE) of the Bulgarian Academy of Sciences, Sofia, Bulgaria.

^{ap} Also at Faculty of Physics, M.V.Lomonosov Moscow State University, Moscow, Russia.

^{aq} Also at National Research Nuclear University MEPhI, Moscow, Russia.

^{ar} Also at Department of Physics, Stanford University, Stanford, CA, United States.

^{as} Also at Institute for Particle and Nuclear Physics, Wigner Research Centre for Physics, Budapest, Hungary.

^{at} Also at Giresun University, Faculty of Engineering, Turkey.

^{au} Also at CPPM, Aix-Marseille Université and CNRS/IN2P3, Marseille, France.

^{av} Also at Department of Physics, Nanjing University, Jiangsu, China.

^{aw} Also at Institute of Physics, Academia Sinica, Taipei, Taiwan.

^{ax} Also at University of Malaya, Department of Physics, Kuala Lumpur, Malaysia.

* Deceased.